SYNTHESIS OF MESOPOROUS CATALYSTS AND THEIR PERFORMANCE IN PYROLYSIS OF POLYETHYLENE

A THESIS SUBMITTED TO
THE GRADUATE SCHOOL OF NATURAL AND APPLIED SCIENCES
OF
MIDDLE EAST TECHNICAL UNIVERSITY

BY

BUĞÇE AYDEMİR

IN PARTIAL FULLFILLMENT OF THE REQUIREMENTS
FOR
THE DEGREE OF MASTER OF SCIENCE
IN
CHEMICAL ENGINEERING

DECEMBER 2010

Approval of the thesis:

SYNTHESIS OF MESOPOROUS CATALYSTS AND THEIR PERFORMANCE IN PYROLYSIS OF POLYETHYLENE

Submitted by **BUĞÇE AYDEMİR** in partial fulfillment of the requirements for the degree of **Master of Science in Chemical Engineering Department**, **Middle East Technical University** by,

Prof. Dr. Canan Özgen _____
Dean, Graduate School of **Natural and Applied Sciences**

Prof. Dr. Deniz Üner _____
Head of Department, **Chemical Engineering**

Assoc. Prof. Dr. Naime Aslı Sezgi _____
Supervisor, **Chemical Engineering Department, METU**

Examining Committee Members:

Prof. Dr. Önder Özbelge _____
Chemical Engineering Dept., METU

Assoc. Prof. Dr. Naime Aslı Sezgi _____
Chemical Engineering Dept., METU

Prof. Dr. Timur Doğu _____
Chemical Engineering Dept., METU

Prof. Dr. Hayrettin Yücel _____
Chemical Engineering Dept., METU

Prof. Dr. Suna Balcı _____
Chemical Engineering Dept., Gazi University

Date: 23.12.2010

I hereby declare that all the information in this document has been obtained and presented in accordance with academic rules and ethical conduct. I also declare that, as required by these rules and conduct, I have fully cited and referenced all material and results that are not original to this work.

Name, Last Name : BUĞÇE AYDEMİR

Signature :

ABSTRACT

SYNTHESIS OF MESOPOROUS CATALYSTS AND THEIR PERFORMANCE IN PYROLYSIS OF POLYETHYLENE

Aydemir, Buğçe
M.Sc., Department of Chemical Engineering
Supervisor : Assoc. Prof. Dr. Naime Aslı Sezgi

December 2010, 159 pages

Plastic materials are widely used throughout the world due to their low prices and easy processing methods. A serious problem of environmental pollution is brought with the widespread use of these materials due to their non-biodegradabilty. For this reason, plastic materials are degraded into lower molecular weight liquid and gaseous products which are potential raw materials and fuels for petrochemical industry. The use of catalysts enhances the formation of more valuable hydrocarbons at lower reaction temperatures and residence times.

In this study, aluminum containing MCM-41 and tungstophosphoric acid (TPA) loaded SBA-15 materials were synthesized by impregnation of Al and TPA into hydrothermally synthesized MCM-41 and SBA-15, respectively to be used in catalytic degradation of polyethylene. Al was incorporated into MCM-41 framework with different Al/Si ratios using aluminum triisopropylate as the aluminum source and TPA was incorporated to the porous framework of SBA-15 with different W/Si ratios, using tungstophosphoric acid hydrate as the acid source.

From XRD analysis, it was observed that introducing acidic compounds did not cause deformations in the regularity and by EDS analysis, it was found out

that at lower loadings, acidic compounds were introduced more effectively for MCM-41 materials. Nitrogen adsorption-desorption isotherms showed that the synthesized materials exhibited type IV isotherms. SEM and TEM pictures showed the hexagonal regularly ordered structure of SBA-15 and MCM-41 materials. FTIR analysis of the pyridine adsorbed synthesized materials revealed the existence of Lewis and Brønsted acid sites in the synthesized materials.

From TGA analysis it was observed that aluminum impregnated MCM-41 samples reduced the temperature of the degradation reaction significantly and TPA loaded SBA-15 samples reduced activation energy of the reaction effectively.

In the degradation reaction system, non-catalytic and catalytic degradation experiments of polyethylene were performed. In non-catalytic degradation and catalytic degradation reactions carried out using aluminum containing MCM-41 materials, selectivity of C3 and C4 hydrocarbon gases was high and in catalytic degradation reactions carried out using TPA impregnated SBA-15 materials, selectivity of ethylene was high. In the liquid analysis of non-catalytic degradation reactions, it was observed that the product distribution was mainly composed of hydrocarbons greater than C18. The use of aluminum loaded MCM-41 and TPA loaded SBA-15 materials resulted in a liquid product distribution in the range of C5-C14, which is the hydrocarbon range of gasoline fuel.

Keywords: Catalytic degradation, polyethylene, mesoporous, MCM-41, SBA-15, tungstophosphoric acid

ÖZ

MEZOGÖZENEKLİ KATALİZÖRLERİN SENTEZİ VE POLİETİLENİN PİROLİZİNDEKİ PERFORMANSLARI

Aydemir, Buğçe
Yüksek Lisans, Kimya Mühendisliği Bölümü
Tez Yöneticisi : Doç. Dr. Naime Aslı Sezgi

Aralık 2010, 159 sayfa

Tüm dünyada plastik malzemeler düşük maliyetleri ve kolay işlenme metodlarından dolayı yaygın olarak kullanılmaktadırlar. Bu malzemelerin yaygın kullanımı, doğada geri dönünüşümlerinin olmaması sebebiyle ciddi bir çevre kirliliği sorununa yol açmaktadır. Bu nedenden ötürü plastik malzemeler, petrokimya endüstrisi için potansiyel birer ham madde ve değerli hidrokarbonlar olan daha düşük molekül ağırlıklı gaz ve sıvı ürünlere parçalanmaktadır. Katalizörlerin kullanımı daha düşük reaksiyon sıcaklığı ve sürelerinde daha değerli hidrokarbonların oluşmasını sağlamaktadır.

Bu çalışmada, polietilenin katalitik pirolizinde kullanılmak üzere alüminyum içeren MCM-41 ve tungstofosforik asit (TPA) içeren SBA-15 malzemeleri, hidrotermal yöntemle sentezlenmiş olan MCM-41 ve SBA-15 malzemelerine emdirme yöntemi kullanılarak sentezlenmiştir. Alüminyum, MCM-41 yapısına farklı Al/Si oranlarında alüminyum kaynağı olarak alüminyum isopropilat kullanılarak, TPA ise SBA-15 yapısına farklı W/Si oranlarında asit kaynağı olarak tungstofosforik asit kullanılarak eklenmiştir. Her iki malzemede de XRD analizi ile, yapıya eklenen asidik bileşenlerin yapının düzenliliğinde deformasyona neden olmadığı, EDS analizi ile düşük yüklemelerde asidik bileşenlerin yapıya daha etkili sokulduğu gözlenmiştir. Nitrojen adsorpsiyon-desorpsiyon izotermleri, sentezlenen malzemelerin Tip IV izoterm gösterdiği

saptanmıştır. SEM ve TEM resimleri, SBA-15 ve MCM-41 malzemelerinin düzenli hekzagonal yapısını göstermiştir. Piridin adsorblanmış malzemelerin FTIR analizi yapıdaki Lewis ve Brønsted acid bölgelerinin varlığını göstermiştir. TG analizi ile alüminyum emdirilmiş MCM-41 örneklerinin piroliz reaksiyonun sıcaklığını önemli ölçüde düşürdüğü, TPA emdirilmiş SBA-15 örneklerinin ise reaksiyon aktivasyon enerjisini etkili bir şekilde düşürdüğü gözlemlenmiştir.

Polietilenin katalitik olmayan ve katalitik deneyleri, degredasyon reaksiyon sisteminde gerçekleştirilmiştir. Katalitik olmayan ve alüminyum içeren MCM-41 malzemelerinin kullanıldığı katalitik piroliz reaksiyonlarında, C3 ve C4 hidrokarbon gazlarının seçicilikleri, TPA içeren SBA-15 malzemelerinin kullanıldığı katalitik piroliz reaksiyonlarında ise etilen seçiciliği yüksektir. Katalitik olmayan piroliz reaksiyonlarında elde edilen sıvı ürünlerin analizinde ürün dağılımı temel olarak C18'den büyük hidrokarbonlardan oluştuğu gözlemlenmiştir. Alüminyum içeren MCM-41 ve TPA içeren SBA-15 malzemelerinin kullanımı, benzin yakıtı hidrokarbon aralığı olan C5-C14 sıvı ürün dağılımı ile sonuçlanmıştır.

Keywords: Katalitik degredasyon, polietilen, mezogözenekli, MCM-41, SBA-15, tungstofosforik asit

To my family, beloved part of my life Barış Zeki Canlı and Zeynep Obalı

ACKNOWLEDGEMENTS

Firstly, I would like to express my deep appreciation to my supervisor Assoc. Prof. Dr. Naime Aslı Sezgi for her patience, guidance and encouragement through my graduate studies. Also I would like to thank her for her wise suggestions and kind attitude.

Also, I would like to thank Prof. Dr. Timur Doğu, for his helpful advises and suggestions on my experimental studies.

I would also like to thank my dear family, my mother Bike Aydemir and my father Nadir Aydemir for their endless love and support throughout my graduate studies.

Also, I would like to thank dear Barış Zeki Canlı, for his patience and great support through this time.

I would especially like to thank Dr. Zeynep Obalı for her help and great friendship. I would also like to thank Didem Özmen, Kenan Cem Tokay, Ayşegül Çiftçi and Dilek Ergun for their kindness and supports through my studies.

I would like to thank Gülten Orakçı for her helps in Gas Chromatography and BET analyses. I would also thank Mihrican Açıkgöz for TGA analysis, Turgut Aksakal for his support in using laboratory equipment, Kerime Güney and Kemal Yıldırım for their kindness and supports.

I would specially thank İsa Çağlar, Nevzat Bekçi, Ertuğrul Özdemir and Süleyman Nazif Kuşhan for their great support through my experimental studies.

I would specially thank METU Chemical Engineering Department for giving me a chance to conduct my thesis studies and making it possible to complete my thesis studies properly.
I would like to thank METU Central Laboratories for TGA, NMR, Surface Characterization, SEM and TEM analyses.

I would also like to thank METU Metallurgy Department for their support in XRD and EDS analyses.

I would like to thank Gazi University Chemical Engineering Department for giving a great support for BET analysis.

TABLE OF CONTENTS

LIST OF TABLES

TABLES

LIST OF FIGURES

FIGURES

LIST OF SYMBOLS

A :Pre exponential factor

A_i :Area of the peak read from gas chromatography

E :Activation energy of the reaction (kJ/mol)

n :Order of the reaction

n_i :Mole number of the compound i

R :Gas constant (8.314 J/kmol)

S_i :Selectivity of the compound i

t :Time (min)

T :Temperature (K)

w_i :Weight fraction of the compound i

x_i :Mole fraction of the liquid compound i

y_i :Mole fraction of the gas compound i

z_i :Volume fraction of the liquid compound i

Greek letters

α :Fraction of polymer decomposed at time t

β_i :Calibration factor of the compound i

Abbreviations

EDS : Energy dispersive spectroscopy

FTIR : Fourier transform infrared

GC : Gas chromatograph

HPA : Heteropoly acid

IUPAC : International Union of Pure and Applied Chemistry

NMR	: Nuclear magnetic resonance
PE	: Polyethylene
PET	: Polyethylene terepthalate
PP	: Polypropylene
PS	: Polystyrene
PVC	: Polyvinyl chloride
SEM	: Scanning electron microscopy
TEM	: Transmission electron microscopy
TGA	: Thermal gravimetric analyzer
TPA	: Tungstophosphoric acid
XRD	: X-Ray diffractometer

CHAPTER 1

INTRODUCTION

Plastic materials are widely used throughout the world due to their low price, high capacity of production and simple processing techniques. These qualifications of plastic materials provide them a great potential of use in plenty of industrial applications. For example, polyethylene itself has a production of 80 million metric tons/year, which can generate an idea of the extent of the plastics' market (http://en.wikipedia.org/wiki/Polyethylene). However, a great drawback is brought by the widespread use of these materials: environmental pollution. Plastic materials are generally non-biodegradable, in other words, incapable of decomposing biologically in the nature. This disability brings the problems of accumulation of plastics with an increasing trend and uncontrollable environmental pollution. Some temporary and ineffective solutions to the problem are presently being applied. Landfilling is one of the previously mentioned solutions, which is highly temporary due to consumption of available, limited landfilling spaces throughout the world. Another ineffective solution is incineration. This technique is not only being temporary, but at the same time dangerous and harmful, due to the emission of highly toxic organic chemicals as the product of burning reaction. These toxic byproducts are extremely dangerous concerning the health of all living things. Therefore, alternative methods are being researched and developed for the safe and effective removal of waste plastics.

The recycling of plastic materials is done by pyrolysis. Pyrolysis is defined as the chemical decomposition of polymeric materials by applying heat under inert atmospheric conditions. As the operation causes chemical change, it involves the breaking of bonds, it is mostly endothermic and therefore heat

supply is necessary for the reaction to proceed. The products obtained at the end of the reaction are olefins and aromatic organic compounds, which can further be processed to be used as raw material of many chemical compounds and fuels. However there exists a problem of high energy consumption of the pyrolysis reaction. A temperature range of generally 450^{o}C-600^{o}C is sufficient for the decomposition to occur in a typical pyrolysis reaction. Also, the distribution of the products has a wide range of carbon numbers, which is an undesired condition due to the fact that the desired products are in a specific range. Therefore, catalysts are being developed in order to overcome those mentioned drawbacks of non-catalytic pyrolysis. By the use of these catalysts, reaction temperature and residence times can be lowered efficiently, providing considerable energy saving and time. Another advantage of using catalysts for the degradation of polymers is obtaining high quality, stable and narrowly distributed products with higher market values.

For polymer pyrolysis reactions, in general, solid acid catalysts are used. Amorphous aluminosilicates, zeolites and some mesostructured catalysts are the most common groups of materials that were studied and presently being studied in the catalytic degradation of polymeric materials. ZSM-5 (Aguado et al., 1997; Garforth et al., 1997; Aguado et al., 2007), HZSM-5 (Ohkita et al., 1993, Miskolczi et al., 2004), HY (Isoda et al., 1998; van Grieken et al., 2001), zeolites Y and Beta (Chaianansutcharit et al., 2007) are the most commonly studied zeolites for pyrolysis of plastic materials. Aluminosilicates (Ohkita et al., 1993, Garforth et al., 1997, Sakata et al., 1997, Uddin et al., 1997) and mesostructured catalysts, MCM-41 (Garforth et al., 1997, Jalil et al., 2002, Marcilla et al., 2002) and SBA-15 are also commonly used in catalytic degradation reactions.

The performance and functionality of the solid catalysts are determined by the structural properties of the material. This dependency on the structure arises from the size and shape of polymeric materials, because the bulky and huge form of polymeric molecules is the determining factor in the choice of the suitable catalyst to be used. In other words, in order to make catalyst to function properly, bulky polymeric molecules have to access the active sites of the catalyst, which can be difficult when microporous materials considered. By

active site, the acidic regions, preferably Brønsted acid sites of the solid acid catalysts are referred. From this point, zeolites which are containing strong Brønsted acid sites are advantageous but microporous structure of the zeolites hinders the access of polymeric molecules to the active sites of the catalyst. On the other hand, mesoporous materials of which aluminosilicates, MCM-41 and SBA-15 are members, have an obvious advantage in allowing the access of polymeric molecules to the pores. The problem with these materials is that acid sites are not present in these as in the zeolites. Therefore, acid sites have to be introduced to these materials in order to maintain the necessary catalytic functionality for the cracking reactions. Aluminum based solutions are widely used as acidic sources to be incorporated into the framework of MCM-41. Widely used aluminum solutions are aluminum sulfate, aluminum nitrate, aluminum hydroxide, aluminum isopropoxide and sodium aluminate (Biz and White, 1999, Cesteros and Haller, 2001, Eimer et al., 2003).

Similarly, pure SBA-15 does not show considerable catalytic activity unless appropriate acidic medium is introduced into the structure (Obali et al., 2009). Therefore, acid sites can also be introduced to the structure in order to produce a functional catalyst for degradation reactions. Heteropoly acids are a good choice for this purpose. Due to their highly strong acidic character, they seem to be very suitable for cracking of polymers. Heteropoly acids cannot be used alone as a catalyst because their thermal stability is very low. It means that at high reaction temperatures, they can easily decompose. Therefore SBA-15 is a suitable material to provide a high thermal and hydrothermal stability when used as a support material for heteropoly acids. High surface area and mesoporosity are also advantageous for the distribution of heteropoly acid molecules over the support material.

In this study, mesoporous MCM-41 and SBA-15 materials were synthesized following a hydrothermal synthesis route and acid sites were introduced to these materials by impregnation method. The synthesized materials were tested by thermogravimetric analysis and then degradation experiments were conducted in the experimental setup. Gaseous and liquid products were then analyzed using gas chromatography

CHAPTER 2

POROUS MATERIALS

According to the IUPAC classification, there are three types of porous materials. These are: microporous (< 2nm), mesoporous (2-50 nm) and macroporous (>50 nm) (Sing et al., 1985). Classification of porous materials according to their sizes is given in Figure 2.1. Porous materials are being widely used as adsorbents, catalyst or catalyst supports and ion exchangers in many chemical reactions and industrial applications (Ciesla et al.,1999, Sayari et al.,1996). In heterogeneous catalysis, mainly two classes of these porous materials are used: microporous and mesoporous materials (Beck et al.,1992).

The most abundant microporous materials are zeolites. Besides zeolites, pillared clays, some metal phosphates like titanium, zirconium etc., amorphous silica, inorganic gels and carbon molecular sieves are the members of microporous materials family (Ciesla et al., 1999, Güçbilmez et al., 2005).

Silica and alumina are an example to mesoporous materials and they have similarly sized fine mesopores. However, the pores of these materials are irregularly arranged.

In 1992, an ordered mesoporous solid structure with uniform hexagonal arrays was discovered by Mobil Oil Corporation researchers, which was a breakthrough in the history of mesoporous materials (Beck et al., 1992, Kresge et al., 1992). The new material was called MCM-41 (Mobil Composition of Matter No.41) which was named after the company.

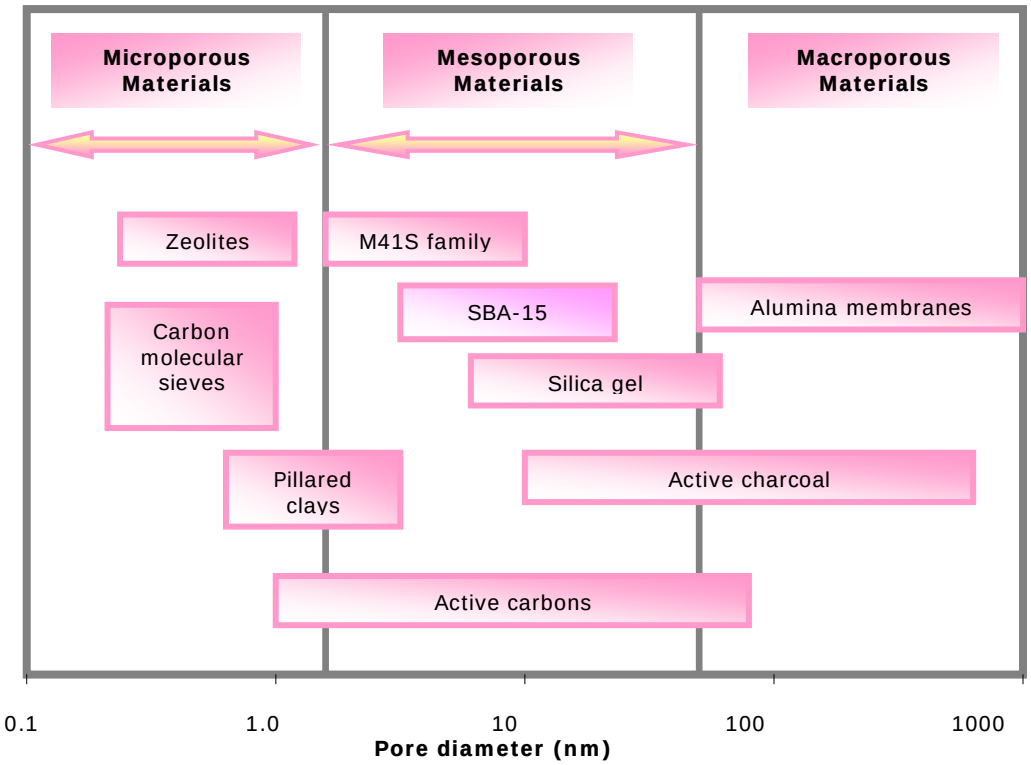

Figure 2.1. Classification of porous materials according to their size ranges (Adapted from Güçbilmez, 2005)

2.1 Mesoporous Materials

2.1.1 M41S Family Members and MCM-41

It is previously mentioned that in the early 90's Mobil researchers developed an idea of preparing porous silicates using supramolecular surfactant templates (Sayari, 1996). The research group defined three main phases: MCM-41 which is a hexagonal structure, MCM-48 which is a cubic structure and MCM-50 which is a lamellar structure (Sayari, 1996, Roth and Vartuli, 2005). These structures are shown in Figure 2.2. Hexagonal phase forms by hexagonal packing of cylindirical micelles, whereas lamellar phase is a result of formation of surfactant bilayers (Sayari, 1996). The structure of MCM-41 is given in Figure 2.3.

MCM-41 is mainly composed of silica (SiO_2). These materials exhibit a remarkably ordered hexagonal structure of unidimensional mesopores,

causing the material to have a particularly narrow pore size distribution, which can vary from 1.6 nm to 10 nm (Schmidt, 1994, Taguchi and Schüth, 2005).

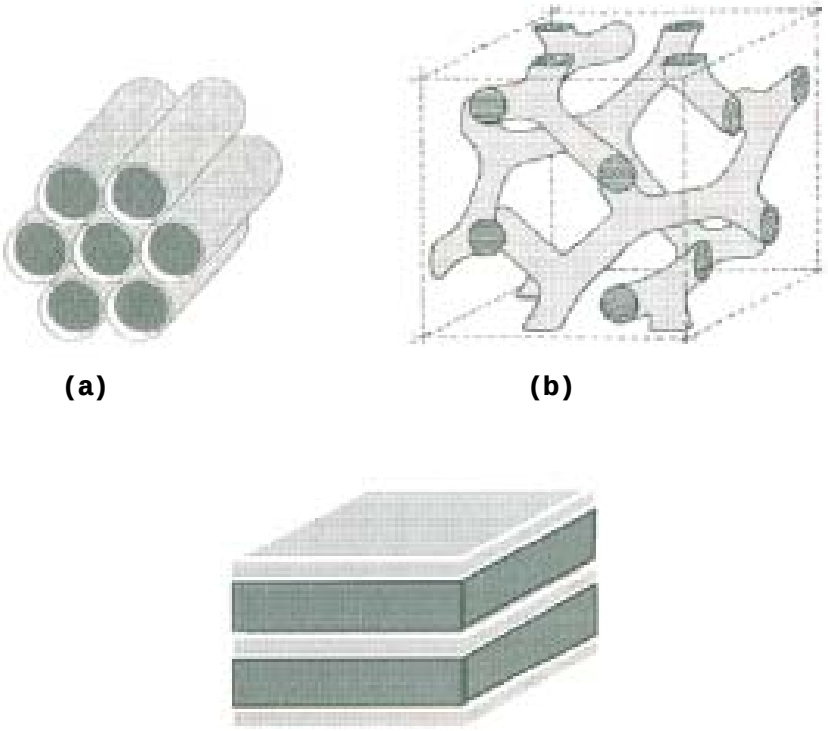

(a) **(b)**

(c)

Figure 2.2. Three silica structures defined by Mobil researchers: (a) MCM-41, (b) MCM-48 and (c) MCM-50 (Roth and Vartuli, 2005)

Members of M41S family are defined and determined by two distinct and general properties:

- After calcination, a thermally stable structure will show at least one low angle in X-ray diffraction pattern greater than 18 Å d-spacing.
- Mesopores that are arranged uniformly, results in a high adsorption capacity caused by capillary condensation of small sorbate molecules in these mesopores (Roth and Vartuli, 2005).

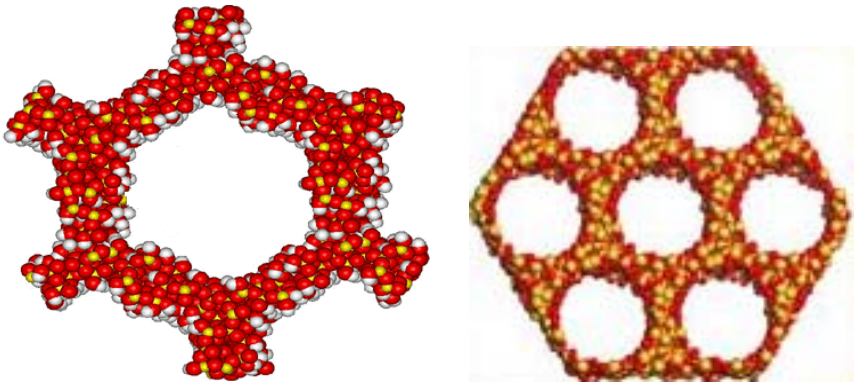

Figure 2.3. Structure of MCM-41 material
(http://www.utdallas.edu/~balkus/drop.jpg)

MCM-41 mesoporous material is very promising considering many kinds of reactions, which include alkylation of aromatics, hydrocarbon cracking, and oil upgrading (Vinu et al., 2004). Existence of uniform hexagonal array of cylindirical pores creates a particular advantage in the catalytic conversion of large, bulky, generally organic or polymeric molecules (Sun et al., 1997).

2.1.1.1 Formation Mechanism of MCM-41

A mechanism for the formation of MCM-41 is proposed, which is called as liquid crystalline templating mechanism (LCT). This mechanism works in such a way that surfactant molecules create an organic template basis for the ordered structure to be formed (Beck et al., 1992). The surfactant molecule contains a hydrophilic head group and a hydrophobic tail group in its structure. According to the temperature and concentration, organization of the surfactant molecules differs. For instance, at lower concentrations, the surfactant molecules tend to locate more randomly. As the concentration increases to a critical level, called as CMC1, surfactant molecules containing hydrophobic and hydrophilic ends, start to form spherical miscelles. The hydrophilic ends of the molecules head towards the outside, whereas the hydrophobic ends head towards inside forming the micellar structure. As the concentration of the surfactant is further increased, the solution reaches to another critical concentration, called as CMC2 at which formation of spherical

or rod like miscelles continues. Continuous increase in the concentration causes the liquid crystals to form. The LCT mechanism proposed by Mobil scientists is given in Figure 2.4 (Sayari, 1996). In the figure, two possible formation pathways are given. In the first pathway, a self-organized liquid crystal phase is formed and this phase is surrounded by inorganic species leading to a condensation into rigid walls. Second pathway includes the participation of inorganic species in the formation of ordered organic-inorganic mesophase which has an effect on the final morphology (Sayari, 1996).

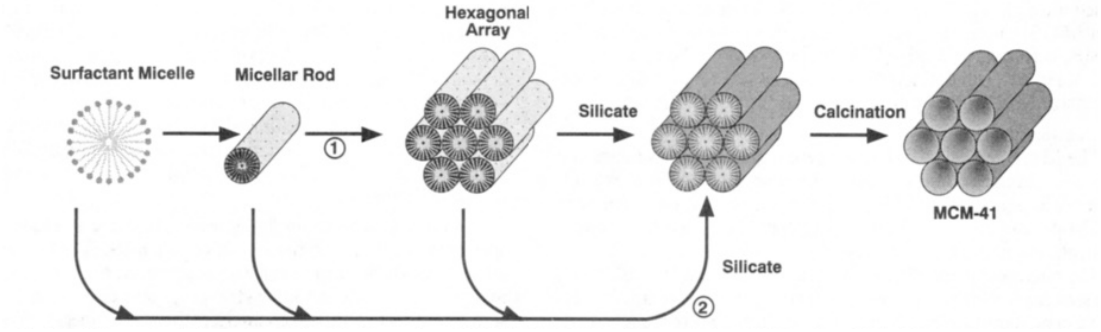

Figure 2.4. Two possible pathways of MCM-41 formation mechanism proposed by Beck et. al (1992)

2.1.1.2 Incorporation of Aluminum into MCM-41 Mesoporous Material

As mentioned earlier, MCM-41 with its structural properties has many advantages in the catalytic conversion of bulky organic molecules. However pure MCM-41 material lacks suitable acid sites, which are sufficient for the catalytic activity of the material. It is known that, when aluminum or transition metal elements are incorporated into the MCM-41 structure, the material ends up with enhanced acidic properties, hence performing a greater catalytic activity. Incorporation of aluminum or transition metals into the silica framework also improves the ion exchange capacity of the material (Cesteros et al., 2001). Many authors investigated the synthesis and characterization of Al-MCM-41 materials from different aspects (Schmidt et al., 1994, Luan et al., 1995, Sun et al., 1997, Cesteros et al., 2001, Jana et al., 2003, Wan et al., 2004). The factors that can be preferred in the synthesis of Al-MCM-41 material are Si/Al ratio and different silica and alumina sources. Widely used

aluminum sources can be listed as; aluminum sulphate, sodium aluminate, aluminum isopropoxide, and pseudoboehmite (Cesteros et al., 2001). Incorporation of aluminum into the silica framework can be carried out using direct synthesis or post-synthesis methods (Jana et al., 2003).

2.1.2 SBA-15

Although M41S family materials are very promising for many catalytic reactions, thermal and hydrothermal stability of these materials are insufficient due to their very thin pore walls (Vinu et al., 2004). Recently, a new material which overcame aforementioned problems has been synthesized, and called as SBA-15, or Santa Barbara Amorphous type material. SBA-15 is a highly ordered, two dimensional and hexagonal mesostructured material which is formed of thick pore walls of 31 to 64 Å (Zhao et al.,1998). This is a polymer-templated silica structure, which has larger pore sizes and thicker pore walls providing higher thermal and hydrothermal stability compared to MCM-41 (Fulvio et al., 2005). Another important characteristic property of SBA-15 material is the presence of micropores in the form of interconnecting channels which binds hexagonal mesopores together (Fulvio et al., 2005). This feature brings better and effective diffusion properties for the catalysis purposes. SBA-15 is synthesized using a triblock copolymer poly(ethylene oxide)-poly(propylene oxide)-poly(ethylene oxide) which functions as templating agent in a highly acidic media (Vinu et al., 2004). In Figure 2.5, three dimensional structure of SBA-15 material is given.

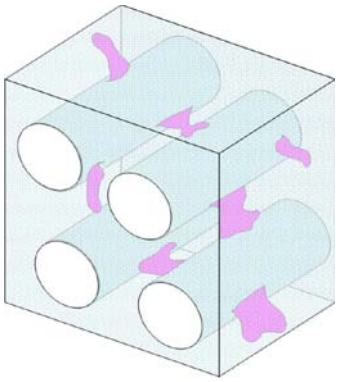

Figure 2.5. Three dimensional structure of SBA-15 material (Sonwane and Ludovice (2005))

According to the synthesis conditions, structural properties of SBA-15 material may differ. In Figure 2.6, TEM images of different pore sized SBA-15 materials are given. Parameters that can be adjusted in the synthesis of SBA-15 are mixture compositions and synthesis conditions like temperature, pH or time.

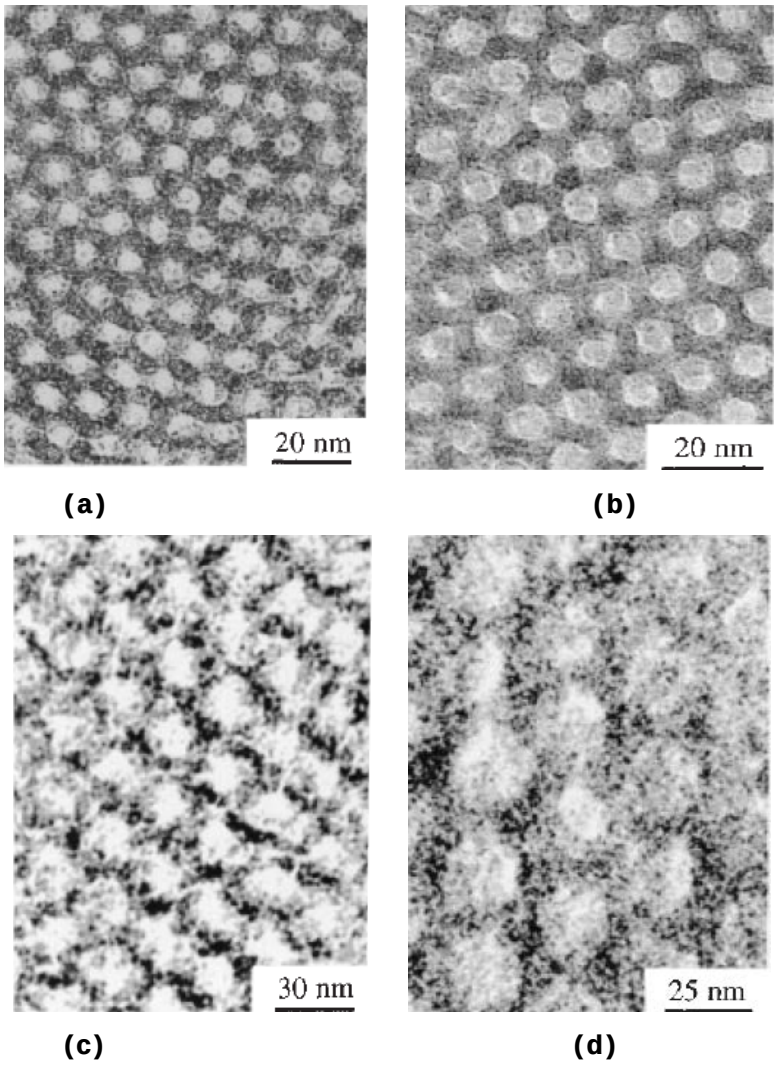

Figure 2.6. TEM images of SBA-15 samples with different pore sizes (a) 6 nm (b) 8.9 nm (c) 20 nm (d) 26 nm (Zhao et al., 1998)

It was reported that, when copolymer weight ratio in the synthesis mixture was higher than 6%, the final product was only consisted of silica gel, whereas when copolymer weight ratio was lower than 0.5%, the resulting product appeared to be amorphous silica. The synthesis of SBA-15 was carried out at a temperature range of 35 ^{o}C to 80 ^{o}C. Below and above this

temperature range, SBA-15 could not be produced. At room temperature amorphous silica powder or poorly ordered products were obtained. Above 80^{o}C, only silica gel is produced. Type of silica source also affects the final product. For SBA-15 synthesis, tetraethoxysilane (TEOS), tetramethoxysilane (TMOS), and tetrapropoxysilane (TPOS) could be used. The pH of the synthesis solution is another critical parameter to be adjusted. To obtain a suitable pH value which is lower than 1 to maintain an acidic medium, HCl, HBr, HI, HNO_3, H_2SO_4, or H_3PO_3 acids could be used. In the range of 2-6 pH values, precipitation or formation of silica gel could not be occurred. At pH 7, amorphous silica could be obtained (Zhao et al., 1998).

2.1.2.1 Heteropoly Acids and Incorporation of Tungstophosphoric Acid into SBA-15

Heteropoly compounds are composed of coordination-type salts and free acids. Condensation of at least two different kinds of oxoanions forms heteropoly compounds (Corma, 1995). Below, given an example for this condensation reaction:

$$12WO_4^{2-} + HPO_4^{2-} + 23H^{+} \rightarrow PW_{12}O_{40}^{3-} + 12H_2O \text{ (Corma, 1995)}$$

Heteropoly compounds contain heteropoly anions, and the central atom of the anion is typically silicon (Si) or phosphorous (P) atom. This central atom is combined with oxygen atoms and surrounded by exterior oxygen-linked metal atoms which are generally molybdenum (Mo), tungsten (W). In some rare occasions metals such as vanadium (V), niobium (Nb), tantalum (Ta) can be also present single or combined with another (Corma, 1995). In Figure 2.7, a schematic representation of a heteropoly compound containing P as the central atom and W as the surrounding metal atom

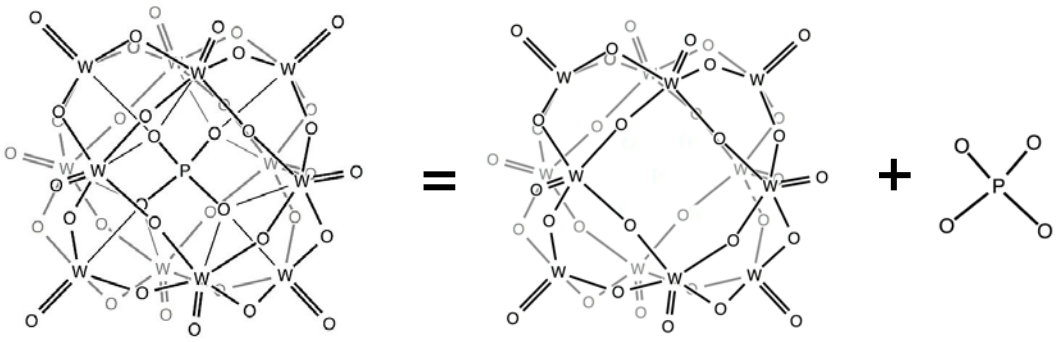

Figure 2.7. Schematic representation of a heteropoly compound (http://en.wikipedia.org/wiki/Keggin_structure)

Two well-known heteropoly acid structures are Keggin and Dawson structures, having the formulas of $H_nXM_{12}O_{40}$ and $H_nX_2M_{18}O_{62}$, respectively, which are given in Figure 2.8. Heteropoly acids are generally used as catalysts, either homogeneous or heterogeneous. Among all heteropoly anions, Keggin type heteropoly anions are the most widely used compound for catalysis due to their stability, acidic strength and availability. Below, the possible forms of heteropoly anions of different chemical formulas in Keggin and Dawson structures are listed (http://en.wikipedia.org/wiki/Heteropoly_acid).

- $H_4X^{n+}M_{12}O_{40}$, X = Si, Ge; M = Mo, W
- $H_3X^{n+}M_{12}O_{40}$, X = P, As; M = Mo, W
- $H_6X_2M_{18}O_{62}$, X=P, As;M = Mo, W

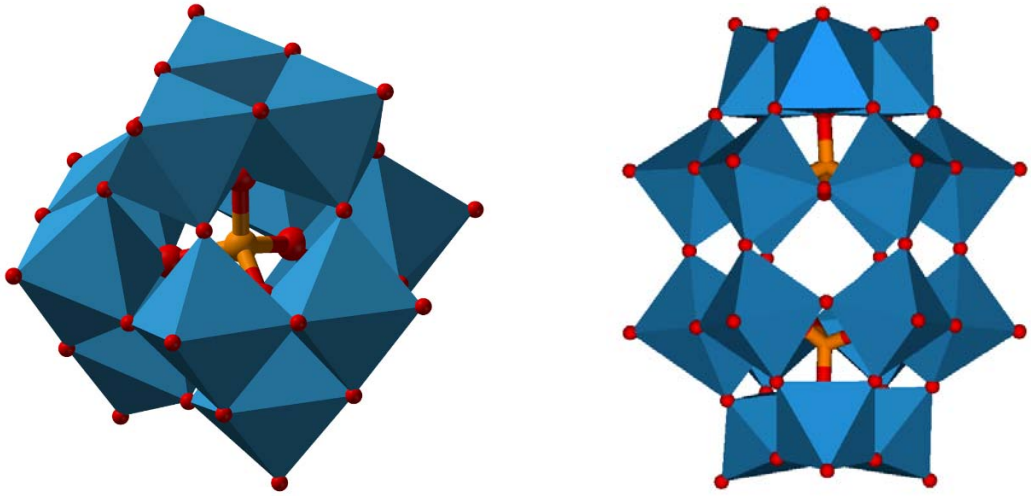

Figure 2.8. Model of two well known heteropoly acid structures (a) Keggin Structure and (b) Dawson Structure (http://en.wikipedia.org/wiki/Heteropoly_acid)

Heteropoly acids are widely and preferably used as catalysts due to their many advantages. First of all, heteropoly acids are environmentally friendly and economic materials. Furthermore, heteropoly acids are very strong Brønsted acids which are almost superacids. Heteropoly acids are also very strong oxidants which can effectively catalyze redox reactions under mild conditions (Kozhevnikov, 1998).

The structural properties of heteropoly acids have a great influence on the acidic character of these compounds. Heteropoly acids are built up of heteropoly anions (polyoxometalate anions) containing metal oxygen octahedral in their structure. As mentioned earlier heteropoly acids are strong Brønsted acids, and understanding the structure is important for understanding the catalytic effect. Three types of oxygen atoms are present in a Keggin type anion (see Figure 2.9). These oxygen atoms are possible protonation sites in the structure. These oxygen atoms are classified as terminal oxygens; M=O, edge sharing and corner sharing bridging oxygens; M-O-M, where M is the metal ion Mo^{6+} or W^{6+}. According to the physical structure of heteropoly anions, the protonation centers differ. For example, in

a Keggin anion in the gas phase edge bridging oxygens are the main protonation sites. On the other hand, for solid heteropoly acids, the terminal oxygen is the predominant acid center due accessibility, because in solid heteropoly acids, bridging oxygens play a role of linking in the formation of the crystal structure (Kozhevnikov, 1998).

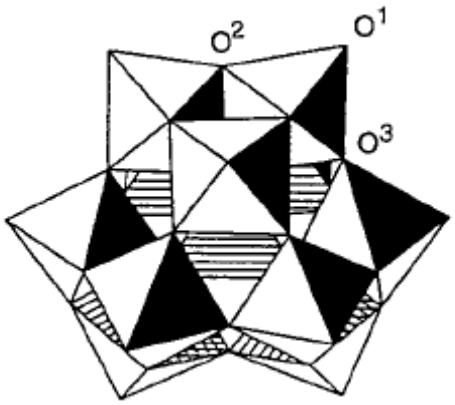

Figure 2.9. A Keggin type anion representing the terminal (O^1), edge bridging (O^2) and corner bridging (O^3) oxygen atoms (Kozhevnikov, 1998)

Solid heteropoly acids are stronger than conventional and common solid acids such as HX, HY zeolites, SiO_2-Al2O_3, and H_3PO_4-SiO_2, due to possession of pure Brønsted acidity. In terms of catalytic mechanism, heteropoly acids' capability of producing carbocations from olefins, make them suitable for catalyzing organic reactions. The acid strength of heteropoly acids is in a decreasing order of; PW > SiW ≥PMo > SiMo, which makes tungstophosphoric acid the most acidic one (Kozhevnikov, 1998).

Thermal stability is another important issue, because many reactions proceed at high temperatures. The decomposition temperatures of Keggin type PW, SiW, PMo, and SiMo are 465 ^oC, 445 ^oC, 375 ^oC, and 350 ^oC, respectively. Reactions that proceed over these temperatures are inappropriate to be catalyzed by these heteropoly acids because decomposition causes the acidity to be lost (Kozhevnikov,1998).

Due to very low surface area (1-5 m^2/g) and comparably low thermal stability, heteropoly acids can be supported on a suitable material to enhance mentioned properties. Zeolites are not suitable as supporting materials for heteropoly acids, because the tiny micropores of zeolites are preventing large heteropoly acid molecules to access inside. On the other hand, mesoporous molecular sieves are very successful support materials for heteropoly acids. Recently, MCM-41 mesoporous material is being used as a support for heteropoly acids. Due to high surface area (1200 m^2/g) and thermal stability, MCM-41 is a suitable support material. It was reported that above 20% heteropoly acid loading, Keggin structure was preserved. For amorphous SiO_2, below this loading level, partial decomposition of heteropoly acid was observed (Kozhevnikov, 1998). More recently, heteropoly acids supported on SBA-15 mesoporous material have been reported (He et al., 2005, Dufaud et al., 2009, Palcheva et al., 2009). In these studies, it was observed that by the incorporation of heteropoly acid into support material SBA-15, high surface area, thermally stable and reactive catalysts were produced.

CHAPTER 3

PYROLYSIS OF POLYMERS

3.1 General Information about Pyrolysis Processes

Pyrolysis is a process in which chemical and thermal decomposition takes place mostly ending up with smaller molecular structures. Pyrolysis or degradation can be performed at different temperature ranges, reaction times and pressures. Also reactive gases or liquids and catalysts may be used in addition for the pyrolysis processes. Plastics pyrolysis or degradation can be carried out at low (<400 ^{o}C), medium (400-600 ^{o}C) or high (>600 ^{o}C) temperature ranges. Pressure for pyrolysis process is mostly atmospheric; but in the case of thermally unstable products formation, the operation may be conducted under the atmospheric pressure, i.e. in vacuum or in the presence of diluents like steam (Scheirs and Kaminsky, 2006).

Products of thermal degradation are generally gases, liquids, and char, but the amounts of these products mostly depend on the type of the polymers used, feed mixtures, and reaction conditions. It is certain that gaseous and liquid products are both mixtures of many organic compounds (Scheirs and Kaminsky, 2006).

Pyrolysis reaction proceeds over breaking of bonds forming the polymeric material in which a significant amount of heat is needed, therefore it is endothermic. An alternative method is partial oxidation but this time products are diluted by oxidation (Scheirs and Kaminsky, 2006).

3.2 Catalytic Pyrolysis of Polymers

Catalytic pyrolysis of polymers has many advantages when compared to non-catalytic thermal pyrolysis. In non-catalytic thermal pyrolysis, decomposition temperature is very high. Therefore a high amount of energy and time is necessary in order to achieve an efficient decomposition process. Also, the quality of the obtained products is low and the distribution of the products forms a broad range in terms of molecular weight or carbon atom numbers, which is actually not a preferred situation. In the presence of catalysts, all the above mentioned disadvantages can be overcome. In catalytic pyrolysis processes, decomposition temperature is efficiently reduced when compared to non-catalytic thermal processes. This provides an efficient use of energy, which is a major concern. Also, the rate of reaction is higher in catalytic degradation, providing time efficiency as well. The quality and distribution of products is also enhanced in the presence of catalysts, making catalytic degradation a promising way to recycle waste polymers.

3.3 Operating Conditions

Pyrolysis of polymers is strongly dependent on the variables and operating conditions of the system. These can be mainly classified as temperature, reaction time, reactor type, and the type of the catalysts that are being used.

3.3.1 Temperature

The major parameter of the degradation reaction is temperature; because it determines both the rate and stability of the products. High temperatures (> 600 ^{o}C) and low pressures (i.e. vacuum) generally favor the production of low molecular weight gaseous products, while low temperatures (< 400 ^{o}C) and higher pressures favor the formation of high molecular weight liquid products, more amount of secondary products and lead to coke formation. Most plastic materials start to degrade at a temperature of ~300 ^{o}C. The presence of additives within commercial polymers also affects the pyrolysis temperature. Generally, pyrolysis operations are conducted in a temperature range of 400-500 ^{o}C (Scheirs and Kaminsky, 2006).

3.3.2 Reaction Time

This parameter is usually dependent on the temperature. The reaction time determines the type of the products formed. For example, in short residence times, generally low molecular weight gaseous products are formed, whereas in longer residence times, products being more thermodynamically stable are formed (Scheirs and Kaminsky, 2006).

3.3.3 Reactor Type

Reactor type for pyrolysis reactions is specifically important for heat transfer, feed and residue keeping concerns. Generally in most of the polymer degradation reactions, firstly polymer is dissolved in a hot molten polymer or in a salt bath in order to reduce its viscosity. If not, heat transfer and mixing properties should be very effective. For this reason thermal or catalytic fluidized bed reactors may be preferred. On the other hand, in fluidized beds, effective filtration should be maintained because residues are also carried with the products through the reactor. Other type of reactors that can be used for polymer degradation reactions are: extruders, tubular reactors, stirred tank reactors, vertical or shaft reactors, fixed bed reactors, salt or lead bath reactors, rotary kilns and autoclaves. For extruders, operation temperature is limited therefore for high temperature reactions, extruders are not very useful. Tubular reactors are simple and widely used, providing simplicity. With stirred tank reactors an efficient mixing and heat transfer can be carried out but clogging of downstream channels should be avoided. Fixed bed reactors are generally used as a second reactor for vapor phase contact modes. The vapor products produced in the first reactor passes from the second fixed bed reactor to obtain products with enhanced quality. Salt or lead bath reactors are efficient in terms of heat transfer, but since the residues are accumulating as a layer, the system should be shut down periodically for maintenance. Rotary kilns are formed of simplified units providing tumbling. Autoclaves are used for pressure sufficient reactions and they generally operate in a batch mode (Scheirs and Kaminsky, 2006).

3.3.4 Catalysts

Catalysts, in general, are special type of compounds or materials, specifically chosen, designed or synthesized to influence the reaction mechanisms in a preferred way. In the presence of catalysts, the reaction rate can be accelerated and the required temperature for decomposition can be reduced effectively, which at the same time means cost efficiency in terms of energy could be managed. The quality of the obtained products is strongly affected by the catalyst used for the pyrolysis reaction, and by quality, formation of gasoline range products are mentioned. Three main points are considered in the selection of the suitable catalyst for a specific reaction: activity, selectivity and stability (Scheirs and Kaminsky, 2006).

3.4 Decomposition Modes of Polymers

Decomposition of polymers is a very complex process in which multiple reactions occur at the same time, and these reactions can not be defined specifically one by one. Moreover, the nature of the proceeding reactions are determined by many factors like molecular structure of the polymers, presence of complex chain systems within the polymer, or presence of catalysts, initiators, etc. Below, the list of decomposition modes of polymers is given (Scheirs and Kaminsky, 2006).

- Unzipping: This type of decomposition is defined as decomposition into monomer units. The decomposition of poly(methyl methacrylate) (PMMA) is an example for the unzipping mode. This type of decomposition is a preferred mode because monomers are formed and they are very valuable. The unzipping of PMMA ends up with methyl methacrylate, and used in acrylic varnishes or as a viscosity index improver for lubricating oil.

- Random fragmentation: This type of decomposition forms products of changing lengths from the main chain. Polyethylene (PE) and polypropylene (PP) undergo this type of decomposition forming a Gaussian type distribution of the final products. PE is fragmented into

PE waxes, containing high amounts of α-olefins. In the case of PP, more branched product mixture is obtained.

- Unzipping and random fragmentation: This type of decomposition is the combined form of unzipping and random fragmentation modes. Polystyrene (PS) and polyisobutylene (PIB) decompose through these two steps. PS by this way could be converted into styrene monomers.

- Elimination of simple stable molecules from adjacent atoms: This type of breaking yields unsaturated charring residues. Polyvinyl chloride (PVC) forms HCl, Polyvinyl acetate (PVAc) forms acetic acid and polyvinyl alcohol (PVOH) forms water when they undergo this type of decomposition.

- Elimination of side chains: Most thermosets and cross-linked polymers follow this type of decomposition mode. Elimination of side chains ends up with cross-linking and forms a porous charred residue. This residue also includes non-volatile additives.

3.5 Polymers

3.5.1 Historical Development

Polymer word comes from the Greek roots “poly” which means “many” and “meros” which means “part”. Polymers are macromolecules (large molecule) containing repeating structural units generally bonded chemically by covalent bonds. In 1811, Henri Bracconot studied on derivative cellulose compounds, which is most probably the first research in polymer science. Then, in 19th century, vulcanization was developed which enhanced the strength of the rubber, which is a natural polymer. In the early 1900s, first completely synthetic polymer was synthesized, named as Bakelite, by Leo Bakeland. Although there were many improvements in the synthesis and characterization of polymeric materials, until 1920s the molecular structure of polymers had not been understood well. In 1922, Hermann Staudinger claimed that polymers are built up of long chains connected by covalent

bonds. For many years, this idea was not accepted until Staudinger was finally awarded the Nobel Prize. In 1920s, Wallace Carother worked on synthesizing polymers from their monomer units. In 1963, German chemist Karl Ziegler and Italian chemist Giulio Natta together developed the Ziegler-Natta catalyst and awarded the Nobel Prize in Chemistry. In 1974, Paul Flory also awarded the Nobel Prize due to his contribution to polymer science by his works of “kinetics of step-growth polymerization”, “addition polymerization chain transfer”, “excluded volume”, the “Flory-Huggins solution theory” and the “Flory convention” (http://en.wikipedia.org/wiki/Polymer).

3.5.2 Properties of Polymers

There are many parameters that directly affect the physical properties of polymers. These parameters can be classified as; chain length, monomer arrangement, tacticity in microstructure level, crystallinity and chain conformation in terms of morphology, tensile strength, and elasticity in terms of mechanical properties.

3.5.2.1 Microstructure

Microstructure is defined as a configuration or physical arrangement of basic monomer units through the backbone chain of the polymer. These units require a breakage of covalent bond in order to be changed. Microstructure strongly influences the properties of a polymer. For instance, two types of polyethylene with different microstructures may exhibit totally different physical and mechanical properties (http://en.wikipedia.org/wiki/Polymer).

3.5.2.1.1 Chain length

The length of the polymer chain strongly affects the physical properties of the material. An increase in chain length directly increases the boiling and melting points of the polymer. Glass transition temperatures, viscosity, resistance to flow in the melt state are also increased with an increase in chain length. Mechanical properties such as impact resistance, strength, and toughness are also increased as the chain length is increased. This situation is caused by the

increase in the amount of entanglements in the polymer chain thus increasing the Van der Walls forces. These interactions results in more stabilized, immobilized and resistant individual chains which remains more strongly in their current positions (http://en.wikipedia.org/wiki/Polymer).

Another way of expressing the chain length is the degree of polymerization, which shows the number of monomers present in the chain. Therefore, the size of the polymer can be defined in terms of molecular weight. Some known types of molecular weight definitions of polymers are number average and weight average molecular weights. These types of molecular weights are defined because as polymers are synthesized, the product polymers consist of a range of molecular weights; therefore statistical definitions are developed. The ratio of number average molecular weight to weight average molecular weight gives the polydispersity index of the polymer. Polydispersity index is used to define the width of molecular weight distribution of a polymer (http://en.wikipedia.org/wiki/Polymer).

3.5.2.1.2 Monomer Arrangement

Monomer arrangement is a concept that can be defined for copolymers. There are five types of monomer arrangement in copolymers which are; alternating copolymers, periodic copolymers, statistical copolymers, block copolymers and graft copolymers (http://en.wikipedia.org/wiki/Polymer).

- Alternating copolymers are consisted of regularly arranged monomer units in the form of $[AB...]_n$

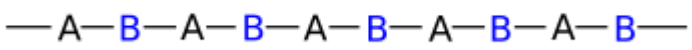

- Periodic copolymers are consisted of monomer units arranged in a repeating sequence, in the given form: $[A_nB_m]; m \neq n$
- Statistical copolymers are consisted of monomer units that are arranged in a definite statistical rule.

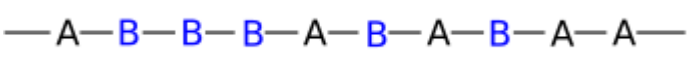

- Block copolymers are consisted of two or more homopolymer sub units connected by covalent bonds. If the number of the same distinct sub units are two or three, they are then called diblock and triblock copolymers.

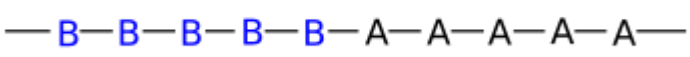

- Graft copolymers are consisted of side chains which have different monomer units than those of the main chain.

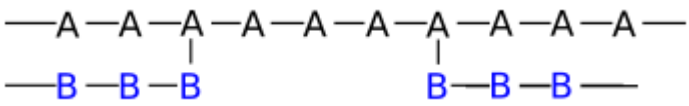

3.5.2.1.3 Tacticity

Tacticity is defined as the "relative stereochemistry of chiral centers in neighboring structural units within a macromolecule" (http://en.wikipedia.org/wiki/Polymer). There exist three types of tacticity. In isotactic polymers all substituents are on the same side, in syndiotactic polymers substituents are arranged alternately and in atactic polymers substituents are arranged randomly.

3.5.2.2 Morphology

Morphology is commonly expressed as the arrangement of chains in space (http://en.wikipedia.org/wiki/Polymer).

3.5.2.2.1 Crystallinity

Crystallinity in synthetic polymers is described theoretically according to the three-dimensional ordering regions on atomic scale they contain. Also, it is

possible for synthetic polymers to contain both crystalline and amorphous regions. In this case, the degree of crystallinity of the structure may be expressed in terms of weight or volume fractions. The degree of chrystallinity changes from zero which appears as transparent to intermediate levels which appears as opaque (http://en.wikipedia.org/wiki/Polymer).

3.5.2.2.2 Chain Conformation

When the chain conformation is being expressed two terms appear: radius of gyration and pervaded volume. Radius of gyration is described as “the average distance from the center of mass of the chain to the chain itself” and pervaded volume is described as “the volume of solution spanned by the polymer chain and scales with the cube of the radius of gyration (http://en.wikipedia.org/wiki/Polymer).

3.5.2.3 Mechanical Properties

Mechanical properties of a polymer determine the behavior of the material at macro-scale.

3.5.2.3.1 Tensile Strength

Tensile strength is the quantity that expresses the amount of stress the polymer withstands before undergoing permanent deformation. Tensile strength is extremely important for polymers to be used for specific applications where physical strength is sufficient. Chain length and amount of cross linking in the polymer are the parameters that increase tensile strength (http://en.wikipedia.org/wiki/Polymer).

3.5.2.3.2 Elasticity

Elasticity in polymeric materials can be defined by Young's Modulus. Elasticity is defined as the ratio of the rate of change of stress to strain. Similar to tensile strength, elasticity is highly important for polymers to be used in specific applications that require physical strength. Young's Modulus is highly dependent on temperature.

3.5.3 Widely Used Polymers

In this section, polymers which are most widely produced and consumed will be listed. These polymers are: polyethylene (PE), polypropylene (PP), polystyrene (PS), polyvinyl chloride (PVC), and polyethylene terepthalate (PET).

3.5.3.1 Polyethylene (PE)

Polyethylene (PE) is the most commonly used plastic material throughout the world with a production of approximately 80 million tons per year. It is widely used in packaging materials. PE is a thermoplastic type polymer and consists of long chains of ethylene monomer units. In Figure 3.1, the repeating unit of PE showing its stereochemistry is given. PE is synthesized by polymerization of ethylene (http://en.wikipedia.org/wiki/Polyethylene).

PE was synthesized firstly by Hans von Pechmann, a German chemist, who found it out by coincidence when he was heating diazomethane. After some characterizations, it was noticed that the material was formed of long -CH_2- chains and named as "Polymethylene". In early 1930s, first industrial synthesis of PE was achieved, again coincidentally, but in late 1930s, by high-pressure synthesis of PE, a reproducible process could be maintained by Michael Perrin. With the discovery of certain catalysts in 1950s (chromium trioxide based), it was seen that the reaction could be carried out under milder conditions in terms of pressure and temperature. In 1953, Karl Ziegler, a German chemist, studied a new catalyst containing titanium halides and organoaluminum compounds. With this new catalyst, the process was carried

out at better conditions. In 1976, a new type of catalyst based on metallocenes was developed by Walter Kaminsky and Hansjörg Sinn. Production of PE by the use of catalysts discovered by Ziegler and Kaminsky constitutes the basis for production of many kinds of PE resins today (http://en.wikipedia.org/wiki/Polyethylene).

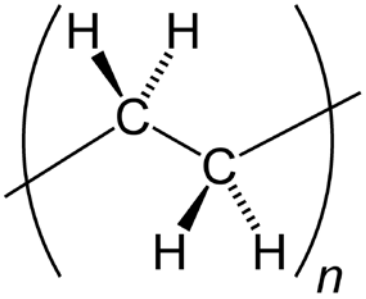

Figure 3.1. The repeating unit of polyethylene revealing its stereochemistry (http://en.wikipedia.org/wiki/Polyethylene)

PE is classified into groups according to the density and branching type. The physical and mechanical properties of PE are highly affected by the molecular weight, crystal structure, and the type of branching of the chains. The most abundant types in terms of consumption are HDPE, LDPE, and LLDPE. Below, all classes of PE are listed.

- Low density polyethylene (LDPE)
- Linear low density polyethylene (LLDPE)
- Very low density polyethylene (VLDPE)
- Medium density polyethylene (MDPE)
- Cross-linked polyethylene (XLPE)
- High density polyethylene (HDPE)
- High density cross-linked polyethylene (HDXLPE)
- Ultra low molecular weight polyethylene (ULMWPE)
- High molecular weight polyethylene (HMWPE)
- Ultra high molecular weight polyethylene (UHMWPE)

In Table 3.1, a summary of different types of PE in terms of density, branching, mechanical properties, and usage areas are given.

Table 3.1. Classification of some types of PE in terms of density, mechanical properties and application fields
(Adapted from http://en.wikipedia.org/wiki/Polyethylene)

Polymer	Density (g/cm^3)	Branching / Mechanical Properties	Application Fields
LDPE	0.910-0.940	High degree of short and long chain branching. Lower tensile strength, increased ductility.	- Rigid containers - Plastic film applications (Plastic bags, film wraps)
MDPE	0.926-0.940	Shock and drop resistance properties are good. Better stress cracking resistance and notch sensitivity properties than HDPE.	- Gas pipes and fittings - Sacks - Shrink film - Packaging film - Carrier bags - Screw closures
HDPE	≥ 0.941	Low degree of branching causing stronger intermolecular forces and higher tensile strength.	- Milk jugs, detergent bottles, margarine tubs - Garbage containers - Water pipes - Toys
LLDPE	0.915-0.925	A linear polymer with a small amount of short branches. Higher tensile strength than LDPE and better stress cracking resistance.	- Agricultural films - Saran wrap - Bubble wrap - Multilayer and composite films. - Cable coverings - Toys - Lids - Buckets, containers
VLDPE	0.880-0.915	A linear polymer with high degree of short-chain branching.	- Hose and tubing - Ice and frozen food bags - Food packaging - Stretch wrap - Impact modifiers (when blended with other polymers)
XLPE	MDPE-HDPE	Contains cross-linked bonds, causing the material to be an elastomer.	-Potable water plumbing systems
UHMWPE	0.930-0.935	Very tough material having good wear and cut resistance with an excellent chemical resistance.	- Can and bottle handling machine parts - Moving parts on weaving machines. - Bearings, joints, artificial joints. - Edge protection on ice rinks. - Butchers chopping boards - Used for constructions of body implants.

3.5.3.2 Polypropylene (PP)

Polypropylene (PP) is a widely used thermoplastic polymer that is synthesized industrially. Polypropylene is used in many applications like packaging, textiles like thermal underwear, containers which are reusable, laboratory equipment, automotive components, etc. Polypropylene is very resistant to many chemical solvents, acids and bases, which makes it an attractive product to be used in storage of such chemicals. In Figure 3.2, the repeating unit of polypropylene is given.

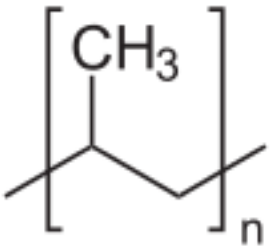

Figure 3.2. The repeating unit of polypropylene (http://en.wikipedia.org/wiki/Polypropylene)

Polypropylene was firstly synthesized by Giulio Natta and his coworkers in 1954. From that year on, the mass production of isotactic polypropylene has started. Mostly, commercially available polypropylene is isotactic, and cristallinity level of isotactic PP is between those of LDPE and HDPE. Polypropylene is cheap and can be produced translucent if not colored, but can not be made transparent like styrene and acrylic presently. Enhanced qualities like, toughness, flexibility, and fatigue resistance makes PP a desired polymer for many engineering applications. Many other qualifications of PP like corrosion and chemical leaching, physical damage, and impact resistances give it a chance to have many fields in the industry. Also, heating is a sufficient method for binding PP parts, rather than gluing, which makes it an attractive option for usage as well.

Nowadays, PP has a lots of application fields. For instance, thin sheets of PP can be used as dielectric inside capacitors. Piping systems which are used in plumbing, hydronic heating/cooling systems, and many water applications are being built up using PP. PP is used in many laboratory equipment like

autoclaves. Heating resistance enables PP to be used in food containers. PP can also be used in clear bags which are produced for the packaging of artistic material, but this is a biaxially oriented form of PP (BOPP) which is crystal clear. Since PP is highly colorfast, it is also being used in the production of carpets, rugs, and mats. PP may also be used for an insulation material in electric cables as an alternative to polyvinyl chloride (PVC).
(http://en.wikipedia.org/wiki/Polypropylene)

3.5.3.3 Polystyrene (PS)

Different from PE and PP, polystyrene (PS) is an aromatic polymer containing styrene monomer in the backbone of the molecule (see Figure 3.3). Styrene is a liquid hydrocarbon produced from petroleum. Polystyrene is a thermoplastic polymer which is produced by polymerization of styrene.

Polystyrene was firstly discovered in 1839 by Eduard Simon who was an apothecary. He formed an oily product by distillation of the resin of the Liquidambar Orientlis (Turkish Sweetgum Tree). He named this product 'styrol'. A few days later, he realized that the oily product he used to obtain became thicker, probably by the effect of oxidation. He named this new product 'styroloxyd'. Later in 1940s, it was found that the same product can also be obtained without the presence of oxygen. In 1900s, it was realized that heating styrene triggers a chain reaction in which macromolecule begin to form.

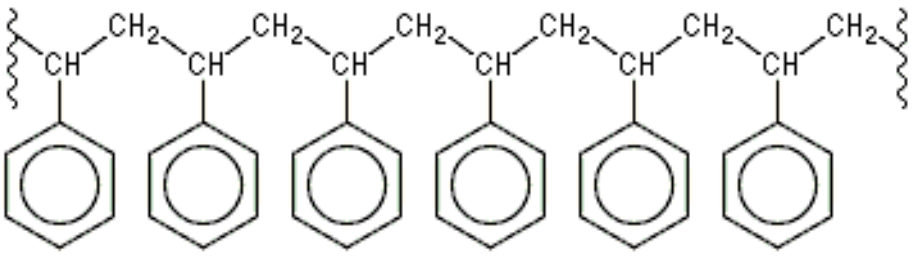

Figure 3.3. Structure of polystyrene
(http://en.wikipedia.org/wiki/Polystyrene)

In a polystyrene chain, the active attraction is mainly caused from van der Waals forces. It is well known that polymeric chains consist of thousands of

monomer units and because of this the total attraction force is quite high. Polystyrene is usually flexible and can be molded or found in a viscous liquid form (http://en.wikipedia.org/wiki/Polystyrene).

3.5.3.4 Polyvinyl Chloride (PVC)

Polyvinyl chloride (PVC) is a thermoplastic polymer as well. As seen in Figure 3.4, it is consisted of vinyl groups that are repeatedly present in the backbone. The production of PVC is very high that it is in the third place after PE and PP. The advantage in producing PVC is that the most of the polymer is consisted of chlorine (nearly 57%), therefore petroleum sufficiency is in smaller amounts. PVC is produced by polymerization of the vinyl chloride monomer.

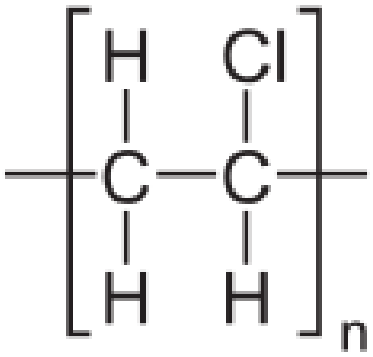

Figure 3.4. The repeating unit of polyvinyl chloride (http://en.wikipedia.org/wiki/Polyvinyl_chloride)

The application field of PVC is very wide as well. The area that PVC is used depends on the specific feature of the polymer. For instance, the resistance to many chemicals and biologic compounds, makes PVC a good choice for sewage pipe systems. With the addition of some stabilizers and modifiers, the very popular PVC window and door frames are being produced. PVC is also used in electric wires because of its insulation feature. Due to the ability of PVC to absorb dust particles and fitting characteristics, it is used as a composite in the accessories of electronic devices (http://en.wikipedia.org/wiki/Polyvinyl_chloride).

3.5.3.5 Polyethylene Terepthalate (PET)

Polyethylene terepthalate (PET) is a thermoplastic polymer resin of the polyester family. The repeating unit of PET, $C_{10}H_8O_4$ is given in Figure 3.5. PET changes from the range semi-rigid to rigid which is a qualification depending on the thickness. It is also a very light plastic. The final form of this polymer is dependent on the processing of the material. According to this, PET can be either amorphous which gives the transparency or semi-crystalline which gives transparency, opacity or whiteness to the material according to the crystal structure and particle size.

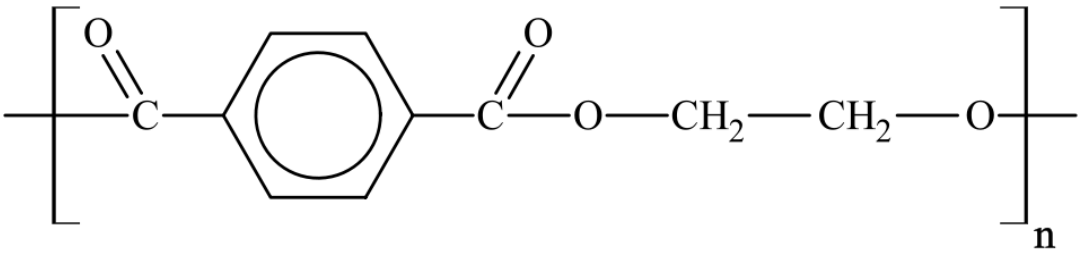

Figure 3.5. The repeating unit of polyethylene terepthalate (http://en.wikipedia.org/wiki/Polyethylene_terephthalate)

The monomer of PET, bis-β-hydroxyterepthalate is synthesized by esterification of terepthalic acid and ethylene glycol. The same monomer can also be produced by esterification reaction of dimethyl terepthalate and ethylene glycol.

PET is used as a container bottle for many soft drinks. Due to being a good barrier to gas, moisture, alcohol and some solvents, it is also used as a container for such ingredients. PET can also be produced in the form of a thin film, then coated by a thin film of aluminum in order to reduce the permeability and to obtain an opaque and reflective surface. Such PET films are used for flexible food packaging and thermal insulation. High mechanical strength of PET makes it available for applications including magnetic tapes and pressure sensitive adhesive tapes (http://en.wikipedia.org/wiki/Polyethylene_terephthalate).

CHAPTER 4

LITERATURE SURVEY

Decomposition of four different kinds of polyethylene (PE) was carried out at 430 ^{o}C in a batch reaction system (Uddin et al., 1997). Degradation reactions were carried out thermally (non-catalytic) and using a solid acid catalyst, silica-alumina. Types of PE used in the degradation reactions were low density polyethylene (LDPE), high density polyethylene (HDPE), linear low density polyethylene (LLDPE) and cross-linked polyethylene (XLPE). Two commercial silica-alumina catalysts were used in the experiment. These catalysts are named as Silica-Alumina-1 (SA-1) and Silica-Alumina-2 (SA-2). SiO_2/Al_2O_3 mole ratio for this two catalysts was 83.3/16.7 and 21.1/78.9, respectively. The resulting products were formed of four types which were classified as: liquid products, gaseous products, wax-like compounds and carbonaceous residues (coke). In terms of thermal degradation, HDPE and XLPE produced high amounts of wax like compounds and the liquid product amount was lower when compared to LDPE and LLDPE thermal degradation products. The amount of wax like compounds in the degradation of LDPE and LLDPE was very low; suggesting that the polymers that have branching in the backbone like LDPE and LLDPE degrade more quickly and easily to liquid products. On the other hand, polymers those have long straight chains end up with more wax like products. When SA-2 catalyst having high alumina ratio was used as catalyst, no wax like compound was obtained in the product and the amount of liquid and gaseous compounds was much higher when compared to non-catalytic thermal degradation. Even XDPE and HDPE were successfully degraded into liquid products. When the two catalysts' liquid product yields were compared, it was observed that SA-2 having higher amount of alumina had achieved higher liquid hydrocarbon yield in the catalytic degradation of the polymers.

In a study, the dependency of the product composition of catalytic degradation of polyethylene to acid strength and amount of silica-alumina (SiO_2/Al_2O_3) catalysts was investigated (Ohkita et al., 1993). In the same study, performances of HZSM-5 and some inorganic catalysts like SiO_2, Al_2O_3, ZnO, TiO_2, and MgO were also investigated. Reaction was carried out at 673 K, having nitrogen as the carrier gas. Thermally degraded low density polyethylene (LDPE), which was located at the bottom of the reactor produced gaseous products which were carried to the middle of the reactor by carrier gas where the catalyst bed is present. Then these products were introduced to cooling chamber where gaseous and liquid products can be separated. The acid strengths of the synthesized catalysts were determined using a titration method with n-butylamine and different color indicators. Results showed that, the inorganic acid catalysts did not show a good performance in the degradation of polyethylene, since nearly no differences observed in catalytic degradation when compared with non-catalytic thermal degradation. On the other hand, by the use of HZSM-5 zeolite as the catalyst, the gaseous product formation is enhanced, giving mostly C_3-C_4 gases. Also the time required for the consumption of 15 g of PE for HZSM-5 catalyst was one-half of the time required in thermal non-catalytic degradation. The acidity of silica-alumina catalysts were adjusted by changing the SiO_2 to Al_2O_3 ratio. This ratio was adjusted between 4 and 1.5 and the most acidic sample had Hammett acidity (H_0) value of -3.0. The increase in acidity of silica-alumina catalysts resulted in the reduction of oil products and increase in the fraction of gaseous products. Also with the increase in acidity, aromatics begin to appear in the oil fraction of the products.

Thermal analysis of catalytic degradation of high density polyethylene (HDPE) using mesoporous and microporous catalysts was carried out (Garforth et al., 1997). In this study, silica-alumina, siliceous and aluminum incorporated MCM-41, HY, HUSY, and HZSM-5 zeolites were used as catalysts for the degradation of HDPE. Before using in the reaction, both siliceous and aluminum incorporated MCM-41 catalysts were calcined in nitrogen atmosphere. Also, polymer-catalyst powders were sieved and then blended by grinding an equal amount of catalyst and polymer together. Two kinds of degradation experiments were carried out. In the first one, polymer/catalyst

mixtures were heated at a rate of 15^{o}C/min to three different temperatures, 275^{o}C, 300^{o}C, and 325^{o}C and held constant at the final temperature for 120 min. In the second experimental procedure, polymer/catalyst mixtures were heated to 600^{o}C, this time at different heating rates of 5^{o}, 5.5^{o}, 10^{o}, and 20^{o} C/min. Catalytic degradation of HDPE was carried out in a flowing nitrogen environment, and the system was done in a thermal analysis instrument. The activity of catalysts were investigated by thermogravimetric method and found out that presence of any catalyst lowers the activation energy of the reaction. When all these catalysts were compared, silica alumina showed minimum effect in lowering the activation energy. Zeolites Y and ZSM-5 had more effect in reducing the activation energy, at the same time resulting more rapid degradation. Aluminum incorporated MCM-41 exhibited maximum reduction in the activation energy of the reaction and showed the promising potential of this family in the cracking of plastic polymers.

In another study (Sakata et al., 1997), the activity of KFS-16 mesoporous catalyst in the degradation of HDPE was investigated. The performance of KFS-16 was compared with performances of other solid acid catalysts like silica-alumina and ZSM-5 zeolite. Two kinds of silica-alumina catalysts were used; silica-alumina-1 (SA-1) having a SiO_2/Al_2O_3 ratio of 83.3/16.7 and silica-alumina-2 (SA-2) having a SiO_2/Al_2O_3 ratio of 21.1/78.9. The SiO_2/Al_2O_3 ratio of ZSM-5 was 97.3/1.3. Non-catalytic and catalytic degradation of HDPE was carried out in a glass reactor under semi-batch conditions. For catalytic degradation, catalyst/polymer loading was 1/10 and the reaction temperature was 430^{o}C. The acidity of the used catalysts was in the following order: SA-1>ZSM-5>SA-2>>KFS-16, which was determined by temperature programmed desorption method. According to these obtained results, SA-2 produced the greatest amount of liquid products, whereas ZSM-5 with high acidity produced less liquid products and more gaseous products. KFS-16 having very low acidity revealed similar results to that of thermal degradation. On the other hand, SA-1 catalyst deactivated quickly due to the coke formation. Deactivation of KFS-16 catalyst was more slowly when compared to that of SA-1 catalyst.

Waste polymers, polyethylene and polystyrene were degraded catalytically in hydrogen atmosphere inside an autoclave which was located in a rotary kiln (Walendzievski et al., 2001). The catalysts used were NiW and 10% HY zeolite containing hydrocracking catalyst and waste commercial fluid cracking catalyst. According to the experimental results, the optimum thermal degradation temperature range was found out to be 410-430^{o}C. When catalytic degradation was carried out, the reaction temperature was around 390^{o}C having a lower reaction time. In very low catalyst contents, the influence of catalyst presence seemed to be very weak. In the presence of hydrocracking catalysts, when the liquid products were analyzed, it was found that the boiling point ranges were lower and the amount of unsaturated hydrocarbons was higher when compared to the reaction with cracking catalyst or non-catalytic thermal reactions. When the catalytic depolymerization of polyethylene and polystyrene compared, with the similar process parameters, both were alike but for polystyrene liquid products were less unsaturated and more aromatic. It was concluded that the physicochemical properties of the products depended on the composition of the waste plastics. It was observed that cracking or hydrocracking of polyethylene gives mainly paraffin fraction products whereas polystyrene mainly gives highly aromatic products.

Catalytic degradation of different types of polyethylene was carried out in the presence of solid acid catalyst MCM-41 (Marcilla et al., 2002). Different polyethylene types were selected according to their characteristics like density, branching degree and melt flow index. Three linear low density polyethylene (LLDPE) samples with different melt flow indices, one low density polyethylene (LDPE) and one high density polyethylene (HDPE) samples were used in the experiments. For thermal degradation, by the thermogravimetrical analysis, no significant differences occurred in terms of the kinetics of the reaction. When 9% of MCM-41 catalyst is added, a significant decrease of 60-79 ^{o}C was observed in the decomposition temperature when compared to non-catalytic thermal process. In thermal degradation, while all types of PE followed a similar behavior, in catalytic process each of them exhibited a different behavior in the presence of catalyst. For instance, LLDPE decomposition temperature was reduced less

than those of LDPE and HDPE by the addition of catalyst. When LLDPE samples were compared, the one with the highest melt flow index value revealed a behavior similar to LDPE and HDPE, while the others with lower melt flow indices behaved differently. This situation was actually attributed to the different structural properties of the polymers.

Polyethylene (PE) was catalytically decomposed under atmospheric pressure and batch conditions at 420 ^{o}C (Jalil et al., 2002). The catalysts used were pure mesoporous MCM-41, pure tungstophosphoric acid ($H_3PW_{12}O_{40}$), water and methanol impregnated $H_3PW_{12}O_{40}$ (HPW) over MCM-41 (HPW/MCM-41). It was observed that pore size of MCM-41 has influence on the product distribution of PE degradation. Smaller pore size promotes pyrolysis into lower molecular weight products, whereas larger pore size ends up with product distribution much alike to that of thermal degradation. On the other hand, as a support material for HPW, larger pore sized MCM-41 was used. When pure MCM-41 and pure HPW were used as a catalyst for the degradation reaction, it was observed that these did not have any effect and presented no catalytic effect at all. Water impregnated HPW/MCM-41 catalyst on the other hand, showed successful catalytic activity by promoting the degradation reaction into lower molecular weight products and by forming higher amount of isobutane in the gaseous products. In non-catalytic and catalytic degradations, in the presence of pure MCM-41 and pure HPW, isobutane was not obtained. By the analysis of gaseous products, in terms of catalytic activity, methanol-impregnated HPW/MCM-41 exhibited similar behaviour as water-impregnated HPW/MCM-41 catalyst. On the other hand, the liquid product distribution in case of methanol impregnated HPW/MCM-41 had similarities with the liquid product distribution of thermal degradation of PE.

Thermal non-catalytic and catalytic degradations of waste plastics were carried out by Walendziewski in 2002. Polymer cracking reactions were divided into two sets. In the first set of the experiments, polymer degradation reaction was carried out in a glass reactor under atmospheric pressure and a temperature range of 350-420^{o}C. In the second set of experiments, polymer degradation reaction carried out in an autoclave under a hydrogen pressure of ~3-5 MPa and in a temperature range of 380-440 ^{o}C. In these experiments

waste polyethylene (PE), polystyrene (PS), and polypropylene (PP) and their mixtures of different combinations were used as raw materials. Also 0-10% cracking catalysts were used for the cracking reaction of waste polymers. As a result of the first set of experiments which were carried out in a batch glass reactor and under atmospheric pressure, the efficiency of the reaction is up to 70-98 wt% with 2-3% coke residue. The presence of cracking catalysts exhibited a decrease in the reaction temperatures about 10-30^{o}C. As the percentage of cracking catalyst increased, the density of the liquid products decreased gradually. Also the composition of the polymers in the feed played a great role in the characteristics of the products. For instance, when PP or PE containing mixtures were degraded, the products' boiling points were below than that of C_7 hydrocarbons. On the other hand, when PS or PS containing mixtures were used as feed, the resulting product was formed of hydrocarbons (mainly styrene and styrene derivatives) having boiling points in the range of 130-180^{o}. In the second set of experiments, which was carried out inside an autoclave, the effect of catalyst was observed at lower temperatures. At the maximum temperature, there are very slight differences in process efficiency between the catalytic and non-catalytic thermal cracking reactions. The presence of catalyst in both set of experiments caused an increase in the gas product yields, but does not have significant effect on the gas composition. Gas product composition is mainly determined by the feed composition and process parameters. When the two sets of experiments were compared, pressure cracking in autoclave caused higher conversion levels including higher gas and gasoline fraction yields.

Thermal degradation of real municipal waste plastics (MWP) and model mixed plastics was carried out in a batch reaction system, at 430 ^{o}C under atmospheric pressure (Bhaskar et al., 2003). Model mixed plastics were PE /PP /PS /PVC (polyethylene /polypropylene /polystyrene /polyvinyl chloride) and PE /PP /PS /PVC /PET (polyethylene /polypropylene /polystyrene /polyvinyl chloride /polyethylene terepthalate). In the degradation of both model mixed plastics and MWP, chlorinated hydrocarbons were observed in the products. It was also found that the presence of PET in model mixed plastic and MPW triggered the formation of new chlorinated hydrocarbons in

liquid products, on the other hand hindering the formation of inorganic chlorine content.

Commercial high density polyethylene (HDPE) was non-catalytically and catalytically degraded in the temperature range of 400-450 ^{o}C in a laboratory scale batch reactor (Miskolczi et al., 2004). Catalysts used in the reaction were fluid cracking catalyst (FCC), HZSM-5, and a clinoptilolite containing rhyolite tuff. The decomposition temperature of HDPE was significantly reduced in the presence of catalysts. Also, yield and composition of the products were highly affected by the presence of catalysts. The yield of the gaseous products was lowest in non-catalytic thermal degradation and highest in the presence of HZSM-5 catalyst. Clinoptilolite and FCC catalysts were both effective than non-catalytic thermal cracking but less effective than HZSM-5 catalyst in terms of yield of the gaseous products. When the liquid product yields were considered, this time FCC was the most effective catalyst and clinoptilolite and HZSM-5 were less effective. Again the yield of liquid products was lowest in non-catalytic thermal cracking. As the temperature of the cracking reactions increased, the effect of catalyzed processes on the product yield and structure became less significant. In non-catalytic thermal degradation, the liquid product distribution in terms of carbon atoms was C_5-C_{28}, whereas in presence of catalysts, it was C_5-C_{25}. It was also observed that degradation temperature has a great effect on the product distribution.

Catalytic degradation of waste polyethylene over commercial catalysts was studied in a semi-batch reactor (Akpanudoh et al., 2005). The main purpose of the study was to investigate the effect of the acidity content on the formation of liquid products. The acidity content was maintained by the polymer/catalyst ratio of the feed. The catalysts used in the degradation were 20% and 40% ultrastable Y zeolite (US-Y) containing commercial catalysts. 20% US-Y and 40% US-Y containing catalysts were named as cracking catalyst 1 and cracking catalyst 2, respectively. When cracking catalyst was used, high conversion values were obtained and the only residue was the coke at the end of the reaction. Maximum liquid yield of 90% and selectivity were obtained in 4:1 polymer to catalyst ratio in the case of cracking catalyst 1. When cracking catalyst 2 is used, similarly high conversion values were

obtained but this time, liquid yield and selectivity were not very high when compared to cracking catalyst 1. It was concluded that higher acidity promoted more coke formation and less liquid product yield. Fraction of catalyst in the polymer catalyst mixture also affected liquid yield of the obtained products. It was observed that as the catalyst amount in the mixture increased more than a significant level, liquid yield decreased gradually.

Catalytic cracking of polyolefins over hexagonal mesoporous silica and effect of aluminum content of the mesoporous material was investigated (Chaianansutcharit et al., 2007). In this study, non-catalytic and catalytic degradation of PE and PP was carried out in a fixed bed catalytic reactor at 380 ^{o}C and 430 ^{o}C reaction temperatures. Two methods, liquid-phase and vapor-phase contact, were used throughout the experiments. System consists of two reactors. In liquid-phase contact experiments, catalyst and PP were loaded in the first reactor to let contact at liquid phase and then the product passed to the second reactor containing quartz grains. In gas-phase contact, polymer was put into the first reactor where it could turn into gas phase, and catalyst was put into second reactor where the polymer in gas-phase could react. Nitrogen was used as the carrier gas with a flow rate of 20 ml/min, and the heating rate was adjusted to 15^{o}C/min. Catalysts used in the catalytic degradation step were pure hexagonal mesoporous silica (HMS) and HMS loaded with aluminum at different ratios. The results obtained from non-catalytic thermal cracking and using pure HMS were similar. When aluminum loaded HMS (Si/Al=99) was used as a catalyst, it was seen that the liquid product yield was decreased, whereas gaseous product yield was increased. There was also a decrease in the residue amount, when compared to thermal degradation. Also, when aluminum containing HMS was used as catalyst, high portion of small molecular weight hydrocarbons were obtained. In vapor-phase contact, since polymers were first broken by thermal degradation and then catalytic degradation, the amount of gaseous products increased whereas the amount of liquid products decreased. When aluminum loaded HMS used as catalyst in vapor-phase and liquid-phase contact, low liquid yield and high gaseous yield were obtained for liquid-phase contact. This showed that the selectivity of products could be controlled by the catalyst contact mode.

The catalytic degradation of polypropylene (PP) was carried out in the presence of Lewis acids and Ziegler-Natta catalysts like $TiCl_4$, $AlCl_3$ (Kaminsky et al., 2007). The reactions took place both in batch and fluidized bed reactors. When compared to non-catalytic thermal reaction, the degradation temperature could be reduced by 100 ^oC. The amount of hydrocarbons with low boiling point was increased in the presence of catalysts. When $AlCl_3$ or combined $TiCl_4$:$AlCl_3$ were used as catalysts, reaction temperature decreased dramatically. Non-catalytic thermal degradation temperature, 500 ^oC, could be reduced up to 400 ^oC by the addition of 0.1% $AlCl_3$. In higher catalyst amounts, the pyrolysis could even be carried out at 300^oC. The increase in the amount of catalyst also causes an increase in the light oil fraction and gaseous products. If the amount of catalyst is further increased, the selectivity of the reaction decreased due to the occurrence of secondary reactions.

Throughout the literature survey, it was observed that there are very few studies on catalytic degradation of polyethylene which uses aluminum impregnated MCM-41. Similarly there is not any study present in the literature on catalytic degradation of polyethylene using tungstophosphoric acid loaded SBA-15 materials as catalysts. For this reason, the objective of this study is:

- To synthesize and characterize aluminum impregnated MCM-41 and tungstophosphoric acid impregnated SBA-15.
- To determine kinetic parameters of polyethylene degradation reaction using thermogravimetric analysis data.
- To design and construct a pyrolysis system.
- To test their activities and to get information about product distribution in polyethylene degradation.

CHAPTER 5

EXPERIMENTAL METHOD

The experimental study is composed of three main parts: first part is the synthesis of catalysts and characterization of the synthesized materials, second part is testing of the performance of the synthesized materials in pyrolysis of polyethylene using thermogravimetric analysis and third part is testing the performance of the catalysts chosen from thermogravimetric analysis results in polyethylene degradation reaction system and analyzing the products using a gas chromatography.

5.1 Synthesis and Characterization of Catalysts

In this part, synthesis and characterization techniques of the catalysts will be described briefly. The synthesized materials to be used in the catalytic degradation of PE are aluminum impregnated MCM-41 and tungstophosphoric acid loaded SBA-15, respectively. The synthesized materials are characterized using X-ray diffraction, energy dispersive spectroscopy, nitrogen adsorption-desorption, nuclear magnetic resonance, scanning electron microscopy, transmission electron microscopy, and Fourier transform infrared spectroscopy methods.

5.1.1 Synthesis of MCM-41 Material

MCM-41 material was synthesized following a hydrothermal synthesis route which is described in detail in the following part. In the synthesis of MCM-41 material, cetyltrimethyl ammonium bromide (CTMABr (Merck)) and tetraethyl orthosilicate (TEOS(Merck)) were used as the surfactant and the silica source, respectively.

5.1.1.1 Synthesis Procedure for MCM-41 material

In this study, MCM-41 catalyst was synthesized following a hydrothermal synthesis route according to the procedure described by Obali, 2010. Firstly, 13.2 gr of CTMABr was dissolved in approximately 87 ml of deionized water and continuously stirred at a rate of 500 rpm at 30 ^{o}C. Then, silica source (TEOS) was added dropwise to the solution while stirring and pH of the solution was adjusted to 11 by adding 1 M sodium hydroxide (NaOH) and kept stirred for an hour. Finally, the solution was taken into a teflon-lined stainless steel autoclave to be kept at 120^{o}C for 96 hours. The obtained mixture was then filtered and washed with deionized water. The solid product was dried at room temperature and afterwards calcined in a tubular furnace at 540 ^{o}C for 8 h with a flow of dry air in order to get rid of the organic materials within the pores of the catalyst. Synthesis procedure for MCM-41 material was given schematically in Figure 5.1.

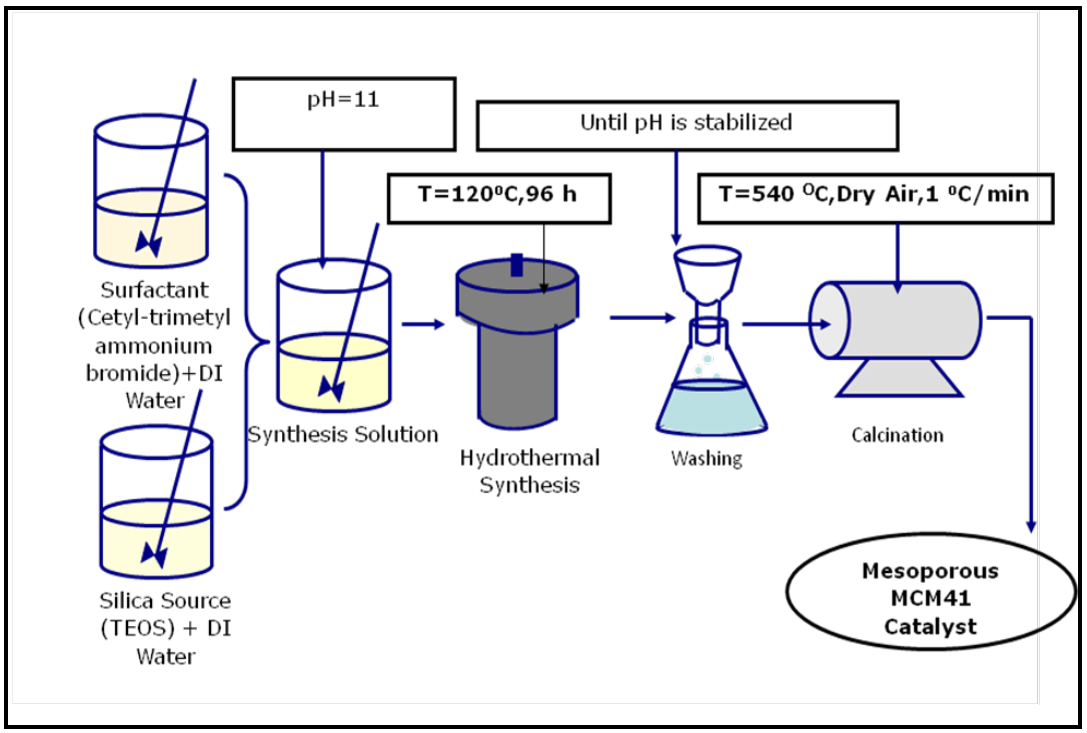

Figure 5.1. Scheme of hydrothermal synthesis route of MCM-41 material

5.1.1.2 Incorporation of Aluminum into Synthesized MCM-41 Materials by Impregnation Method

Aluminum was introduced to MCM-41 material by impregnation method. Aluminum isopropoxide (Merck) was used as the aluminum source. In this method, firstly, approximately 1 g of MCM-41 sample was dispersed in deionized water and kept stirred at room temperature for 2 h. According to the desired Al/Si molar ratio, determined amount of aluminum isopropoxide was dissolved in deionized water. An example of calculation of the desired amount of aluminum is given in Appendix A. Then, as the silica source was being stirred, aluminum source is added dropwise to the solution and the obtained mixture was kept stirred for 24 h. Finally, water of the mixture was evaporated and the resulting solid product was kept in oven at 110 ^{o}C for 16 hours. Impregnation of aluminum into synthesized MCM-41 material is given schematically in Figure 5.2.

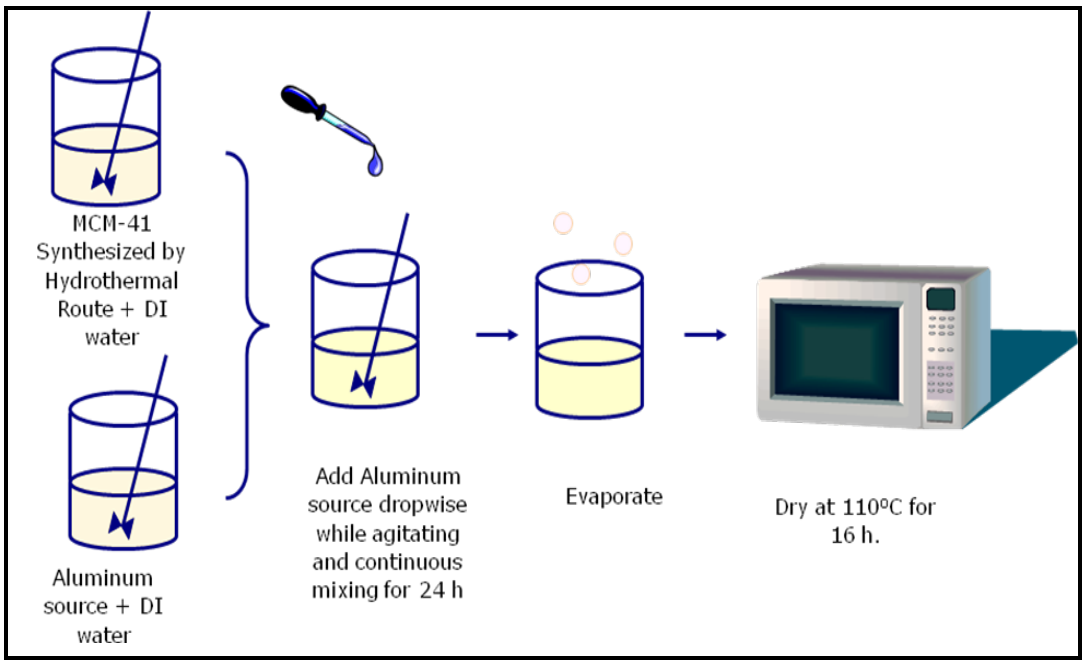

Figure 5.2. Scheme of aluminum incorporation into hydrothermally synthesized MCM-41 material by impregnation method

5.1.2 Synthesis of SBA-15 Material

SBA-15 material was synthesized following a hydrothermal synthesis route which is described in detail in the following part. In the synthesis of SBA-15, triblock copolymer poly(ethylene glycol)-poly(propylene glycol)-poly(ethylene glycol) (Sigma-Aldrich Co.) and tetraethyl orthosilicate (TEOS) (Merck) were used as the surfactant and the silica source, respectively.

5.1.2.1 Synthesis Procedure for SBA-15 Material

SBA-15 catalysts were synthesized following a hydrothermal synthesis route according to the procedure described by Fulvio et al, 2005. Firstly, 4 g of surfactant was dissolved in 120 ml of 2M HCl solution and continuously stirred at a rate of 350 rpm at 40 ^{o}C for 4h to allow the polymer to be dissolved. Then, 8 g of silica source was dropwisely added to the solution while stirring and kept stirred for another 2 h. The final solution was transferred into a teflon-lined stainless steel autoclave for the hydrothermal synthesis at 100^{o}C for 48 hours. The obtained mixture was filtered and washed with deionized water. The solid product was then dried in the oven and calcined in a tubular furnace at 540 ^{o}C for 8 h with a flow of dry air in order to get rid of the organic materials within the pores of the catalyst. Synthesis procedure for SBA-15 material is given schematically in Figure 5.3.

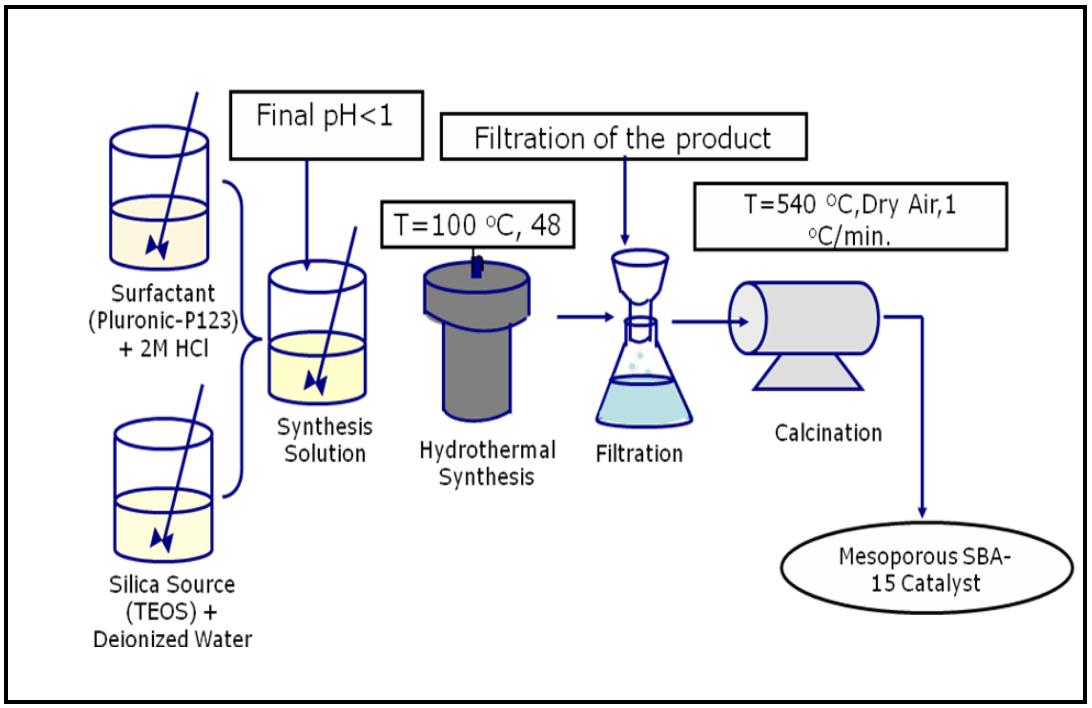

Figure 5.3. Scheme of hydrothermal synthesis route of SBA-15 material

5.1.2.2 Incorporation of Tungstophosphoric acid into Synthesized SBA-15 Materials by Impregnation Method

Phosphotungstic acid hydrate (Acros Organics) was used as the tungstophosphoric acid source. TPA was introduced to the structure of SBA-15 materials by impregnation method. In this method, firstly, approximately 1 g of SBA-15 sample was dispersed in deionized water and kept stirred at room temperature for 2 h. According to the desired W/Si molar ratio, determined amount of TPA was dissolved in deionized water (Appendix A). Then, as the SBA-15 solution was being stirred, TPA previously dissolved in water was added dropwisely to the solution and the mixture was kept stirred for 24 h. Finally, water of the mixture was evaporated and the solid product was kept in oven at 80 ^{o}C for 16 hours. Impregnation of tungstophosphoric acid into synthesized SBA-15 material is given schematically in Figure 5.4.

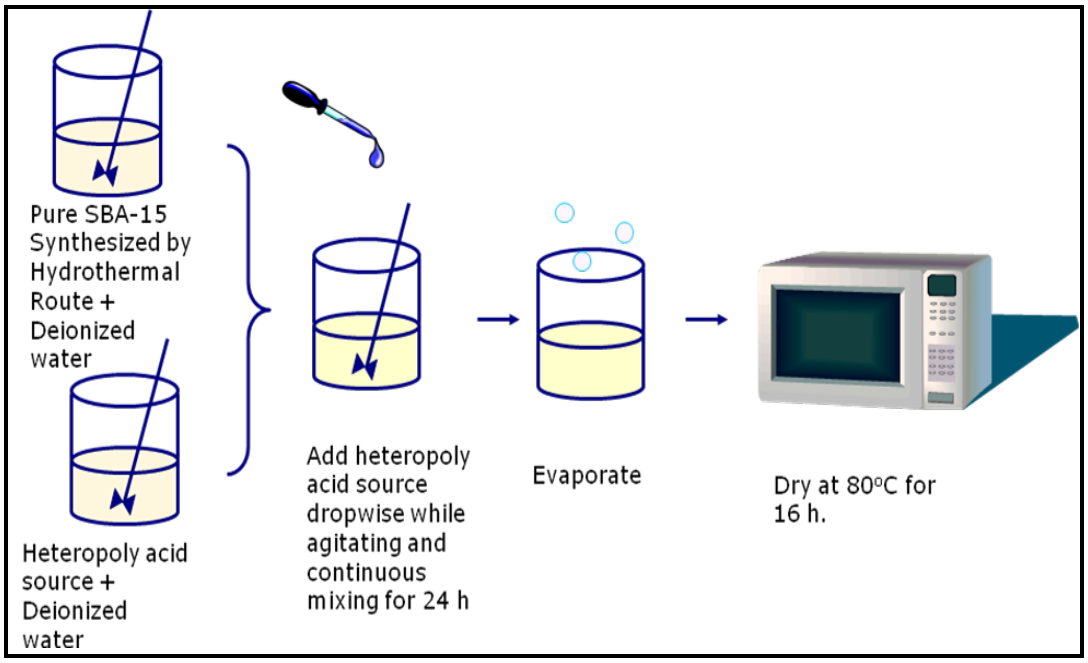

Figure 5.4. Scheme of incorporation of tungstophosphoric acid into hydrothermally synthesized SBA-15 material by impregnation method

5.1.3 Notation

The synthesized materials were named as PMCM41 and PSBA15 for pure MCM-41 and SBA-15 materials, respectively. Aluminum impregnated samples were given as: Al-X where X stands for the ratio of Al/Si and TPA impregnated SBA-15 samples were given as SBA15-X where X stands for the ratio of W/Si.

5.2 Characterization Techniques for the Synthesized Materials

Physical and structural properties of the synthesized materials were determined using the following techniques: X-Ray Diffraction, Energy Dispersive Spectrometry, Nitrogen Adsorption-Desorption, Nuclear Magnetic Resonance (^{27}Al-NMR), Scanning Electron Microscopy, Transmission Electron Microscopy and Fourier Transform Infrared Spectroscopy.

5.2.1 X-Ray Diffraction

To get information about the regularity of the structure, synthesized materials were analyzed by X-Ray Diffraction method. The equipment used for the analysis was Rigaku D/MAX2000 Diffractometer with nickel filtered CuK_{α} radiation having a characteristic wavelength of 1.5406 Å. The Bragg angle values were adjusted in the range of 1^{o}-10^{o} for pure and aluminum impregnated MCM-41 samples, and 0.8^{o}-10^{o} for pure SBA-15 sample and 0.8^{o}-80^{o} for TPA impregnated SBA-15 samples. The step size was adjusted as 0.01. During analysis the voltage and current were 40 kV and 40 mA, respectively.

5.2.2 Energy Dispersive Spectroscopy

The percentage of the elements within the synthesized materials was analyzed by energy dispersive spectroscopy technique. This method is an analytical method, in which elemental composition of a material is analyzed. The EDS analysis of the samples was carried out by Energy Dispersive Spectrometry analysis using JSM 6400 Electron Microscope equipped with NORAN system 6X-Ray Microanalysis System & Semafore Digitizer. All the samples were coated with gold for the analysis.

5.2.3 Nitrogen Physisorption

5.2.3.1 Multipoint BET Surface Area Measurement

Physical properties of the synthesized materials, such as surface area, pore diameter, pore volume and pore size distributions were determined by nitrogen adsorption technique. Multipoint BET surface area, adsorption-desorption isotherms and average pore size of the materials were measured using Quantachrome Autosorb-1C/MS equipment. The samples were degassed at 120^{o}C overnight before the analysis. The analyses were performed at a relative pressure range of 0.05 to 0.99 at liquid nitrogen temperature.

5.2.3.2 Single Point BET Surface Area Measurement

Single point surface area measurements of the synthesized materials were carried out using Quantachrome Monosorb Direct Surface Analyzer. This device is designed to give very quick and accurate single point BET surface area measurement under nitrogen-helium gas mixture flow at the relative pressure of 0.30. There are preeliminary steps for the material to be analyzed before the measurements. These steps were keeping the material at 140^{o}C in an oven overnight to enable drying and degassing at 140^{o}C for 30 minutes under nitrogen-helium gas mixture flow for further drying. The analysis was performed under the flow of nitrogen-helium gas mixture which consists of 30% nitrogen and 70% helium gases. The temperature of the liquid nitrogen was 77 K. Calibration of the device was required before beginning the analysis. For the calibration, 1 cm^3 of air at atmospheric pressure was used. The surface area value equivalent to the nitrogen amount of this much air should be 2.84 m^2. After the calibration and degassing steps were completed, the sample was taken to the analysis station where the measuring proceeded. Air entering the system during the placement of the sample was removed by adjusting the indicator to zero value. The adsorption begun when the sample cell rose up to be met with the liquid nitrogen. When the adsorption finished, the tank was lowered down and then desorption was started at a relative pressure value of 0.30. The value was read from the digital panel of the device and divided by the weight of the sample which is approximately 0.02 grams. This value gives the surface area of the material per gram.

5.2.4 Nuclear Magnetic Resonance (^{27}Al NMR)

Coordination environment of aluminum atoms was analyzed using ^{27}Al magic angle spinning nuclear magnetic resonance (MAS NMR) spectrometer. The equipment was Bruker AVANCE 300 MHz with a magnetic field of 7 Tesla. The spin rate of the sample was 5 kHz and the resonance frequency was 78.1 MHz. Spectra were recorded at room temperature.

5.2.5 Scanning Electron Microscopy

Morphology of the catalysts was analyzed using a QUANTA 400F Field Emission Scanning Electron Microscope. Before the analysis, the samples were prepared. This preparation was consisted of two steps: attaching material on a carbon tape and coating with gold. First of all, a small amount of sticking carbon tape was attached onto the metal apparatus inserted in the machine during the analysis. Then, a trace amount of sample was taken onto this carbon tape and it was spread to the surface of the tape homogeneously. In the second step, the materials were coated with gold to be ready for the analysis.

5.2.6 Transmission Electron Microscopy

TEM images of the synthesized materials are taken by JEOL model JEM 2010 transmission electron microscope equipped with SIS Megallion CCD camera at the Electron Microscopy Center of the Faculty of Biology and Geology of Babes-Bolyai University in Romania. Before taking the images, the samples were dispersed in water medium and put on a 300 mesh copper (Cu) grids with collodium film.

5.2.7 Fourier Transform Infrared Spectroscopy

DRIFT spectra of the synthesized materials were obtained using Perkin Elmer-Spectrum One FTIR spectrometer in the wavenumber range of 400-4000 cm^{-1}. In order to observe the nature of the acid sites of the synthesized materials, DRIFT analysis of the pyridine adsorbed samples was performed using the same equipment. Before the analysis of the pyridine adsorbed samples, 2 ml of pyridine was added to 0.0025 g of the material and kept for 2 hours under the hood to allow pyridine to be evaporated. Then, the pyridine adsorbed samples were mixed with potassium bromide (KBr) in a weight ratio of 1:20. For the samples that shall not be pyridine adsorbed, also mixed with KBr in a 1:20 weight ratio. Before performing the analysis of the samples, a background spectrum of pure KBr was taken and then, the samples which were prepared with and without pyridine were analyzed. In order to obtain the

spectra giving the acid sites within the synthesized material, the spectra of pyridine free sample was subtracted from the spectra of pyridine adsorbed sample.

5.3 Thermogravimetric Analysis

To test the performance of synthesized materials in the decomposition reaction of polyethylene, thermogravimetric analysis was carried out using Perkin Elmer Pyris 1 TGA and Spectrum 1 FT-IR Spectrometer. The polymer was polyethylene (Aldrich Co.) of M_n 1700, density 0.92 g/ml, polydispersity index 2.35 and melting point range of 90-110 ^oC.

Thermogravimetric analysis experiments were performed under nitrogen atmosphere having a flow rate of 60 cc/min, in the temperature range of 30-550 ^oC with a constant heating rate of 5 ^oC/min. Testing samples were prepared with a catalyst to polymer weight ratio of 1/2.

5.4 Polyethylene Degradation Reaction System

5.4.1 Experimental Setup

In Figure 5.5, the experimental setup for pyrolysis reactions is given. The carrier gas was selected as nitrogen; therefore a nitrogen gas tank was present in the system. There was a rotameter connected to the nitrogen tank in order to adjust the gas flow rate to the desired value. The gas entered the reaction chamber from the bottom of the reactor, which was placed inside a tubular reactor. The furnace was covered with an isolating material in order to prevent the heat loss inside.

The reactor, which was located in the tubular furnace, was mainly made of three parts. The bottom part of the reactor was the spiral part in order to increase the surface area and contact time of the flowing gas for efficient heating. In this spiral portion, there were tiny glass particles within the spirals to help increasing of the surface area. Above the spiral part, there was a special porous glass, where the polymer and catalysts were put. This was the

place where the reaction took place; therefore a thermocouple was inserted to this location in order to measure the exact reaction temperature. This porous glass also prevented the backflow of the polymer and catalyst to pass to the bottom part of the reactor. The third and the upper part of the reactor was cylindrical and connected to the condenser by a steel pipe. This pipe was covered with a heating tape and isolation material to be heated up to reaction temperature to prevent early condensation of the products before reaching the condenser. There was another thermocouple which was connected to a controller in this area to control the temperature of the heating tape.

The condenser and liquid collecting bottles were connected to the water bath which maintained adequate cooling for liquids to be condensed. For collecting the liquid products efficiently, an extra liquid collecting bottle was present in the system. Non-condensed gaseous products were collected in the gas balloon and by an injector, gas samples were taken to be analyzed in gas chromatograph. At the end of the system, there was a soap bubblemeter where the flow rate of the gas was measured, and the excess gas was passing to the vent.

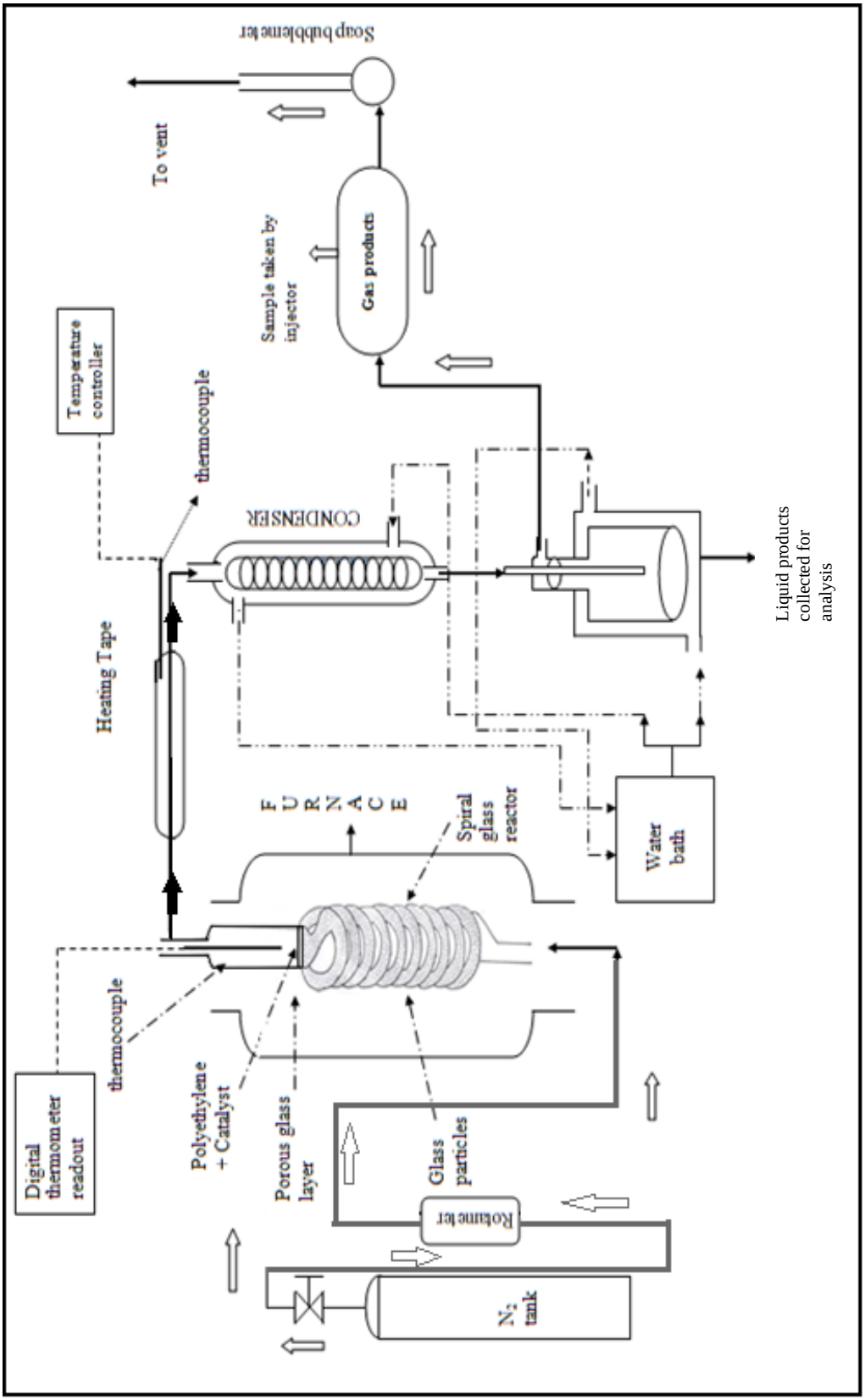

Figure 5.5. Experimental setup for catalytic degradation of polyethylene

5.4.2 Experimental Procedure

1.0 g of polymer and 0.5 g of catalyst were weighed and mixed to be put inside the reactor from the upper part. After placing the polymer-catalyst mixture into the reactor, the thermocouple was inserted and the system was closed tightly using the fittings and the system was checked for potential gas leakage after giving the nitrogen gas to the system. After checking for the gas leak, the flow rate of nitrogen gas was adjusted to 60 cc/min. Then, the furnace was adjusted to the desired temperature with a constant heating rate of 5^{o}C/min. The temperature of the heating tape surrounding the pipe connecting the exit of the furnace to the entrance of the condenser was adjusted exactly to the same temperature that the reaction took place. The cooling system of the reaction setup was composed of a condenser and two liquid collecting containers. The apparatus was cooled with the water coming from the cooling water bath, which is adjusted to approximately 0^{o}C. During the experiment, in every 15 minutes, the temperature of the furnace, reaction chamber, and cooling bath and flow rate were recorded in order to control the experimental system better. Gas samples were collected with the injector at the time interval which the reaction took place. Liquid samples and solid residue/catalysts were collected after the system was cooled down to room temperature. Solid residue remaining in the system was collected by turning the reactor upside down and reheating it in the furnace until the remaining material melted. The collected liquid products, catalyst and solid residue was weighed and recorded.

The amount of the polymer kept constant for all experiments, which was 1.0 g. In catalytic degradation experiments, the amount of the catalyst that was mixed with 1.0 g polymer was 0.5 g, which was 1:2 ratio in terms of weight.

In Table 5.1, experimental conditions for non-catalytic and catalytic eperiments are given. The reaction temperatures were selected accroding to the obtained thermogravimetrical data.

5.4.3 Product Analysis Procedure

Analysis of the gas and liquid produts were performed in a gas chromatograph (GC). Gas samples were taken from the gas collecting bubble using a gas-tight syringe during the reaction and injected to the gas chramotograph to be analyzed. Liquid products were collected in the liquid collecting bottle and injected to the gas chromatograph using a microliter liquid syringe.

Table 5.1. Experimental conditions for non-catalytic and catalytic thermal degradation experiments

Material	Temperature (^{o}C)	Time (min)
Polyethylene	420	45
Polyethylene	430	10
Polyethylene	430	15
Polyethylene	450	10
Polyethylene	450	15
Polyethylene	480	5
Polyethylene	480	10
Polyethylene + SBA-0.10	390	15
Polyethylene + SBA-0.10	430	15
Polyethylene + SBA-0.25	390	15
Polyethylene + SBA-0.25	430	15
Polyethylene + SBA-0.40	390	15
Polyethylene + SBA-0.40	410	15
Polyethylene + SBA-0.40	430	15
Polyethylene + SBA-0.40	460	15
Polyethylene +Al-0.03	390	15
Polyethylene +Al-0.03	430	15
Polyethylene +Al-0.25	390	15
Polyethylene +Al-0.25	430	15

5.4.3.1 Analysis of Gas Products

Gas samples were taken at several time intervals through the reaction and analyzed using a GC equipped with a packed column (Propac Q). Gas analysis

conditions are given in Table 5.2. Varian Star Chromatography Workstation version 6.2 program was used for the data analysis.

Table 5.2. Gas chromatography analysis conditions for gas products obtained from the degradation reactions

Oven Temperature	80^{o}C (isothermal)
Injection Temperature	110^{o}C
Detector Type and Temperature	TCD, 120^{o}C
Column Pressure	30 psi
Analysis Time	35 minutes
Carrier Gas	He
Carrier Gas Rate	30 ml/minute

5.4.3.2 Analysis of Liquid Products

Liquid samples taken from the liquid collecting bottles were analyzed in GC equipped with a capillary column of 0.320 mm I.D and 30 meters length (HP-5 capillary column). Liquid analysis conditions are given in Table 5.3.

Table 5.3. Gas chromatography analysis conditions for liquid products obtained from the degradation reactions

Oven Temperature	40^{o}C (for 10 min) to 150^{o}C (for 15 min) with a heating rate of 5^{o}C/min and then to 200^{o}C (for 70 min) with heating rate of 1^{o}C/min
Injection Temperature	210^{o}C
Injection amount	0.1 µL
Detector Type and Temperature	FID, 225^{o}C
Column Pressure	5 psi
Analysis Time	167 minutes
Carrier Gas	He at 1.5 ml/min
Split Ratio	100:1

CHAPTER 6

RESULTS AND DISCUSSION

In this study, mesoporous Al loaded MCM-41 and TPA impregnated SBA-15 catalysts were synthesized and characterized using XRD, BET, SEM, TEM and FTIR. These catalysts were tested in polyethylene degradation reaction.

6.1 Characterization Results of Synthesized Materials

6.1.1 Characterization Results of MCM-41 and Aluminum Impregnated MCM-41 Materials

6.1.1.1 X-Ray Diffraction Results of MCM-41 and Aluminum Impregnated MCM-41 Materials

The X-Ray Diffraction patterns of pure MCM-41 and aluminum impregnated MCM-41 samples are given in Figure 6.1. The main peak of the PMCM41 sample was obtained at the Bragg Angle value of 2.61°. Secondary, tertiary and quaternary peaks were observed at 2θ values of 3.01°, 4.75° and 4.91°. For aluminum impregnated samples, the main peak was observed at Bragg angle value of 2.66°. These samples exhibited the other three peaks at 2θ values of approximately 3.02°, 4.70° and 4.92°. All the peaks matched with the characteristic peaks of the ordered mesostructure of MCM-41 material given in the literature (Güçbilmez, 2005). According to these results, the slight deviations in the XRD patterns showed that aluminum incorporation to MCM-41 sample which was synthesized following a hydrothermal synthesis route, did not cause any deformation in the ordered structure of the mesoporous material. It was observed that the well ordered regular structure of the material was preserved even in high loading levels.

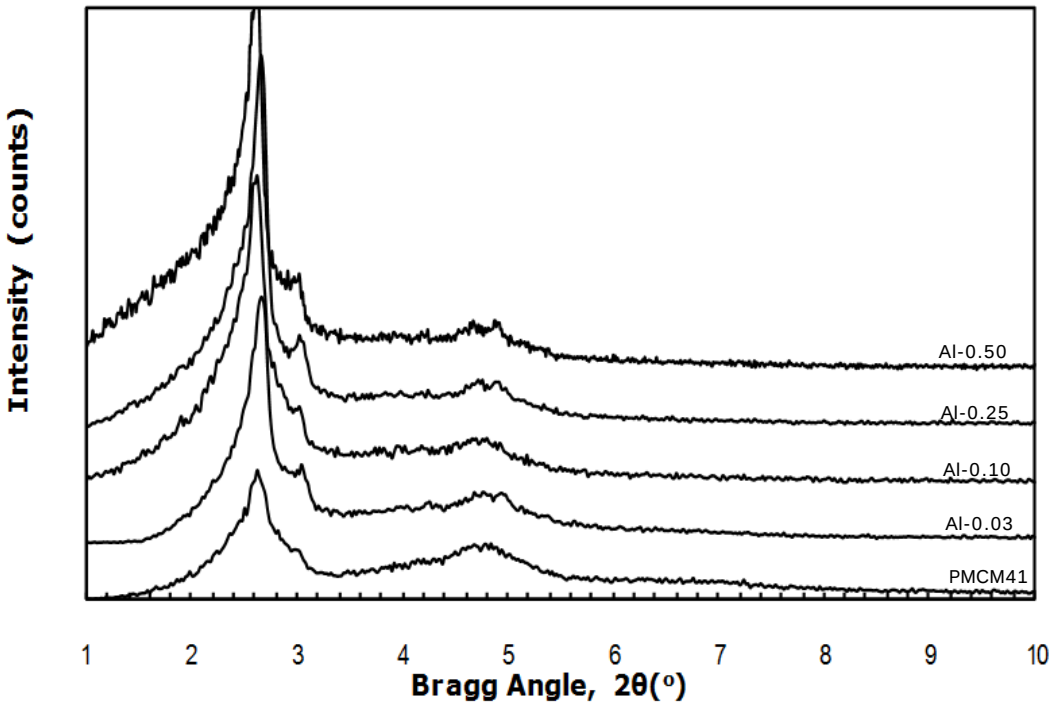

Figure 6.1. X-Ray Diffraction patterns of synthesized MCM-41materials

6.1.1.2 Energy Dispersive Spectroscopy Results of MCM-41 and Aluminum Impregnated MCM-41 Materials

Energy Dispersive Spectrometry analysis results of aluminosilicate catalysts prepared by impregnation method is given in Table 6.1. It was observed that as the aluminum amount in the synthesis solution was increased, the amount that was introduced to the structure was decreased gradually. As the amount of aluminum introduced to the pores of the material increased, the capacity of the pores was lowered preventing more aluminum getting inside. It was observed that in low loading levels the incorporation of aluminum into the structure was more successful. EDS spectra of all the aluminum loaded MCM-41 catalysts are given in Appendix B. In addition to aluminum and silicon peaks, gold, oxygen and carbon peaks were observed. Gold peak came from the coating of the sample with gold. Oxygen and carbon came from the formation of SiO_2 and the organic template not removed from the material during washing and calcination steps, respectively.

Table 6.1. EDS results of aluminum impregnated MCM-41 materials

Sample	Al/Si Ratio (EDS)	Al/Si Ratio (in the initial solution)
Al-0.03	0.03	0.03
Al-0.1	0.12	0.1
Al-0.25	0.18	0.25
Al-0.5	0.36	0.5

6.1.1.3 Surface Characterization Results of MCM-41 and Aluminum Impregnated MCM-41 Materials

Nitrogen adsorption-desorption isotherms of synthesized MCM-41 and aluminosilicates are shown in Figure 6.2. According to the IUPAC classification, the synthesized samples exhibited isotherms of Type IV, which is a typical of mesoporous materials. Type IV isotherm belongs to microporous solids containing mesopores in their structure. A sharp increase in the adsorbed N_2 volume was observed at a narrow relative pressure range of 0.25-0.35. This indicates a narrow pore size distribution. For the samples PMCM41, Al-0.03 and Al-0.10, no hysteresis formation was observed. Type H2 hysteresis was clearly observed for samples Al-0.25 and Al-0.50 for relative pressures above 0.6 due to the capillary condensation of nitrogen in the mesopores of the structure. It resulted from the differences between the adsorption and desorption mechanism. The desorption branch was much steeper than the adsorption branch. In Table 6.2, BET surface area, pore volume and pore diameter of MCM-41 and aluminosilicates are shown. As the aluminum was incorporated into the structure, it was observed that surface area of the sample decreased with an increase in aluminum loading. This may be due to accumulation of aluminum inside the pores of the structure causing such a drop in the surface area values.

Pore diameters of the samples, which were calculated by BJH model were in the range of mesoporosity, as expected. Average pore size distributions of the synthesized materials were similarly given in terms of BJH model and this

value was approximately 24.4 Å (Figure 6.3). For all samples, pore size distribution showed a narrow range of 20 to 100 Å, which was again an indication of the mesoporous structure.

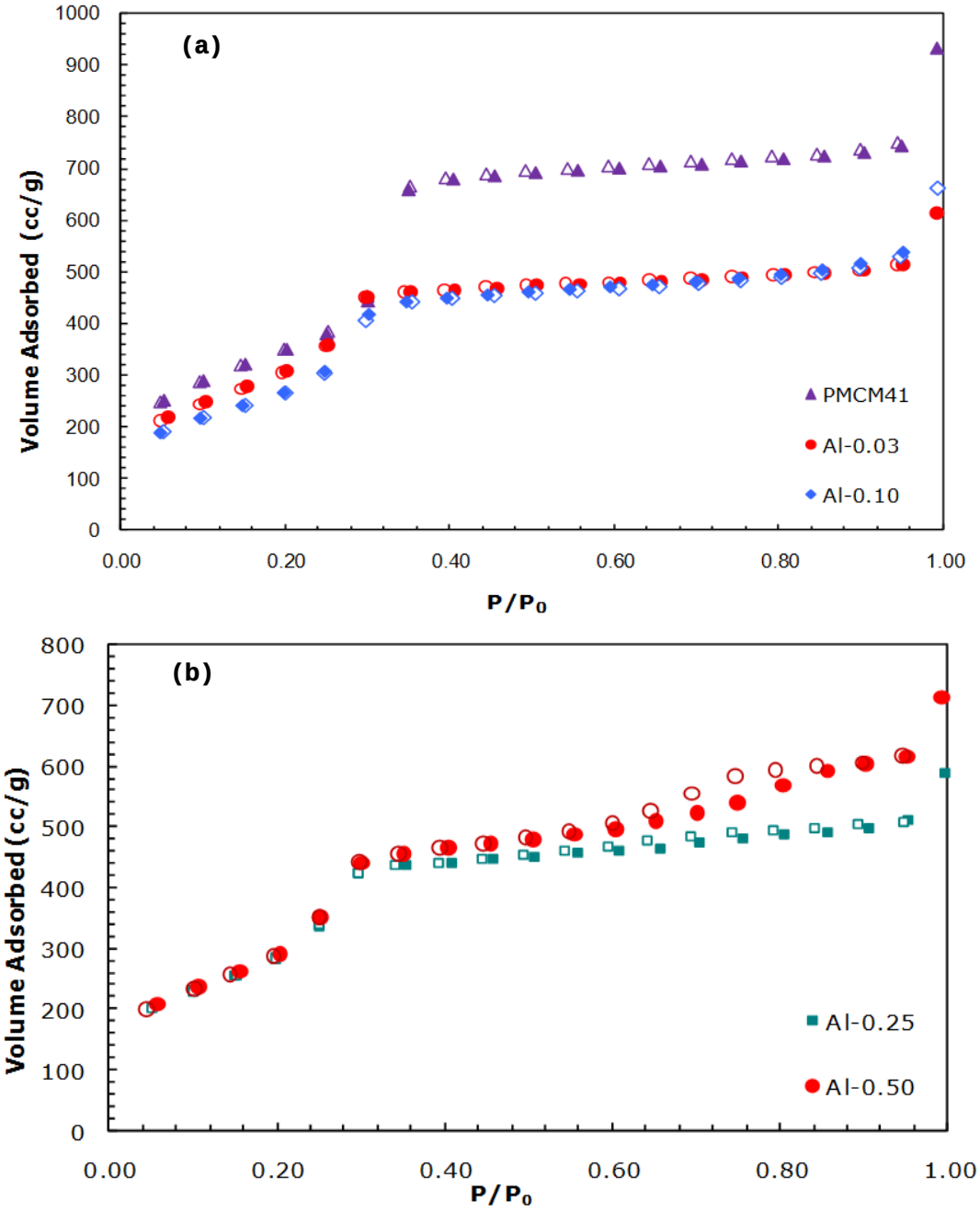

Figure 6.2. Nitrogen adsorption and desorption isotherms for (a) PMCM41, Al-0.03, Al-0.10 and (b) Al-0.25, Al-0.50 materials (Filled symbols: adsorption and empty symbols:desorption)

Table 6.2. Surface area and pore size values of the synthesized pure and aluminum impregnated MCM-41 materials

Sample	Surface Area Single Point BET, (m^2/g)	Surface Area Multi Point BET, (m^2/g)	Pore Volume BJH Des., (cc/g)	BJH Des. Av. Pore Diameter (Å)
PMCM41	1262	1290	1.58	27.5
Al-0.03	1254	1227	1.01	24.4
Al-0.1	1098	1031	1.1	24.5
Al-0.25	1024	1146	0.97	24.4
Al-0.5	967	1197	1.19	24.5

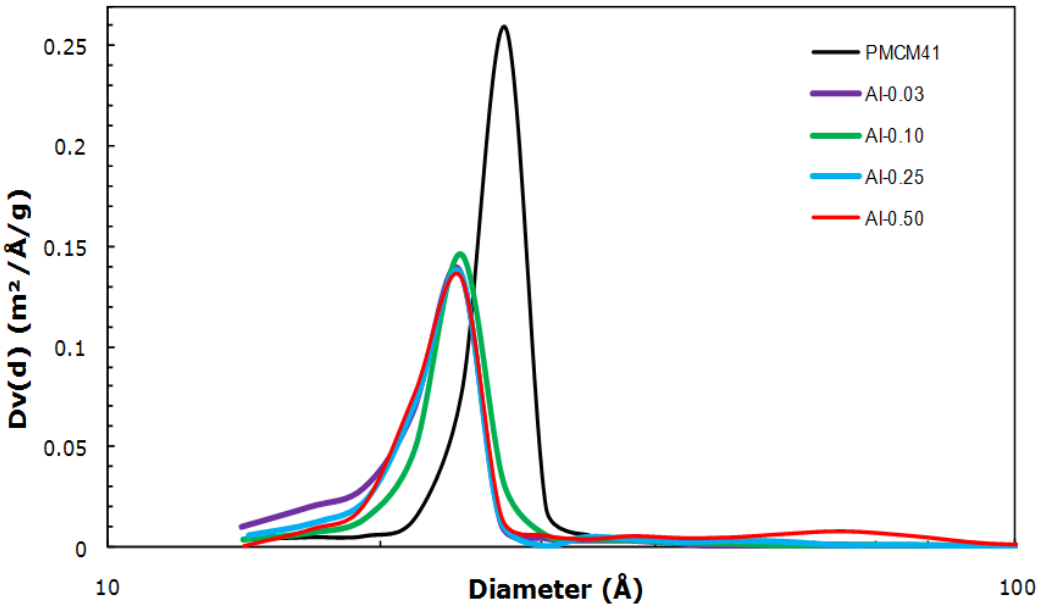

Figure 6.3. Pore size distributions of the synthesized pure and aluminum impregnated MCM-41 materials

6.1.1.4 Scanning Electron Microscopy Results of MCM-41 and Aluminum Impregnated MCM-41 Materials

SEM images of the synthesized samples are given in Figure 6.4 and 6.5. SEM images of aluminosilicate materials revealed the hexagonal array of well known structure of MCM-41. It was observed that agglomerations occurred in the material when aluminum was incorporated into the structure (Figures 6.4-b and 6.5). For Al-0.03 sample, the approximate particle size was 0.1 μm whereas for the sample Al-0.25, this value was around 0.7 μm. The loading of aluminum did not affect the general shape of the particles.

6.1.1.5 Transmission Electron Microscopy Results of MCM-41 and Aluminum Impregnated MCM-41 Materials

TEM images of aluminosilicate samples are given in Figure 6.6 and 6.7. The honeycomb structure of the pores can easily be distinguished in these images (Figure 6.6-6.7). Pore channels were arranged very regularly within the particle. These channels were in a cylindirical form. The average wall thickness and pore diameter read from the images were; 1.6 nm and 2.1 nm, respectively, which are in good agreement with nitrogen-adsorption and desorption analysis.

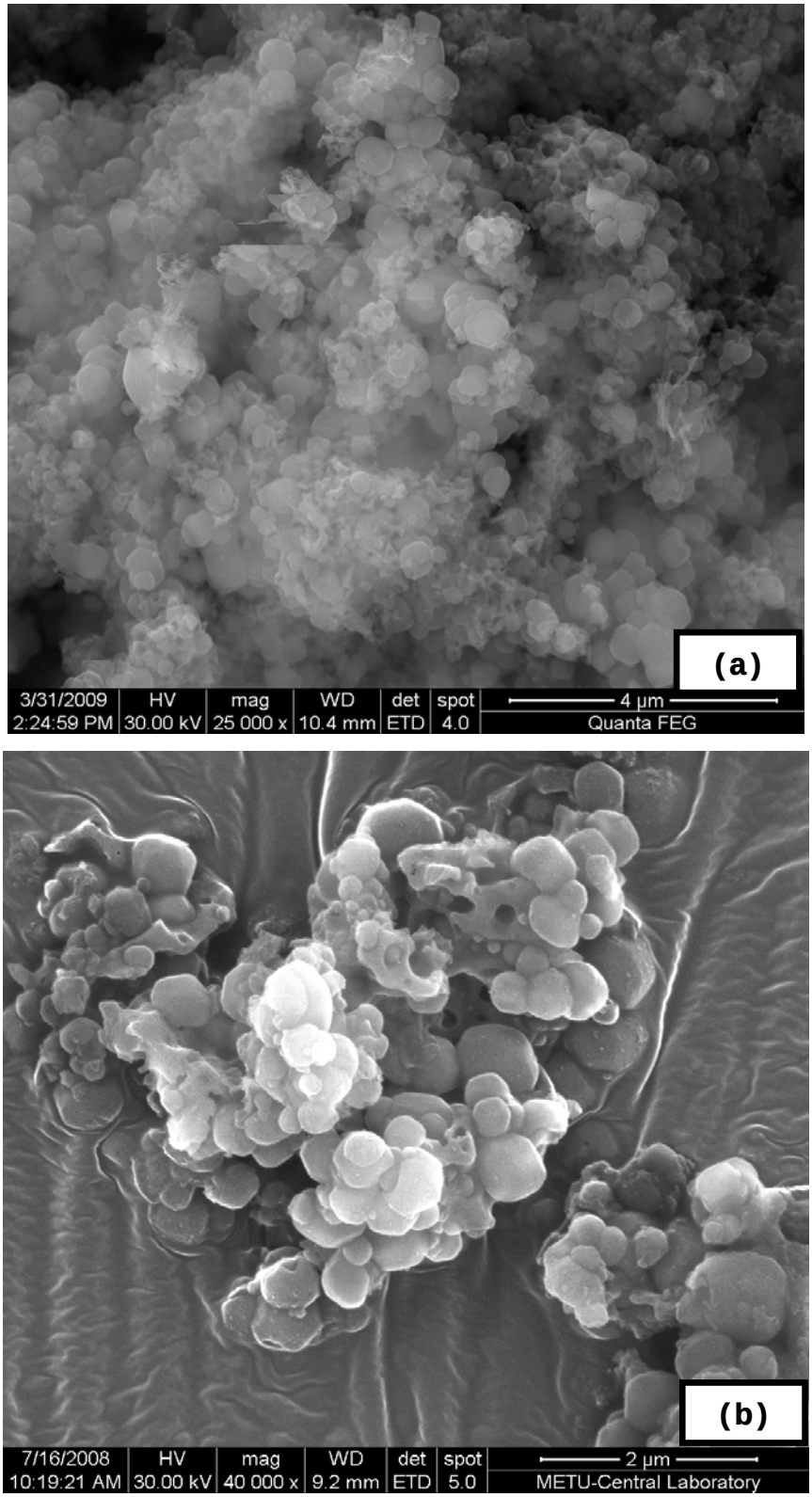

Figure 6.4. SEM images of (a) Al-0.03 and (b)Al-0.50 materials

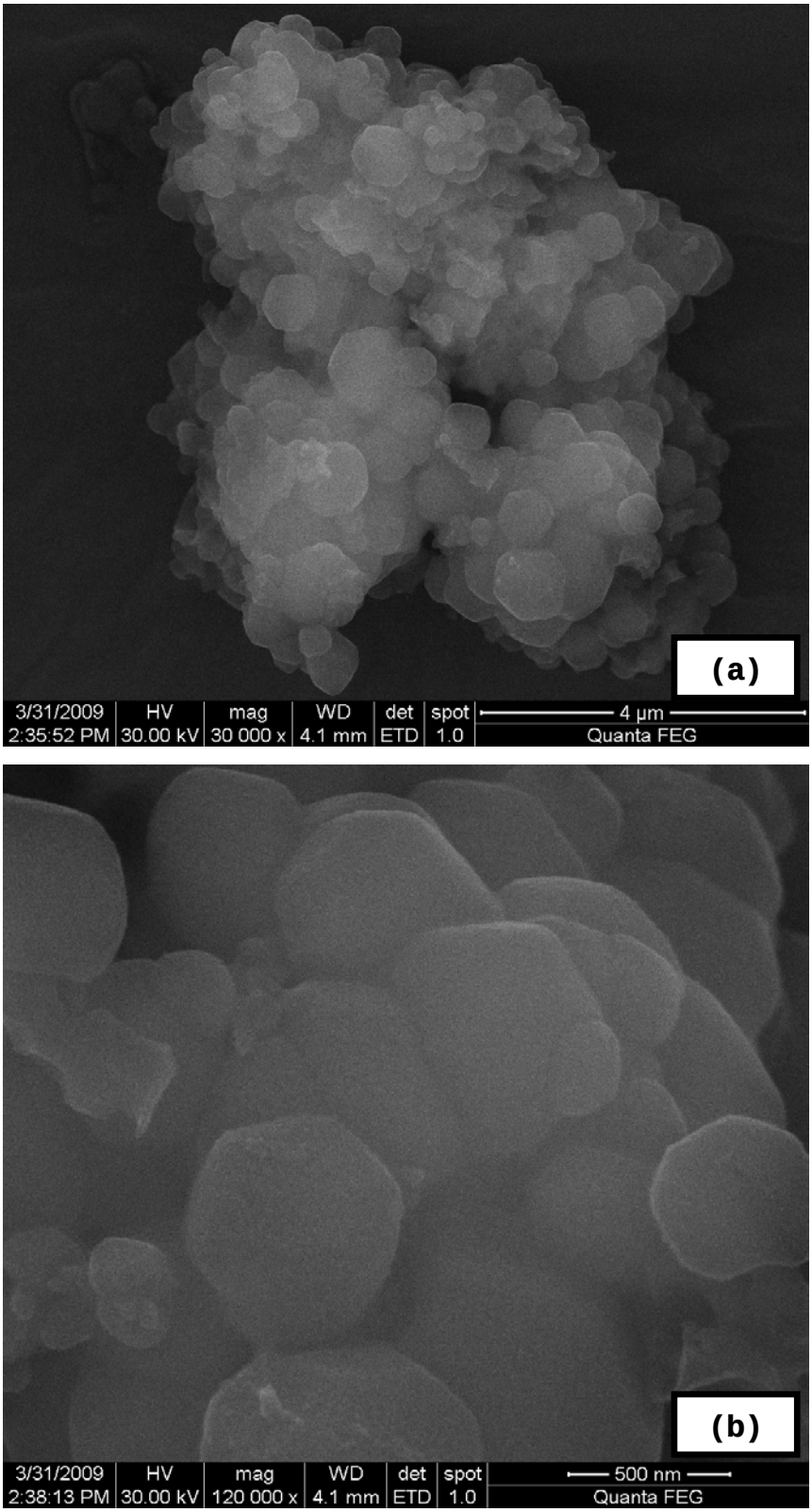

Figure 6.5. SEM image of Al-0.25 material (a)30000x magnification, (b)120000x magnification

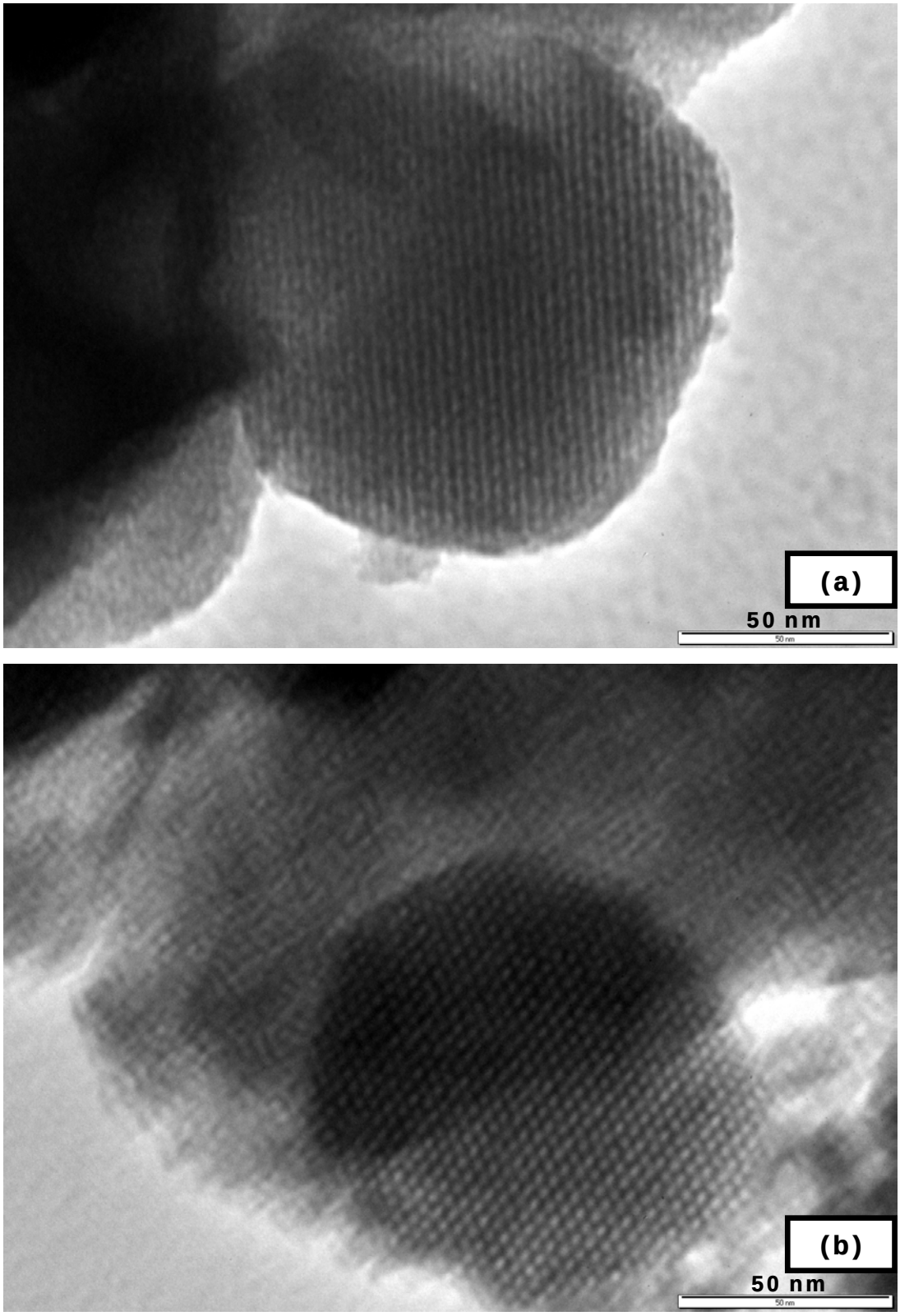

Figure 6.6. TEM images of (a) Al-0.03 and (b) Al-0.1 materials

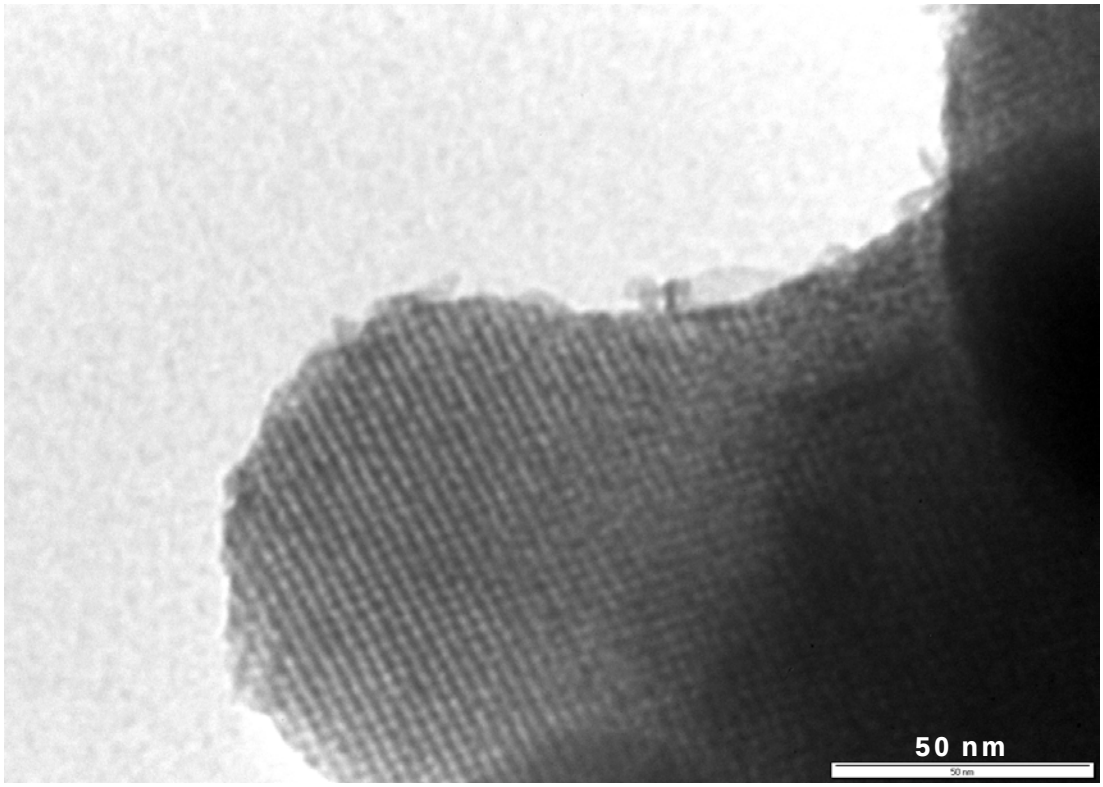

Figure 6.7. TEM image of Al-0.5 material

6.1.1.6 Nuclear Magnetic Resonance Results of MCM-41 and Aluminum Impregnated MCM-41 Materials

^{27}Al magic angle spinning nuclear magnetic resonance spectrometry results are shown in Figure 6.8. The spectra of these materials showed two peaks at around 0 and 50 ppm. The peak at 0 ppm belongs to 6-coordinate aluminum and the peak at 50 ppm belongs to 4-coordinate aluminum. Except for Al-0.50 sample, it was observed that; as the aluminum amount increased, octahedral aluminum in the structure was increased for all samples.

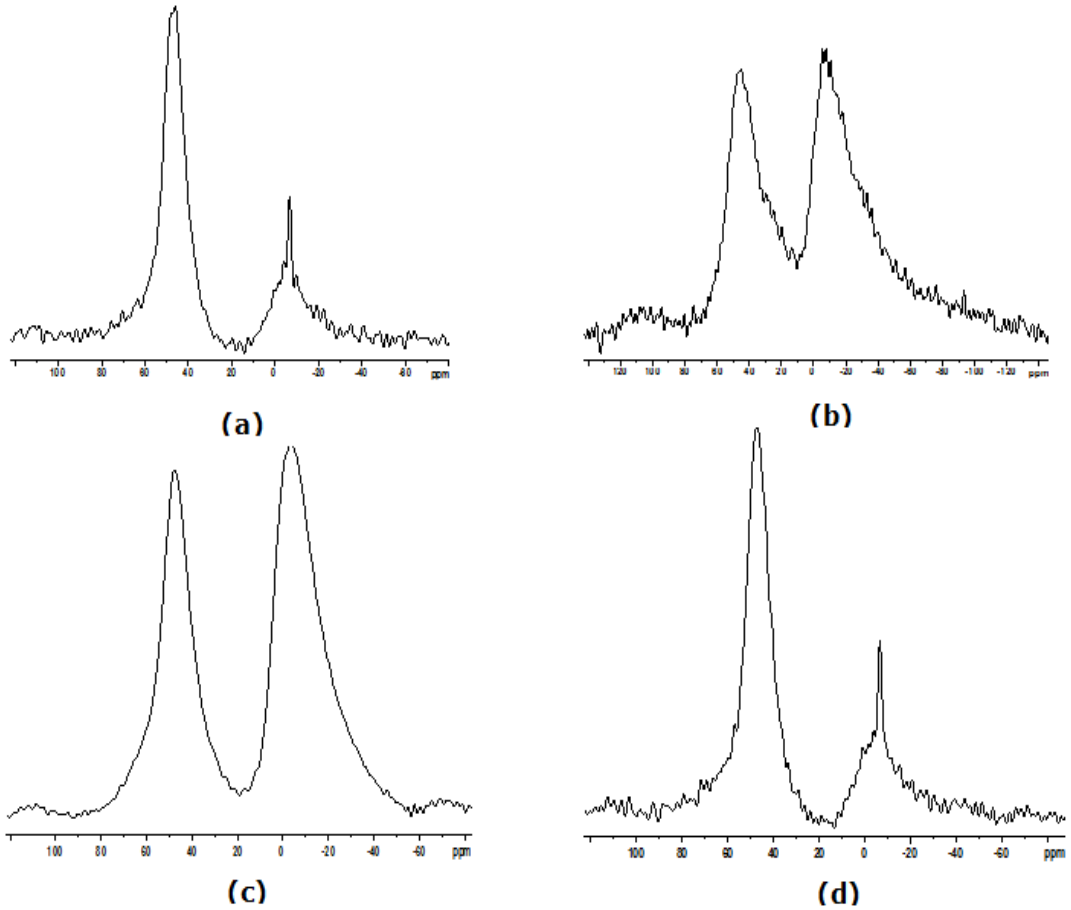

Figure 6.8. ^{27}Al MAS NMR spectra of (a) Al-0.03, (b) Al-0.10, (c) Al-0.25, and (d) Al-0.50 materials

For Al-0.03 and Al-0.50 samples, high intensity line at 50 ppm resonance indicates that most of the aluminum was introduced to the framework and low intensity line at 0 ppm indicated that inconsiderable amount of aluminum impregnated was non-framework. However, Al-0.10 and Al-0.25 samples showed the existence of both framework and non-framework aluminum introduced to the structure in comparable amounts. NMR results showed that aluminum loaded MCM-41 materials exhibited tetrahedrally and octahedrally coordinated aluminum species in the structure.

6.1.1.7 DRIFT Results of MCM-41 and Aluminum Impregnated MCM-41 Materials

DRIFT results of fresh catalysts are given in Figure 6.9. Bands obtained at ~1070 cm^{-1} with a shoulder obtained at 1200 cm^{-1} are due to the asymmetrical Si-O-Si stretching vibrations (Holmes et al., 1998) and the band obtained at 3738 cm^{-1} is due to the existence of free Si-OH (silanol) groups in the material. The peak at 798 cm^{-1} was due to Si-O-Si symmetrical stretching vibration (Zhao et al., 1997). The band at 3738 cm^{-1} was obtained only for the pure MCM-41 sample and not for Al impregnated samples and this peak was disappeared with the aluminum loading, which may be lost due to the bonding of aluminum to those free silanol groups.

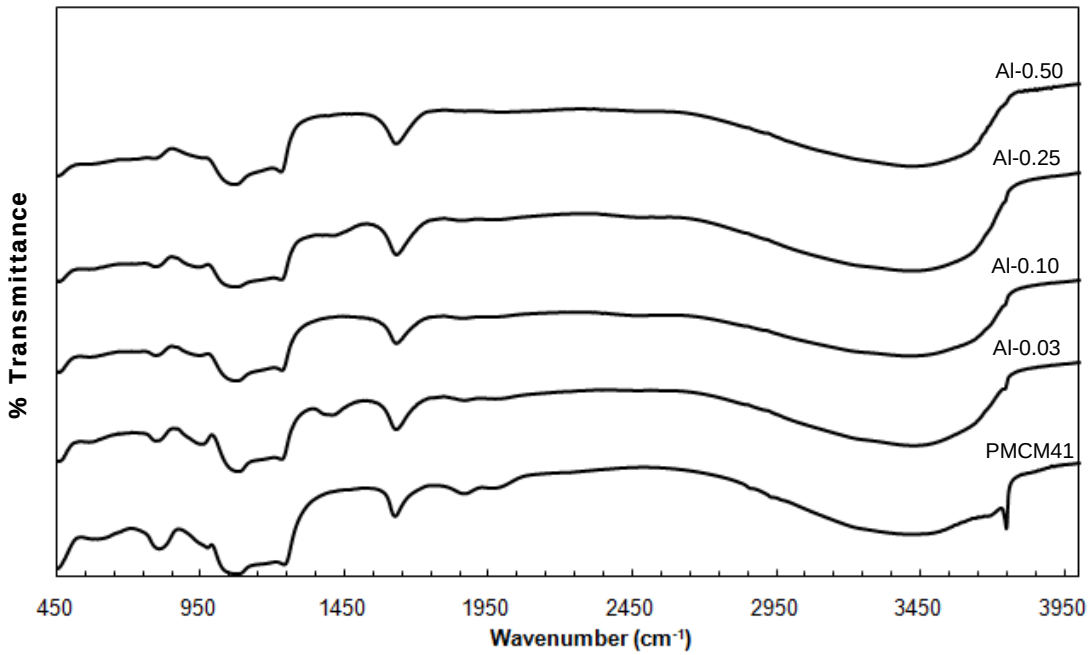

Figure 6.9. DRIFT spectra of the synthesized pure MCM-41 and aluminum impregnated MCM-41 materials

Peak at a wavenumber of 1650 cm^{-1} was assigned to the bending vibration of adsorbed water (Liu et al., 2004). A broad peak with a maximum of 3400 cm^{-1} (Brodie-Linder et al., 2008) belongs to the hydrogen bonded silanol groups and adsorbed water.

In order to observe the existence of Lewis and Brønsted acid sites in the pure and aluminosilicate samples, pyridine was adsorbed. The difference between DRIFT spectra of pyridine adsorbed and fresh catalysts helped to obtain characteristic peaks that gave information about Lewis and Brønsted acid sites in the synthesized materials. For instance, bands obtained at 1447 cm^{-1} and 1598 cm^{-1} showed the existence of Lewis acid sites that adsorbed pyridinium ion, whereas bands obtained at 1540 cm^{-1} and 1640 cm^{-1} showed the existence of Brønsted acid sites. The band observed at 1489 cm^{-1} was due to the contribution of both Lewis and Brønsted acid sites within the structure (Corma, 1995). In Figure 6.10, DRIFT spectra of pyridine adsorbed samples can be seen. For pure MCM-41 sample, the bands obtained at 1447 cm^{-1} and 1598 cm^{-1} are related with the Lewis acidity. On the other hand, when DRIFT spectra of all the aluminum impregnated samples are examined, in addition to the aforementioned bands obtained due to the Lewis acidity, there are small bands obtained at 1540 cm^{-1} and 1640 cm^{-1} indicating Brønsted acidity. Also, the band seen at 1489 cm^{-1} is regarded as the contribution of both Lewis and Brønsted acid sites in the structure. Therefore, impregnation of aluminum into pure MCM-41 sample led the formation of Brønsted acid sites within the structure.

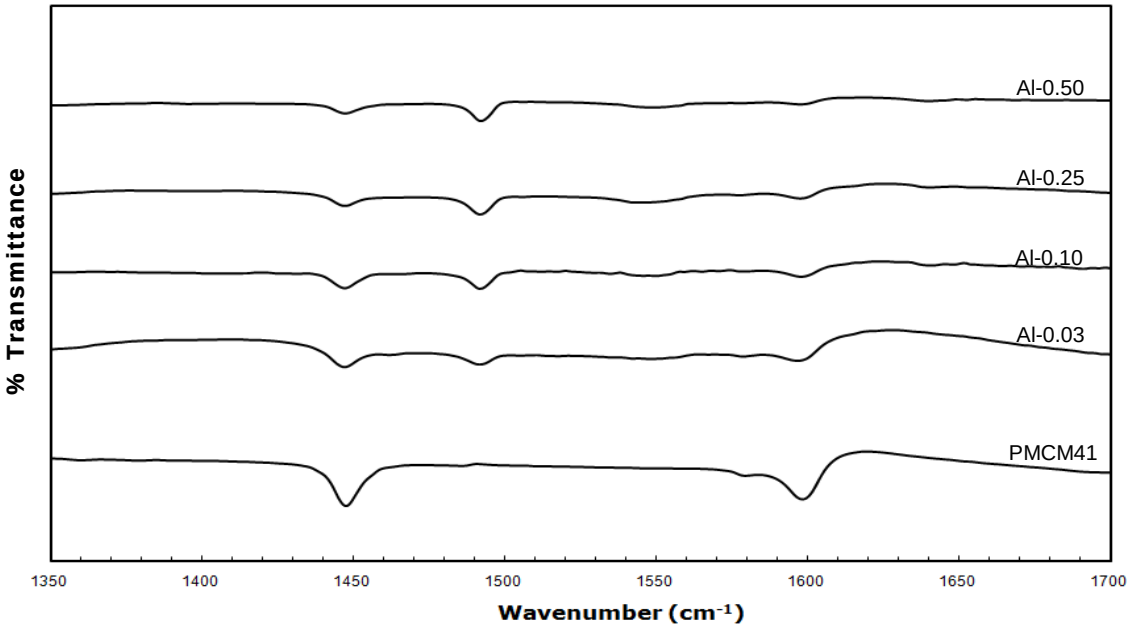

Figure 6.10. DRIFT spectra of the pyridine adsorbed pure MCM-41 and aluminum impregnated MCM-41 materials

6.1.2 Characterization Results of SBA-15 and Tungstophosphoric Acid Impregnated SBA-15 Materials

6.1.2.1 X-Ray Diffraction Results of SBA-15 and Tungstophosphoric Acid Impregnated SBA-15 Materials

The X-Ray Diffraction patterns of pure and TPA containing SBA-15 materials at the low Bragg angle are shown in Figure 6.11. The main peak of pure SBA15 sample was at the Bragg Angle value of 1.08^o. Secondary, tertiary and quaternary peaks were observed at 2θ values of 1.42^o, 1.72^o and 1.92^o which match well with the characteristic pattern of the ordered mesostructured (Kumar et al., 2006). For TPA modified samples, the main peaks were observed at the same Bragg Angle value of 1.08^o. The intensities of all the peaks decreased with an increasing TPA loading. In other words, in low TPA loading levels, there were not any major distortions in the ordered structure of the material, on the other hand at high loading values it was observed that the regular and ordered structure was not preserved. In Figure 6.12, wide angle X-Ray diffraction patterns of TPA impregnated materials are given. A broad peak at a Bragg Angle value of 24^o was observed in all of these materials corresponding to the amorphous structure of silica. TPA modified materials exhibited a peak at 2θ value of 8.84 ^{o} which actually is the characteristic peak of tungstophosphoric acid and the increase in loading amount caused an increase in intensity of the TPA characteristic peak. In low loading levels, the distribution of TPA within the structure is more enhanced than the distribution in higher loading levels.

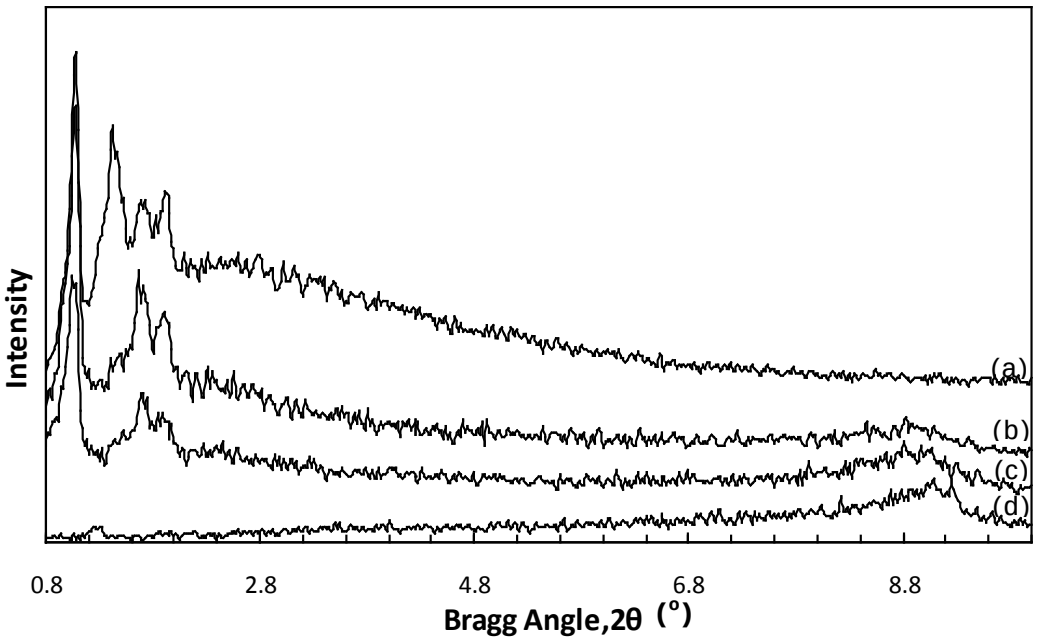

Figure 6.11. Low angle X-Ray Diffraction patterns of (a) pure SBA-15 (b) SBA15-0.1, (c) SBA15-0.25, and (d)SBA15-0.40 materials

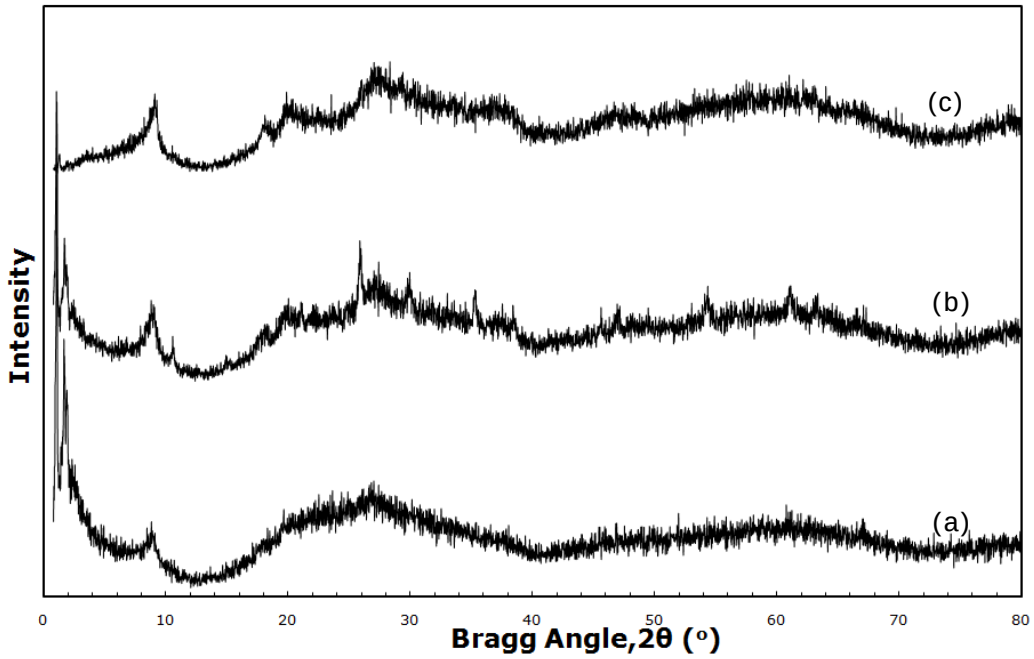

Figure 6.12. Wide angle X-Ray Diffraction patterns of (a) SBA15-0.1, (b) SBA15-0.25, and (c) SBA15-0.40 materials

6.1.2.2 Energy Dispersive Spectroscopy Results of SBA-15 and Tungstophosphoric Acid Impregnated SBA-15 Materials

EDS analysis results of TPA impregnated SBA-15 materials are given in Table 6.3. EDS spectra of all TPA containing catalysts are given in Appendix B. It was observed that TPA was introduced to the structure more effectively, at different TPA loadings. This situation was regarded to the wider mesopores of SBA-15 which provide more TPA to pass into the pores of the structure (Obalı et al., 2009).

Table 6.3. EDS results of tungstophosphoric acid impregnated SBA-15 materials

Sample	W/Si Ratio (EDS)	W/Si Ratio (in the initial solution)
SBA15-0.1	0.096	0.10
SBA15-0.25	0.25	0.25
SBA15-0.40	0.41	0.40

6.1.2.3 Surface Characterization Results for SBA-15 and Tungstophosphoric Acid Impregnated SBA-15 Materials

Nitrogen adsorption-desorption isotherms of synthesized SBA-15 and TPA impregnated SBA-15 materials are shown in Figure 6.13. According to the IUPAC classification, the synthesized materials exhibited isotherms of Type IV, which is a typical of mesoporous material (Sing et al., 1985). H1 type hysteresis was also observed for all of them at a relative pressure range of 0.65-0.80 due to the capillary condensation of nitrogen in the mesopores of the structure, which indicates uniform, narrow pore size distribution. This hysteresis loop was narrow and the adsorption and desorption branches were quite sharp and nearly parallel in most of the synthesized materials. With high TPA loading, the adsorbed nitrogen volume significantly decreased. This might be due to the blocking of these materials' pores by TPA molecules. In Table 6.4, BET surface area, pore volume and pore diameter values of the samples

are tabulated. Incorporation of TPA to the silica at high loading above 0.25 of W/Si ratio caused a sharp decrease in the surface area values. This sharp decrease might be due to the blocking of synthesized materials' pores by TPA species. Pore diameters which were calculated using BJH model (Table 6.4) are approximately 65 Å. This indicates the mesoporosity of the material, as expected.

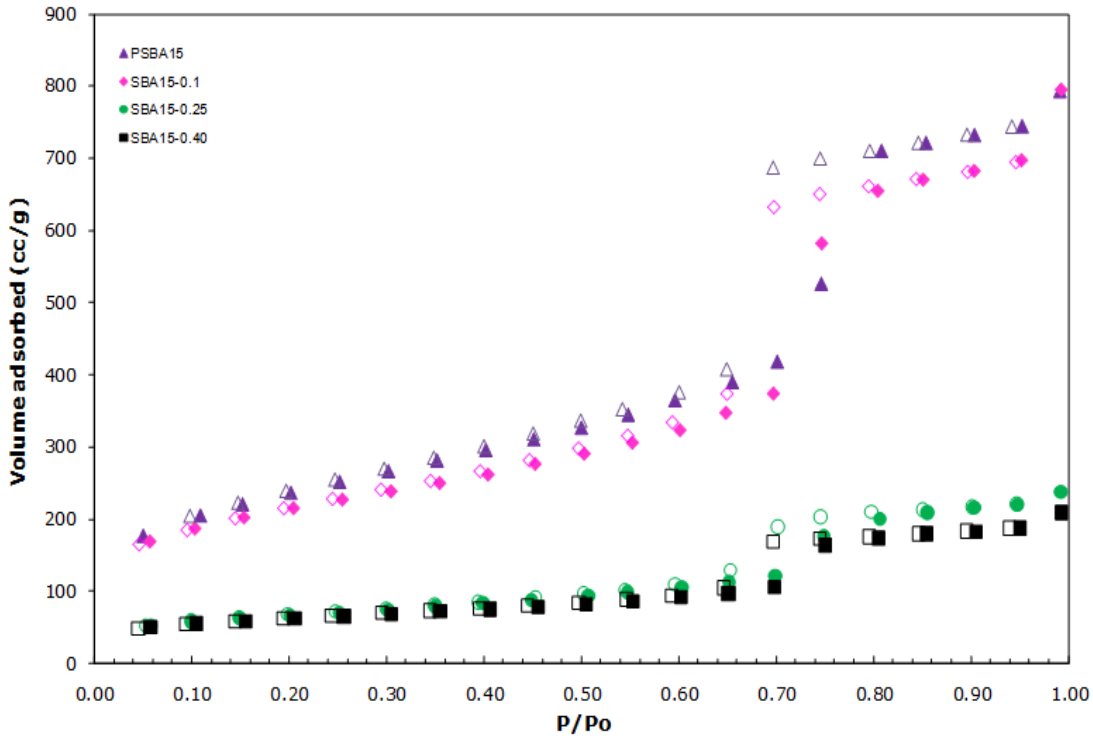

Figure 6.13. Nitrogen adsorption and desorption isotherms of the synthesized materials: (Filled symbols:adsorption, empty symbols: desorption)

Table 6.4. Surface area and pore size values of the synthesized pure SBA-15 and tungstophosphoric acid impregnated SBA-15 materials

Sample	Surface Area Multi Point BET, (m^2/g)	Pore Volume BJH Des., (cc/g)	BJH Des. Av. Pore Diameter (Å)
PSBA15	825	1.183	65.2
SBA15-0.1	749	1.19	65.1
SBA15-0.25	230	0.357	66.0
SBA15-0.40	212	0.306	64.8

In Figure 6.14, pore size distributions of the synthesized materials obtained using BJH model are given. For all samples, pore size distribution shows a narrow pore diameter range of 20 to 100 Å, which is again an indication of the mesoporous structure (Sing et al., 1985). Hence TPA loading did not cause a dramatic change in the pore diameter of the samples. On the other hand, pore volume decreased drastically as the amount of TPA loading increased. This situation might be arisen from the fact that TPA molecules were distributed all over the external surface of the silicate structure and blocked the pores. These results were consistent with nitrogen adsorption-desorption isotherm results (Figure 6.13).

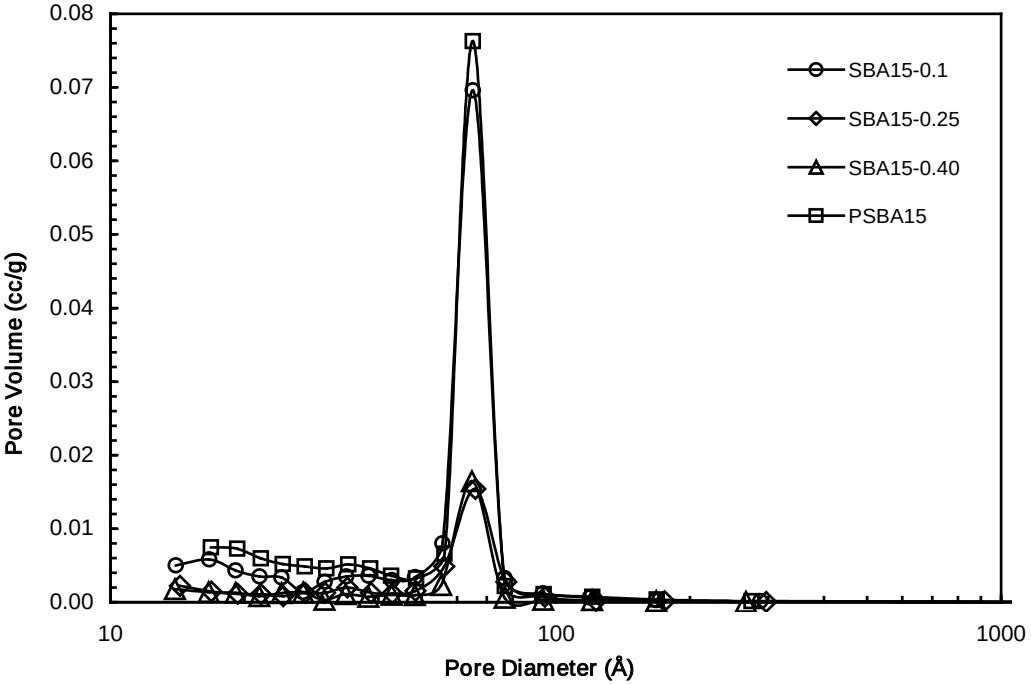

Figure 6.14. Pore size distributions of the TPA loaded SBA-15 materials

6.1.2.4 Scanning Electron Microscopy Results of SBA-15 and Tungstophosphoric Acid Impregnated SBA-15 Materials

SEM images of the synthesized samples are given in Figures 6.15, 6.16, and 6.17. SEM images of synthesized SBA-15 catalysts revealed the hexagonal array of the material (Figure 6.16). Agglomerations were observed in the material when TPA was incorporated into the structure (Figure 6.16). The loading of TPA did not affect the general shape of the particles. For pure SBA-15 material, the approximate particle size is 0.6 μm whereas for materials SBA15-0.1 and SBA15-0.40, the measured average particle size values are 0.66 μm and 0.82 μm, respectively.

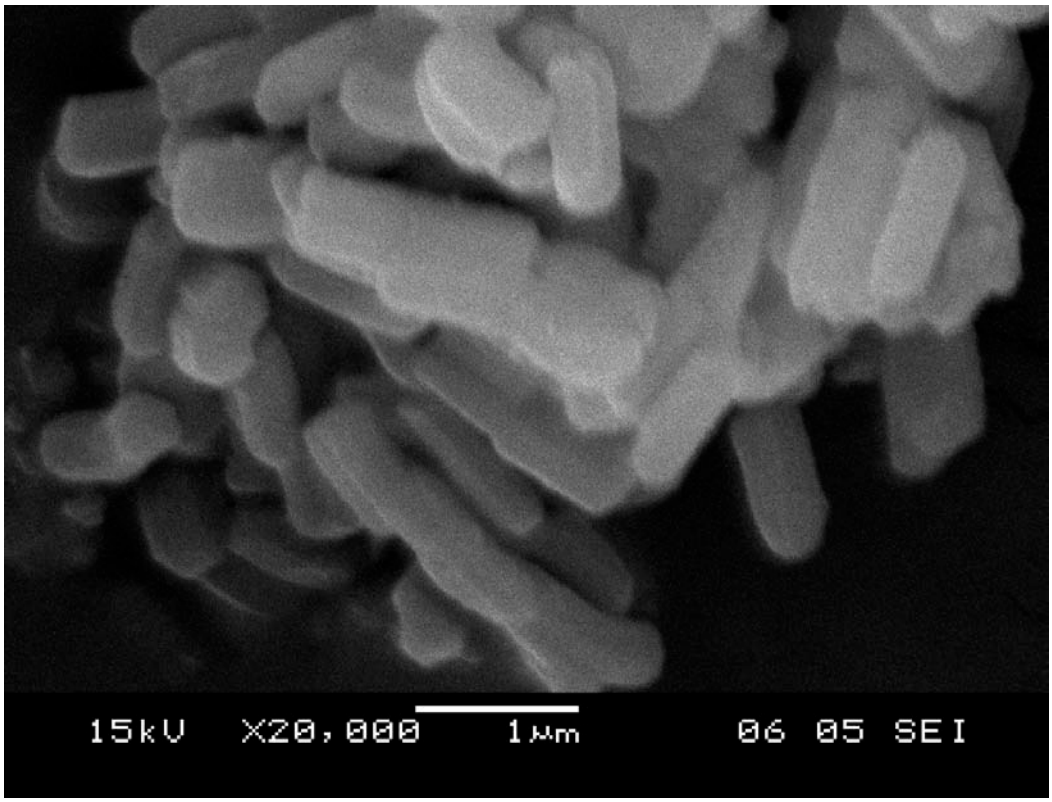

Figure 6.15. SEM image of SBA15-0.25 material

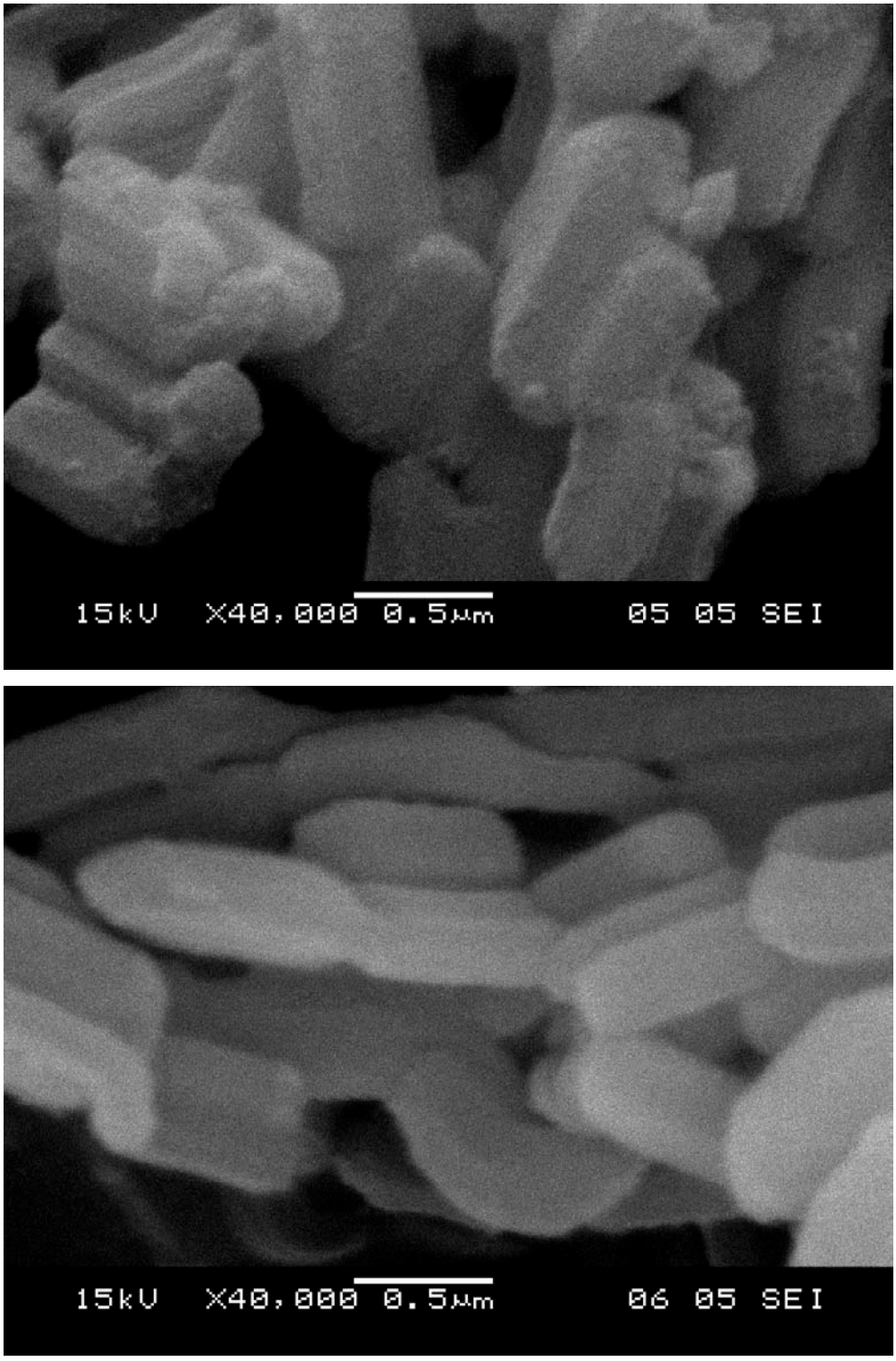

Figure 6.16. SEM image of SBA15-0.10 material taken from different areas of the sample

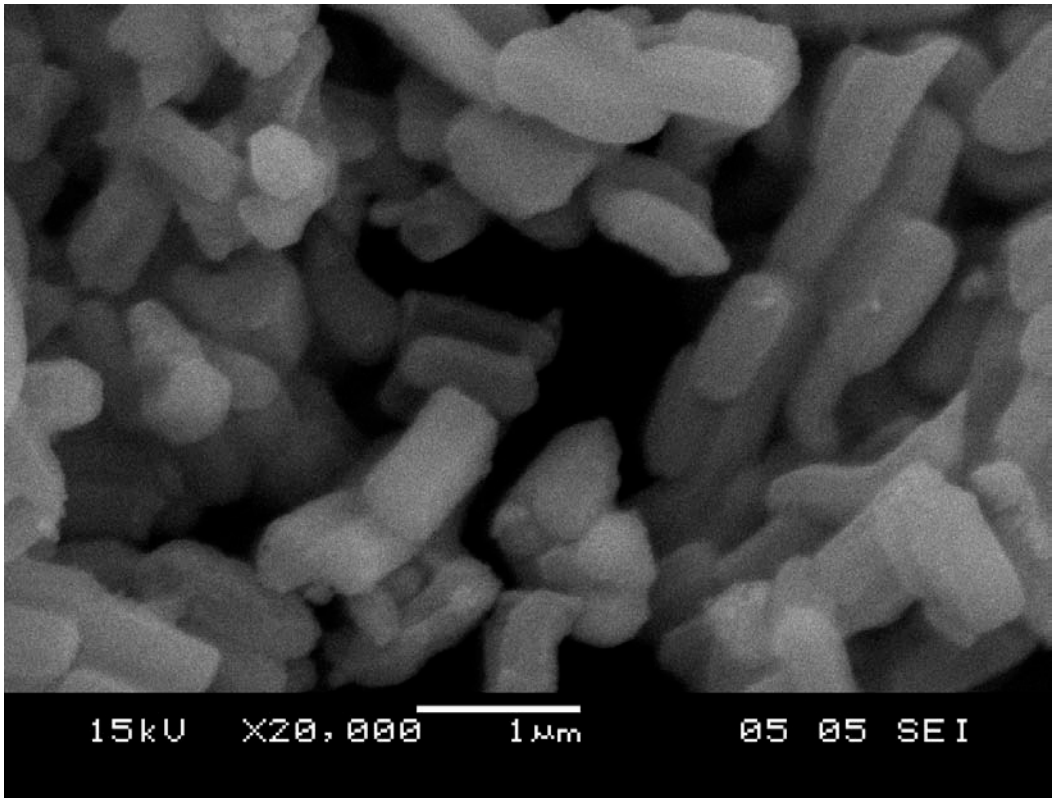

Figure 6.17. SEM image of SBA15-0.40 material

6.1.2.5 Transmission Electron Microscopy Results for SBA-15 and Tungstophosphoric Acid Impregnated SBA-15 Materials

TEM images of pure and TPA impregnated SBA-15 materials are shown in Figure 6.18 and 6.19. As seen from these figures, the pores are in honey-comb structure (Figure 6.19a) and pore channels are arranged very regularly within the particle. The channels are in a cylindrical form (Figure 6.18a, b, and Figure 6.19b) and particles are combined with each other in an ordered manner (Figure 6.18b). The average measured particle sizes were 0.76 µm and 0.83 µm for SBA15-0.1 and SBA15-0.40, respectively and are in a good conformity with SEM images. The distance between two consecutive centers of hexagonal pores was ~10.2 nm. The average wall thickness was ~4.1 nm. The pore diameter was ~6.2 nm. These results are in agreement with the results obtained from N_2 physisorption analysis.

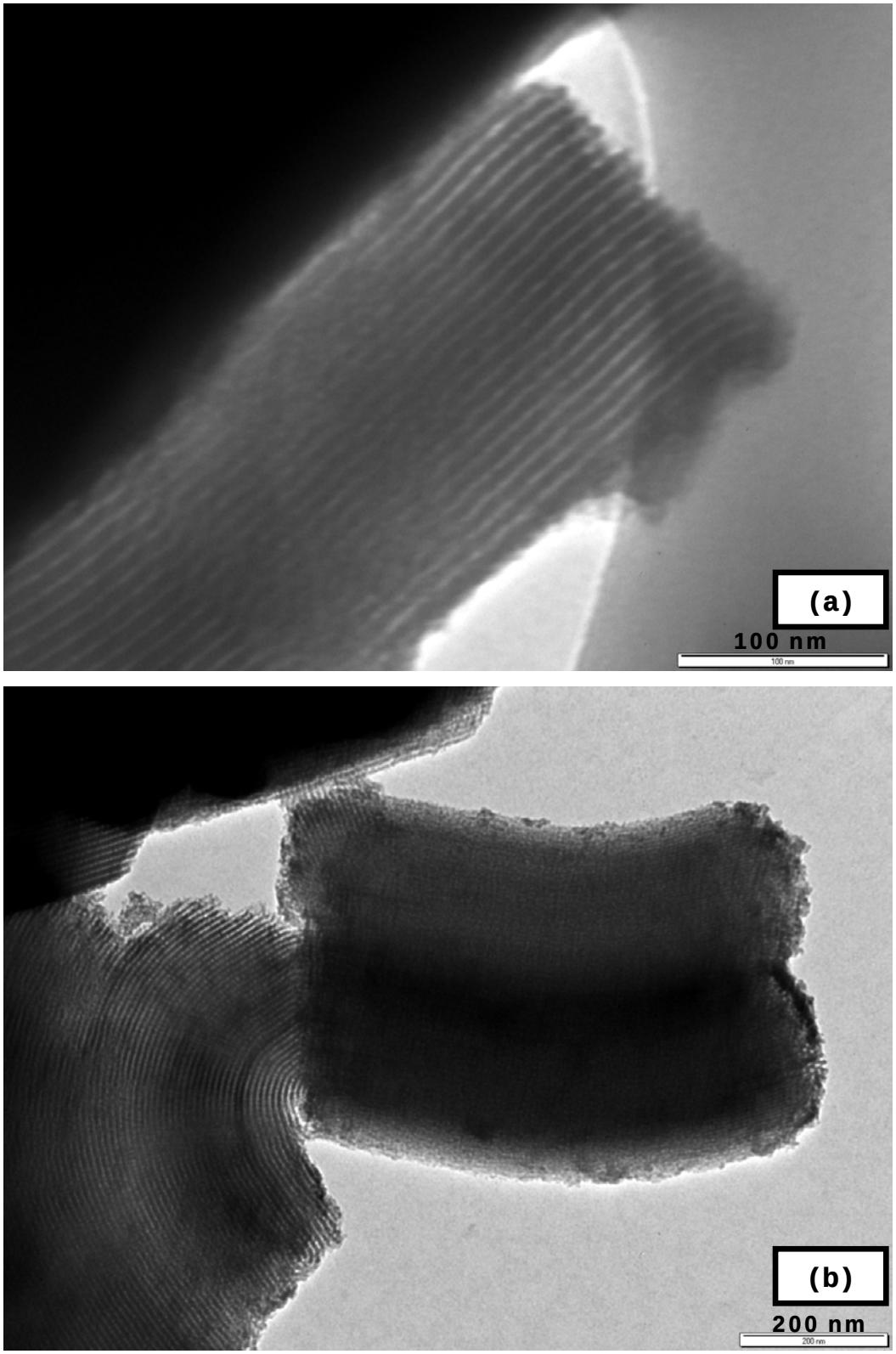

Figure 6.18. TEM images of (a) pure SBA15 and (b) SBA15-0.10 materials

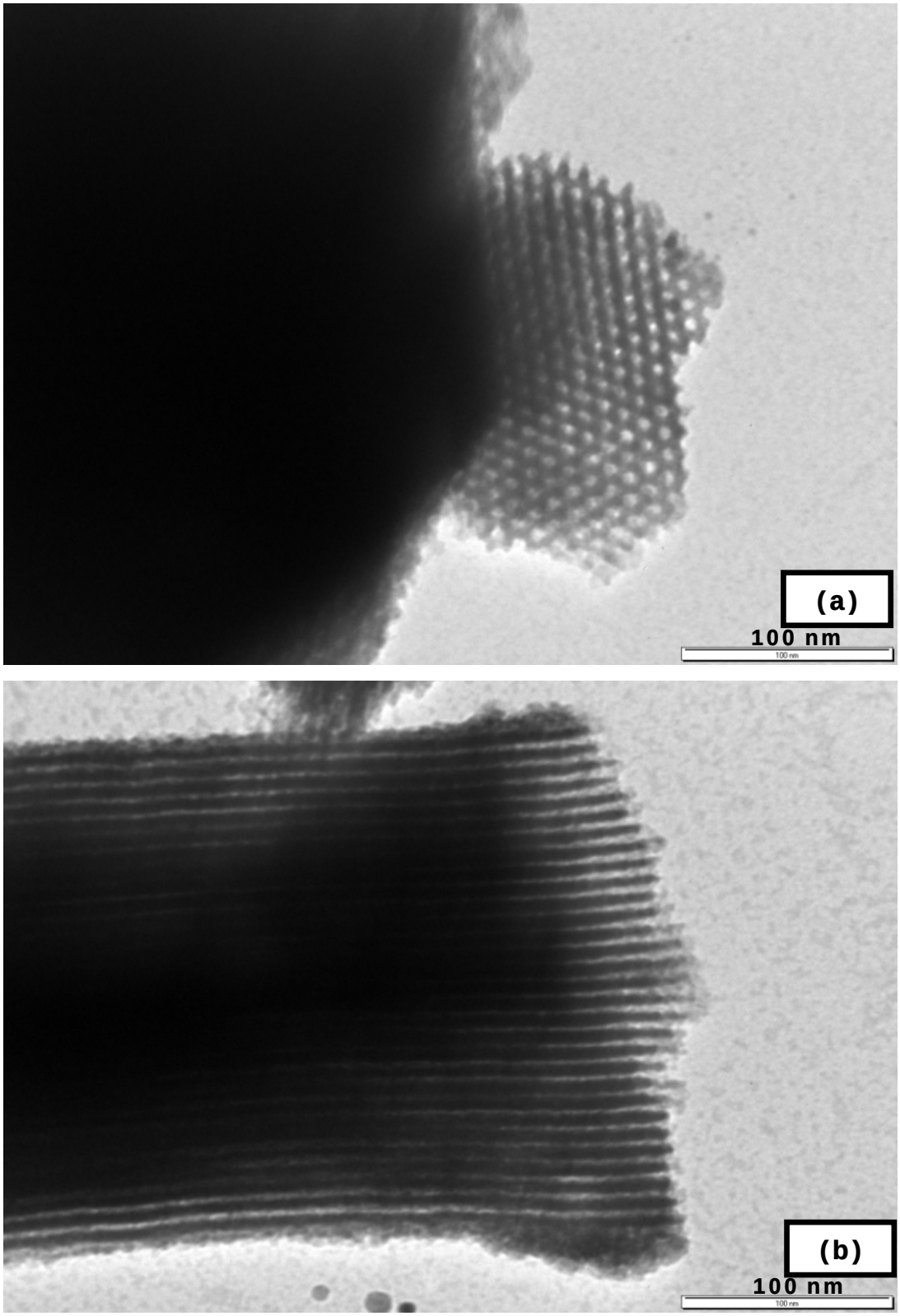

Figure 6.19. TEM images of (a) SBA15-0.25 and (b) SBA15-0.40 materials

6.1.2.6 DRIFTS Results of SBA-15 and Tungstophosphoric Acid Impregnated SBA-15 Materials

DRIFT results of fresh catalysts are given in Figure 6.20. Peaks obtained at 798 cm^{-1} and 886 cm^{-1} are due to W-O_c-W and W-O_b-W stretching vibrations. Here, subscripts b and c stand for the oxygen bridging to W, corner-sharing and edge sharing belonging to WO_6, respectively (Vazquez et al., 2000). The bands at 968 cm^{-1} and 1070 cm^{-1} are assigned to W=O_t and P-O vibrations (Sawant et al., 2005). These peaks at 798 cm^{-1}, 886 cm^{-1}, 968 cm^{-1}, and 1070 cm^{-1} showed Keggin structure in the synthesized materials (Kumar et al., 2006). Bands obtained at around 1070 cm^{-1} with a shoulder at 1200 cm^{-1} are due to the asymmetric Si-O-Si stretching vibrations (Holmes et al., 1998) which overlaps with P-O vibration peak and the band at around 798 cm^{-1} is due to Si-O-Si symmetric stretching which overlaps with W-O_c-W (Zhao et al., 1997) stretching vibration peak. Only the TPA peaks at 886 cm^{-1} and 968 cm^{-1} are discernable in the spectra of the synthesized materials. In pure SBA-15, the bands at 886 cm^{-1} and 968 cm^{-1} were not observed. The intensities of peaks at 886 cm^{-1}, 968 cm^{-1}, and 1070 cm^{-1} increased with TPA loading levels, which indicates incorporation of TPA species to the structure of SBA-15 material and also shows that the Keggin structure is preserved well. A broad peak with a maximum of 3450 cm^{-1} belongs to the hydrogen bonded silanol groups and adsorbed water (Brodie-Linder et al., 2008). Peak at a wavenumber of 1612 cm^{-1} is assigned to the bending vibration of adsorbed water (Liu et al., 2004). The band obtained at 3748 cm^{-1} is due to the existence of free Si-OH (silanol) groups in the material (Liu et al., 2004). The band obtained at 3748 cm^{-1} for the pure SBA-15 sample was disappearing as the amount of TPA loaded increased, which may be lost due to the bonding of tungstophosphoric acid to those free silanol groups.

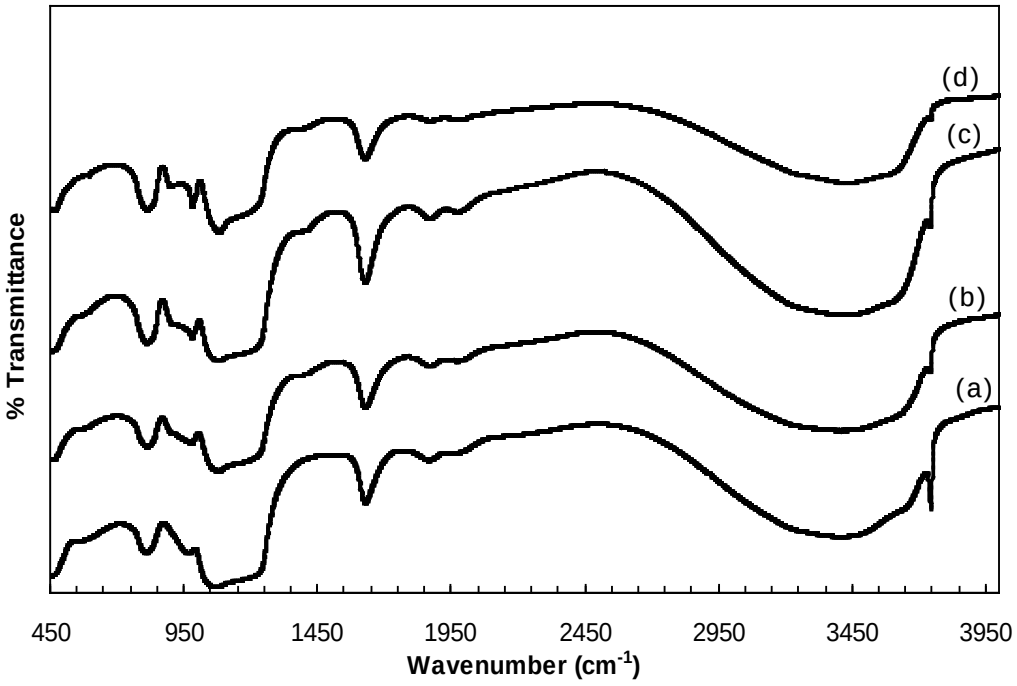

Figure 6.20. DRIFT spectra of the synthesized materials: (a) PSBA15, (b) SBA15-0.1, (c) SBA15-0.25, and (d) SBA15-0.40

In order to observe the existence of Lewis and Brønsted acid sites in the pure and TPA modified samples, pyridine was adsorbed on catalysts. The difference between DRIFT spectra of pyridine adsorbed and fresh catalysts helped to obtain characteristic peaks that give information about Lewis and Brønsted acid sites in the synthesized materials. In Figure 6.21, DRIFT spectra of pyridine adsorbed samples can be seen. For pure SBA-15 sample, peaks regarding to Brønsted acid sites were not observed, only one band at 1447 cm^{-1} related with the Lewis acid sites in the material was observed. On the other hand, when DRIFT spectra of all the TPA impregnated samples are examined, in addition to the aforementioned band obtained due to the Lewis acidity, there are small bands at 1540 cm^{-1} indicating Brønsted acidity. Also, the band at 1489 cm^{-1} is regarded as the contribution of both Lewis and Brønsted acid sites in the structure. Therefore, impregnation of TPA into pure SBA-15 sample led the formation of Brønsted acid sites within the structure and as the amount of TPA increased, the intensities of the peaks regarding to Brønsted acidity were increased.

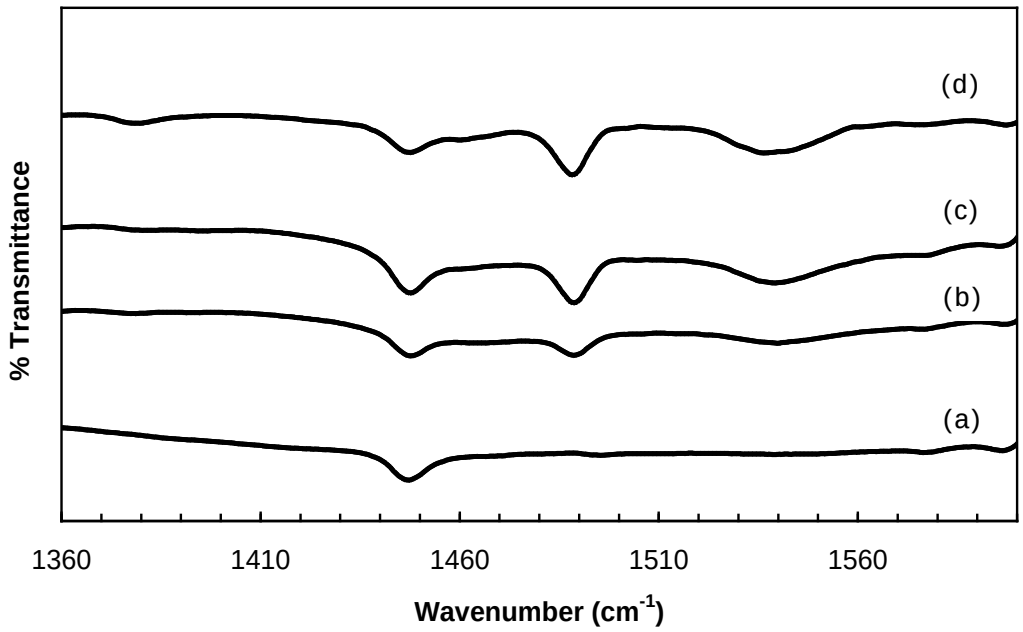

Figure 6.21. DRIFT spectra of the pyridine adsorbed catalysts (a) PSBA15, (b) SBA15-0.1, (c) SBA15-0.25, and (d) SBA15-0.40

6.2 Thermogravimetric Analysis Results

6.2.1 Thermogravimetric Analysis Results of Synthesized MCM-41 and Aluminum Impregnated MCM-41 Materials

Thermogravimetric analysis of the synthesized samples showed the behavior of the prepared polymer-catalyst mixtures at a given temperature interval .In Figure 6.22,TGA plots of polymer-catalyst mixtures at different weight ratios are given. With an increase in catalyst amount, decomposition temperature shifted to lower temperatures. Catalyst to polymer ratio of 1/2 decreased the degradation temperature most. That determined the ratio used in the TG analyses and catalytic degradation experiments.

In Figure 6.23, TG plots of pure polyethylene and polyethylene with synthesized catalysts prepared in 1/2 weight ratio can be seen. As the TG curve of pure polyethylene was examined, it was seen that the decomposition

started at 410 °C and ended up at 500 °C. Pure polyethylene showed a steep weight loss. This steep weight loss may be due to the chain degradation. Those temperatures are very high as the energy consumption for the decomposition reaction is considered. Also, for the polymer prepared with pure MCM-41 sample, the same condition exists, as a small change in decomposition temperature is observed. This is related to the fact that pure MCM-41 being lack of Brønsted acid sites within the structure. The existence of Lewis acid sites obviously have no significant effect in decomposition temperature, since the initiation step of the polyethylene degradation reaction proceeds over Brønsted acid sites causing protolysis. (Scheirs and Kamisky, 2006) When aluminum impregnated samples were used as a catalyst, a remarkable decrease occurred in decomposition temperature of polyethylene. It seems that the acid sites introduced to the structure by impregnation method play a great role in this decrease.

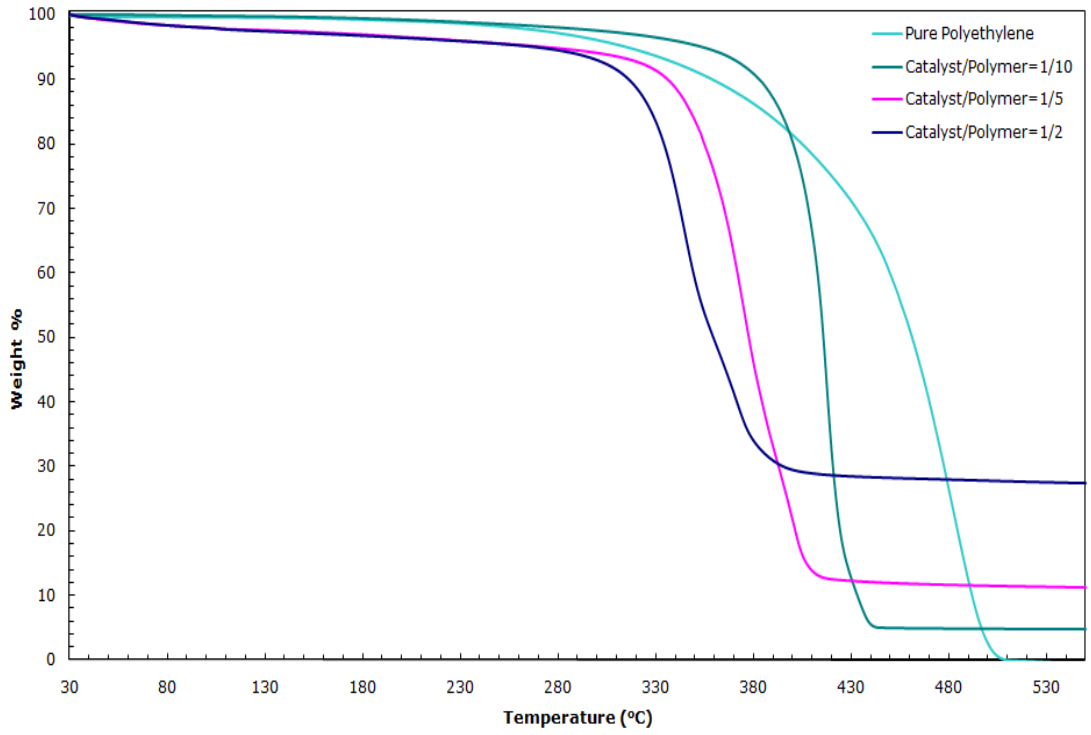

Figure 6.22. TGA plots for comparison of different catalyst/polymer ratios (Catalyst: Al-0.50)

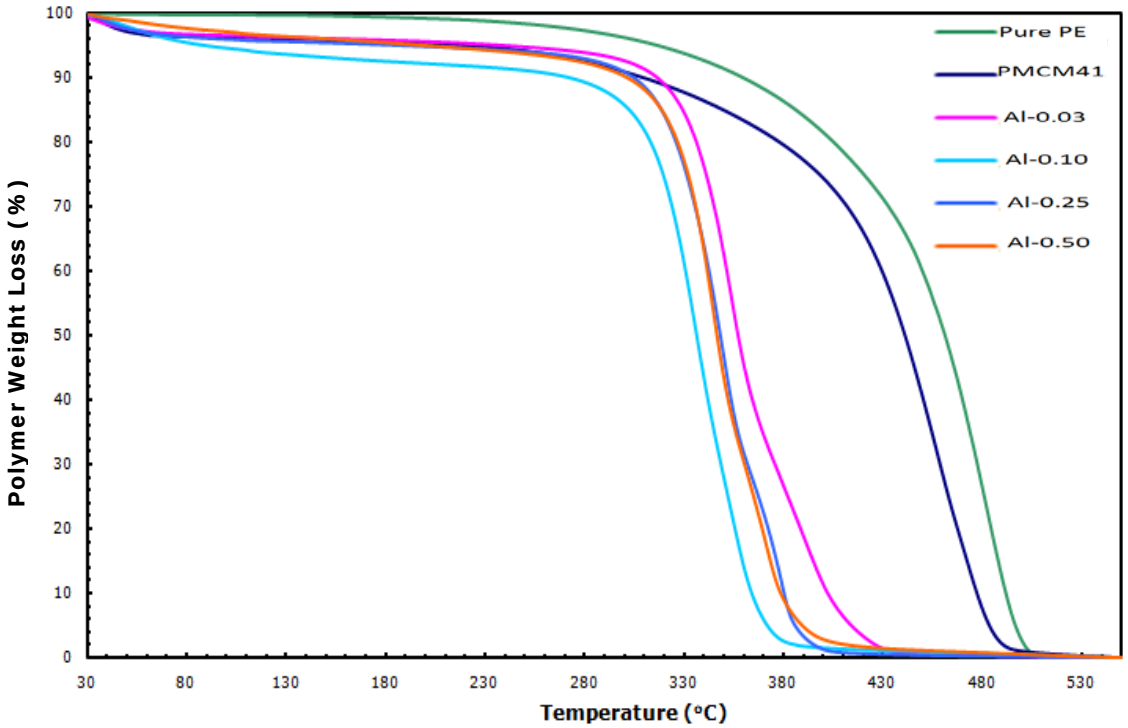

Figure 6.23. TGA plots of pure and aluminum impregnated MCM-41 samples ($w_{Catalyst}/w_{polymer}$: 0.5)

6.2.2 Thermogravimetric Analysis Results of Synthesized SBA-15 and Tungstophosphoric Acid Impregnated SBA-15 Materials

Figure 6.24 illustrates the TG analysis under nitrogen flow corresponding to polyethylene in the presence of the synthesized materials. In the presence of TPA impregnated SBA-15, polyethylene shows a steep weight loss at a lower temperature range than in the absence of catalyst. This temperature range shifted to a lower range with an increase in TPA loading. This is the indication of a significant decrease in degradation temperature of polyethylene. It was observed that the acid sites introduced to the structure by impregnation method play a great role in this decrease. Increase of acidity had a positive effect on the activity of the catalyst for degradation of PE. The increase in the amount of acidity, which is caused by loading of higher amount of TPA, caused a decrease in the polyethylene decomposition reaction temperature.

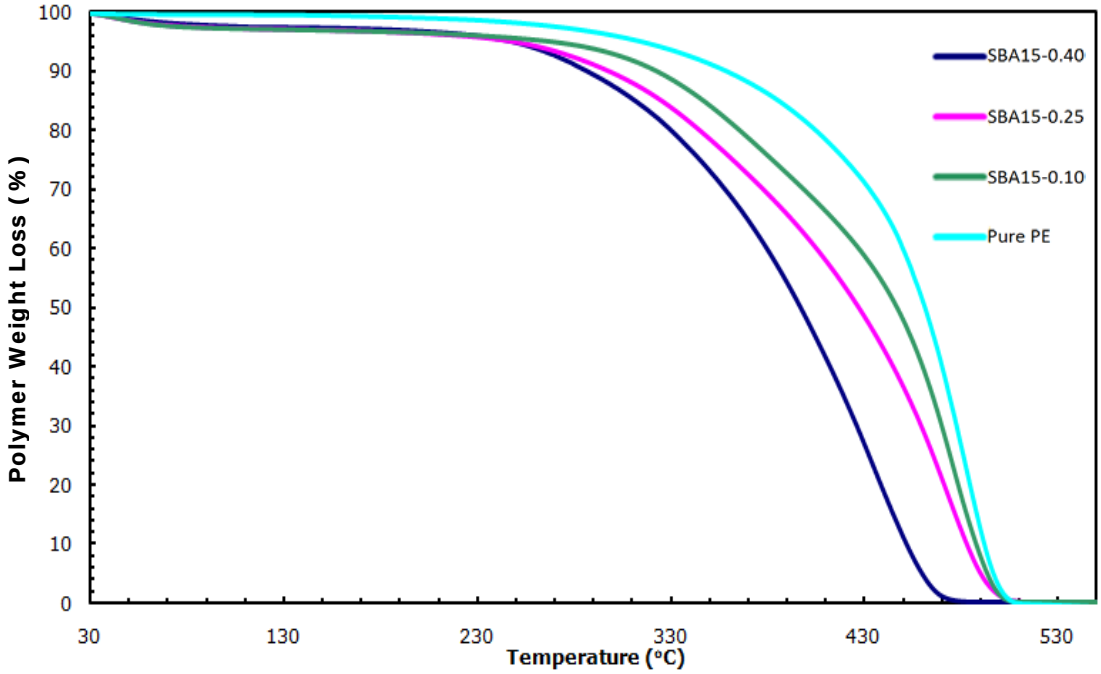

Figure 6.24. TGA plots of tungstophosphoric acid impregnated SBA-15 samples ($w_{Catalyst}/w_{polymer}$: 0.5)

6.3. Determination of Kinetic Parameters from TGA Data

In order to determine kinetic parameters from TGA data of the degradation reaction with and without the synthesized catalysts, a similar method in the literature was applied (Coats and Redfern, 1964). The model applied to define the kinetics of the reaction is given below,

$$\frac{d\alpha}{dt} = Ae^{-E/RT}(1-\alpha)^{n} \qquad (6.1)$$

where A is pre-exponential factor and E is activation energy of the reaction. α is the fraction of polymer decomposed at time t and defined as follows,

$$\alpha = \frac{w_0 - w_t}{w_0 - w_\infty} \qquad (6.2)$$

where w_0, w_t, and w_∞ are the initial weight of the sample, weight at time t, and weight at infinity, respectively. Assuming a linear heating rate;

$$a = \frac{dT}{dt} \tag{6.3}$$

By inserting equation (6.3) into equation (6.1), and after rearranging and integrating, it becomes;

$$\frac{1-(1-\alpha)^{(1-n)}}{(1-n)T} = \frac{AR}{aE}\left(1-\frac{2RT}{E}\right)exp\left(\frac{-E}{RT}\right) \qquad \text{(for } n \neq 1\text{)} \tag{6.4}$$

For simplification, assuming that $2RT / E << 1$ and taking the natural logarithm of both sides, the following relation is obtained.

$$ln\frac{1-(1-\alpha)^{(1-n)}}{(1-n)T^2} = ln\frac{AR}{aE} - \frac{E}{RT} \qquad \text{(for } n \neq 1\text{)} \tag{6.5}$$

equation (6.6) can be applied for first-order reaction where n=1, as well:

$$ln\frac{-ln(1-\alpha)}{T^2} = ln\frac{AR}{aE} - \frac{E}{RT} \qquad \text{(for } n=1\text{)} \tag{6.6}$$

By using TGA data, α values can be inserted into equation (6.5) and (6.6), and after plotting the term on the left-hand side of equations (6.5) and (6.6) as a function of 1/T, activation energy and pre-exponential factor can be obtained from slope and intercept of the straight line. In Figure 6.25, plots for a first and second order assumptions for the experiment conducted for pure polyethylene are given. The highest correlation coefficient is the determining factor in deciding the order of the reaction. Therefore, since R^2 value is around 0.96 and greater than the one obtained for a second order assumption, the order of the reaction is accepted as 1. Activation energies for pure polyethylene and catalyst/polymer mixtures are given in Table 6.5.

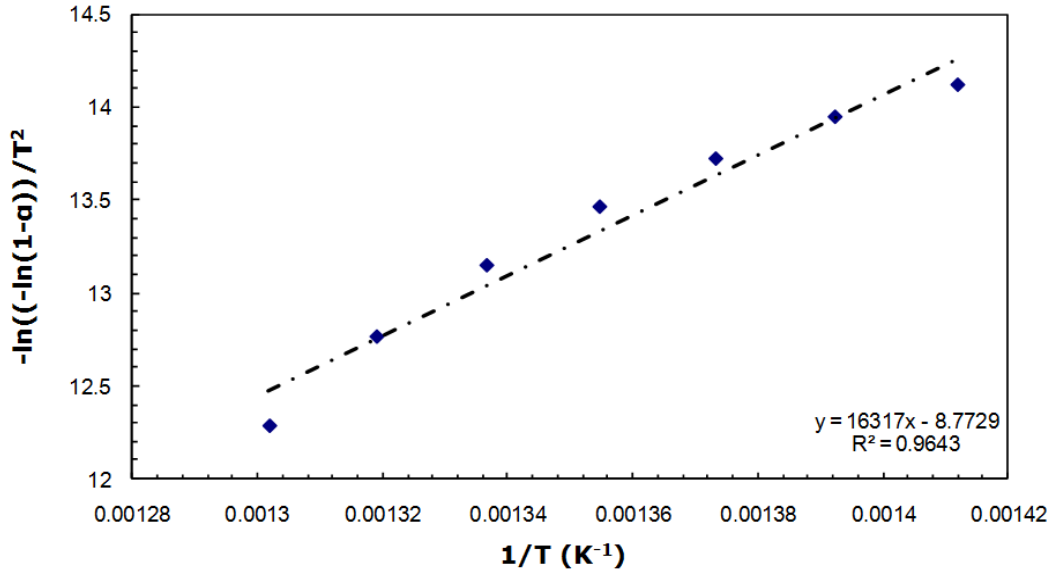

(a)

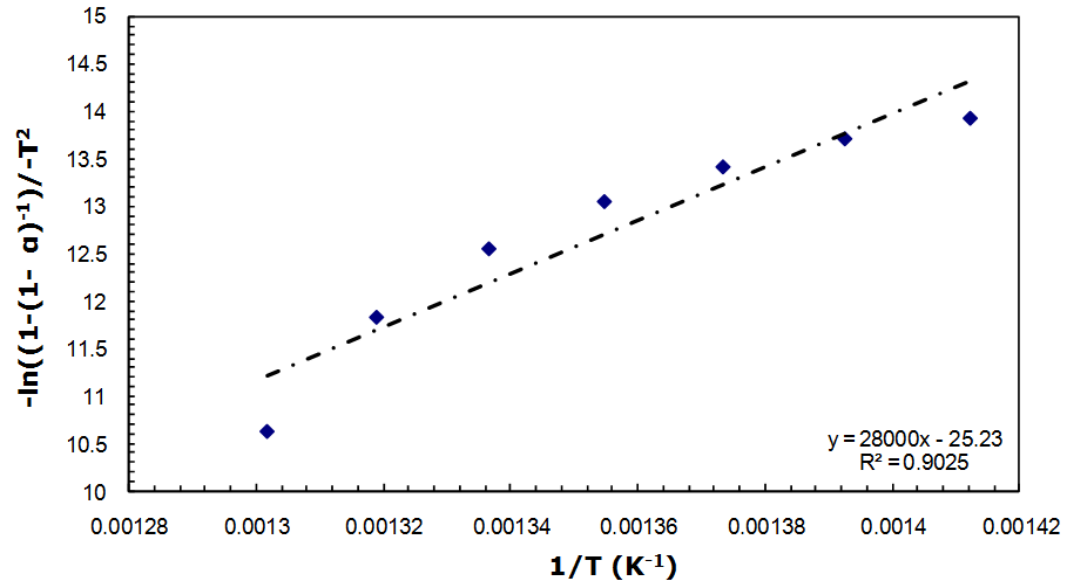

(b)

Figure 6.25. Determination of the order and the activation energy of the reaction (a) for a 1st order assumption (b) for a 2nd order assumption

Table 6.5. Activation energies of the degradation reaction calculated for pure polyethylene and catalyst added samples

Catalyst ($W_{catalyst} / W_{polymer} = 0.5$)	Activation Energy (kJ/mol)
Pure PE	136.0
PMCM41	137.0
Al-0.03	106.0
Al-0.10	131.4
Al-0.25	127.5
Al-0.50	137.0
SBA15-0.10	74.5
SBA15-0.25	60.4
SBA15-0.40	62.5

The overall order of the PE degradation reaction was found to be 1 for all types of catalysts. The activation energy for the polyethylene degradation reaction in the absence of the catalyst was around 136 kJ/mole. This activation energy value is in good agreement with literature (Peterson et al., 2005). In the presence of pure MCM-41, the activation energy is the same as non-catalytic degradation of pure PE. Similarly for Al-0.10, Al-0.25, and Al-0.50 samples the activation energy of PE degradation reaction remained almost constant. On the other hand, for TPA impregnated samples, it was observed that there was a great decrease in the activation energy of PE degradation reaction. Among all TPA introduced SBA-15 materials, SBA15-0.25 and SBA15-0.40 reduced the activation energy the most. This was regarded to the increase in the Brønsted acid sites in the structure with more TPA loading amounts. According to these results, Al-0.03, Al-0.25, SBA15-0.10, SBA15-0.25, and SBA15-0.40 materials were chosen to be used in the catalytic degradation experiments of polyethylene.

6.4 Results of Polyethylene Degradation Experiments

The non-catalytic and catalytic thermal degradation reactions were carried out isothermally in polymer degradation reaction system under nitrogen atmosphere with a flow rate of 60 cc/min and a constant heating rate of 5^{o}C/min.

6.4.1 Gas, Liquid, and Residue Yields Obtained from the Degradation Experiments

For each experiment, 1 g of polyethylene was loaded to the reactor. Non-catalytic and catalytic degradation products were hydrocarbon gases, liquids, and residues. The mass of gaseous products was found by subtracting the sum of polymer melt (residue) and condensate masses from the initial polymer mass. Yield was defined as;

$$\text{Yield (wt\%)} = \frac{P(g)\times 100}{Polymer\ Feed\ (g)} \qquad (6.7)$$

where P and Polymer Feed are: catalytic pyrolysis hydrocarbon product in grams, and amount of the polymer fed to the reactor in grams, respectively.

The reaction yields of polyethylene degradation with and without catalyst are given in Table 6.6.

In non-catalytic pyrolysis experiments, at low pyrolysis temperatures, solid residue was observed. This amount was 14.1% for a pyrolysis temperature of 420^{o}C and 7.5% for a pyrolysis temperature of 430^{o}C. Above these temperatures, no solid residue was observed. This showed that, with an increase in reaction temperature, the amount of solid residue decreased. The increase in reaction temperature increased the liquid product yields. This was also correct for the experiments conducted at the same temperature with different reaction times, where the higher reaction time resulted with higher liquid product yield. These results emphasized the importance of experimental parameters such as temperature an reaction time on the quantity of product

yields. Liquid products obtained from the non-catalytic experiments were in a gel-like form, which might be an indication of the existence of high molecular weight hydrocarbons in the product.

Table 6.6. Summary of the main products of PE degradation at different reaction conditions

Material	Temperature (°C)	Time (min)	Yield (wt %)		
			Residue	Liquid	Gas
Polyethylene	420	45	14.1	56.3	29.6
Polyethylene	430	10	7.5	52.8	39.7
Polyethylene	430	15	0	58.5	41.5
Polyethylene	450	10	0	58.9	41.1
Polyethylene	450	15	0	73.5	26.5
Polyethylene	480	5	0	67.9	32.1
Polyethylene	480	10	0	74.1	26.0
Polyethylene + SBA-0.10	390	15	0	09.8	90.2
Polyethylene + SBA-0.10	430	15	0	18.9	81.1
Polyethylene + SBA-0.25	390	15	0	12.1	87.9
Polyethylene + SBA-0.25	430	15	0	23.8	76.2
Polyethylene + SBA-0.40	390	15	0	11.6	88.4
Polyethylene + SBA-0.40	410	15	0	28.5	71.5
Polyethylene + SBA-0.40	430	15	0	30.8	69.2
Polyethylene + SBA-0.40	460	15	0	42.0	58.0
Polyethylene +Al-0.03	390	15	0	36.2	63.8
Polyethylene +Al-0.03	430	15	0	18.1	81.9
Polyethylene +Al-0.25	390	15	0	27.1	72.9
Polyethylene +Al-0.25	430	15	0	46.3	53.7

The results of degradation reactions conducted using TPA containing SBA catalysts at two different temperatures showed that the liquid product yield was increased with the increasing temperature. The increase in TPA percent of the catalyst also resulted in an increase in liquid yields. For Al-MCM-41 catalyzed reactions, it was seen that temperature and acidity increase also caused an increase in the liquid product yields. Unlike non-catalytic degradation reactions, the liquid product obtained in the catalytic reactions

was light, flowing liquid, which might be an indication of the existence of lower molecular weight hydrocarbons. When liquid and gas product yields of non-catalytic and catalytic degradation of polyethylene conducted at 430^{o}C for 15 min reaction time was compared, it was observed that the liquid yields were obtained much higher for non-catalytic degradation reaction. For catalytic degradation reactions performed using TPA loaded SBA-15 materials, the gaseous product yields was very high when compared to liquid product yields obtained. For non-catalytic degradation reactions on the other hand, the liquid and gaseous product yields was very close. This showed that the catalytic degradation of polyethylene favored the production of gaseous products. For aluminum loaded MCM-41 materials, the liquid product yield obtained was also lower than that of non-catalytic degradation, but the ratio of liquid and gaseous yields obtained for MCM-41 materials was closer to each other.

6.4.2 Gas Analysis of Non-Catalytic and Catalytic Degradation Reactions

6.4.2.1 Gas Analysis of Non-Catalytic Degradation Experiments

Gas products were analyzed qualitatively and quantitatively using GC. To determine mole fraction of these products, calibration factors for each gas product were found. Calculation of calibration factors for gas products is given in Appendix C. Ethane, acetylene, propane, propylene, n-butane, and i-butane gases were observed in the studied reaction temperatures.

Mole fraction and selectivity of gas products obtained from non-catalytic degradation of polyethylene are given in Figure 6.26 and Figure 6.27, respectively. Mole fraction and selectivity calculations of the gas products are given in Appendix D. Mole and weight fractions and selectivity results of gas products obtained from the non-catalytic degradation of PE are tabulated in Appendix E. It was observed that, ethylene (C_2H_4) mole fraction and selectivity were considerably high when compared with other gas products. The amount of ethylene increased up to 450^{o}C creating a maximum at this point and then decreased gradually to a half value at 480^{o}C. It was noticeable

that the mole fraction and selectivity of the other compounds made a minimum at 450°C and increased to a higher amount at 480°C. This might be due to re-polymerizing of hydrocarbon molecules at 480°C which were degraded to ethylene monomer units at lower temperatures.

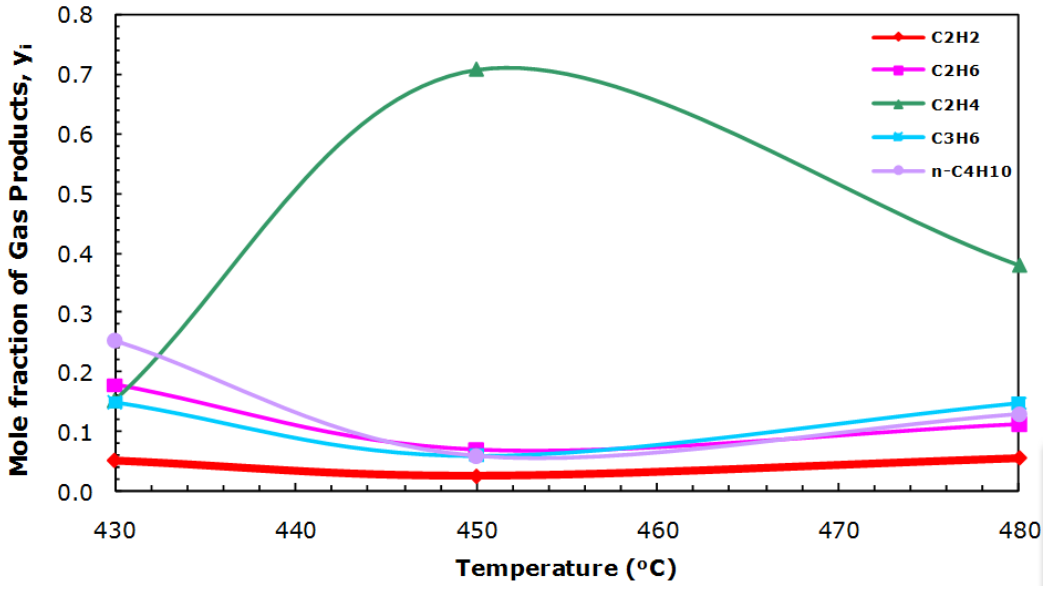

Figure 6.26. Mole fractions of gas products obtained from the non-catalytic degradation reactions performed at different temperatures (430°C, 450°C, & 480°C) for 10 min reaction time

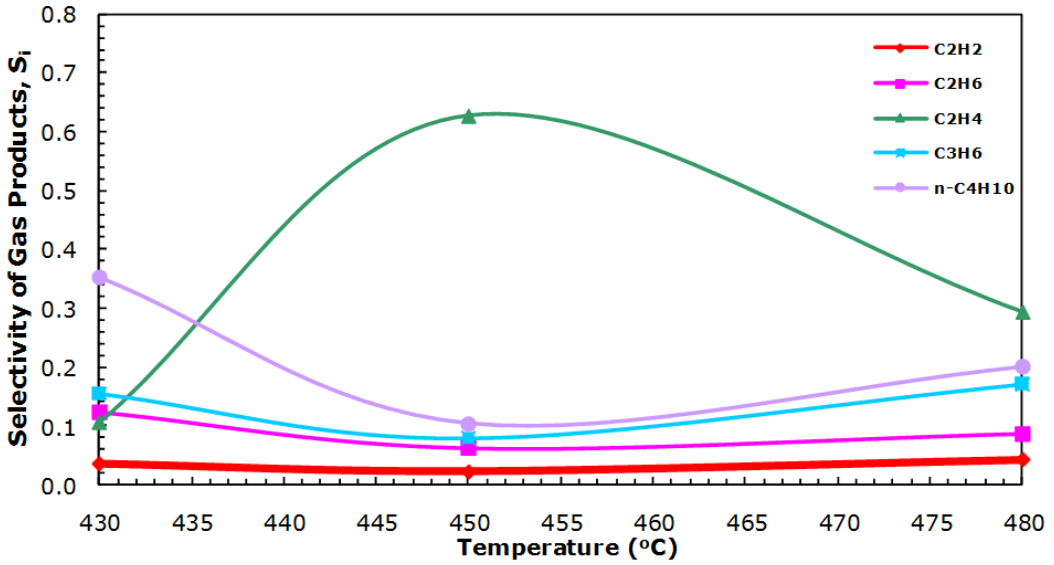

Figure 6.27. Selectivities of gas products obtained from the non-catalytic degradation reactions performed at different temperatures (430°C, 450°C, & 480°C) for 10 min reaction time

6.4.2.2 Gas Analysis of Catalytic Degradation Experiments

The effect of temperature on gaseous product distribution for catalytic degradation of polyethylene was observed by a set of experiments conducted at different temperatures. Mole fraction and selectivity of gas products obtained in the presence of SBA-0.40 catalysts are given in Figure 6.28 and 6.29. Mole and weight fractions and selectivity results of gas products obtained from the catalytic degradation of PE are tabulated in Appendix E. It was observed from these figures that maximum mole fraction of the gaseous products belongs to ethylene. Following ethylene, propylene (C_3H_6), n-butane (n-C_4H_{10}), i-butane (i-C_4H_{10}) and propane (C_3H_8) exhibited high mole fraction and selectivity values at lower temperatures. The fractions of these compounds decreased at higher temperatures and the amount of smaller hydrocarbon gas products increased. The increase in the fraction of lighter hydrocarbons, acetylene and ethane, was promoted by the higher degradation reaction temperature.

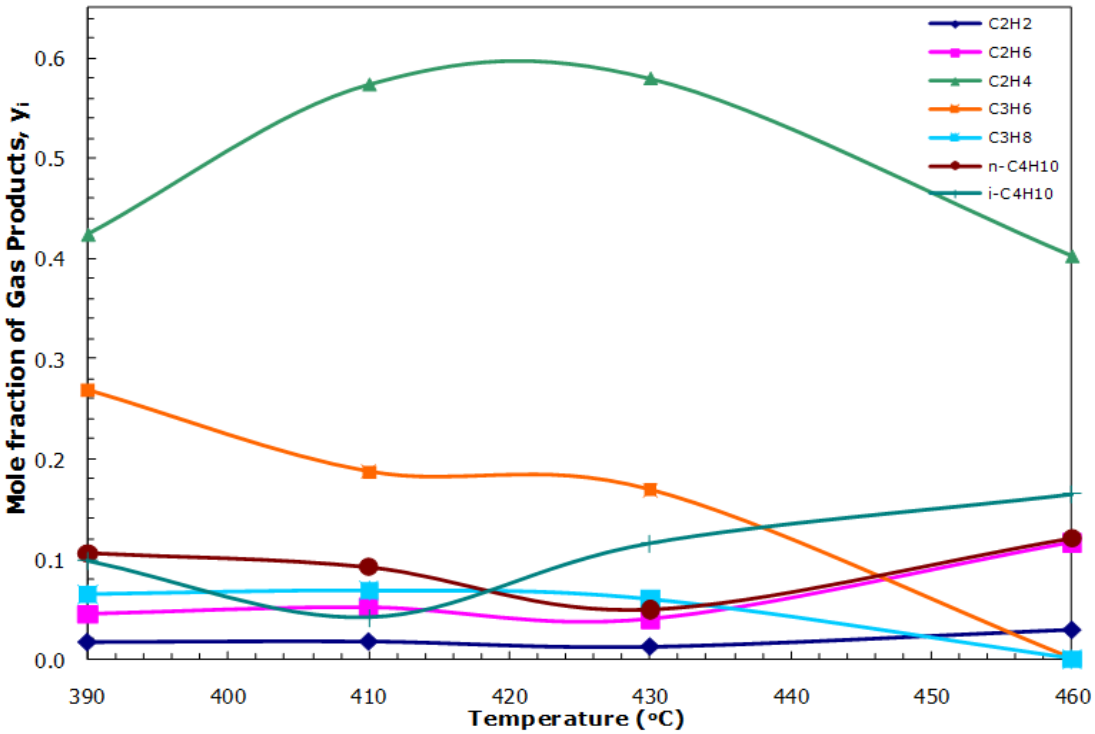

Figure 6.28. Mole fractions of gas products obtained from the degradation reactions performed using SBA-40 catalyst at different temperatures (390°C,410°C, 430°C, & 460°C) for 15 min reaction time

The decrease in the mole fraction and selectivity of C3 hydrocarbons, propane and propylene might be due to the effective decomposition of PE at higher reaction temperatures. The change in molar fraction and selectivity of C4 hydrocarbons (n-butane and i-butane) was considerable, since the fractions decreased to make a minimum and then increased to a higher level at 460°C. This might be due to the promoting effect of high reaction temperatures on the formation of C4 hydrocarbons.

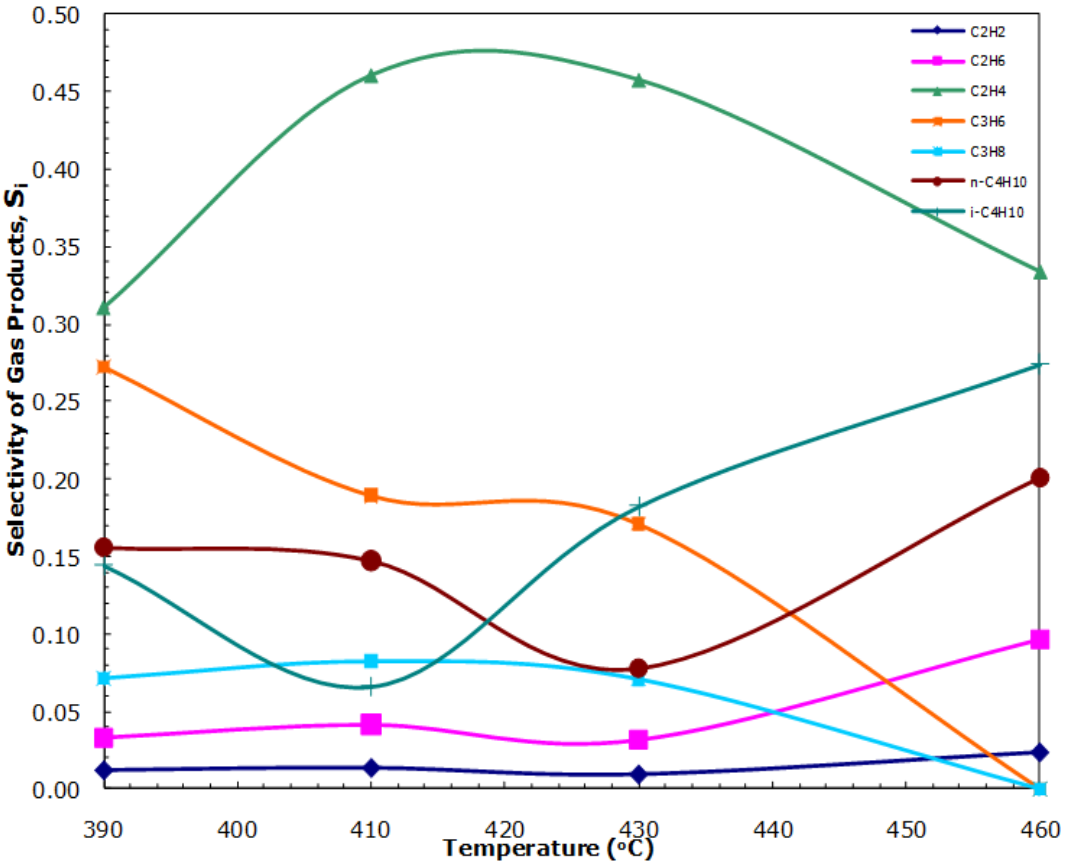

Figure 6.29. Selectivities of gas products obtained from the degradation reactions performed using SBA-40 catalyst at different temperatures (390°C, 410°C, 430°C, & 460°C) for 15 min reaction time

To observe the effect of acidity of the catalyst on PE degradation reactions, degradation experiments were conducted at the same temperature with different TPA loadings for SBA-15 catalysts and Al contents for MCM-41 catalysts. In Figures 6.30-6.33, the effect of TPA content on mole fraction and selectivity of gas products at two different temperatures are shown. At 390°C

(Figures 6.30 and 6.31) the highest fraction in the gas products was obtained for ethylene. Propylene and n-butane had also high fractions in the gas products obtained. The other gaseous products remained constant with TPA loading.

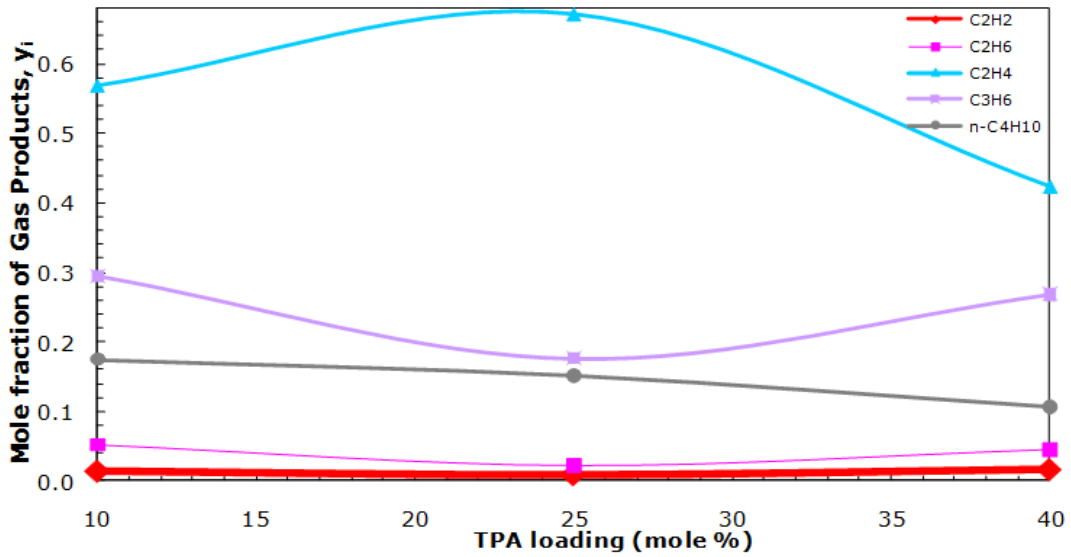

Figure 6.30. Mole fractions of gas products obtained from the degradation reactions performed at 390°C using SBA-15 catalysts with different TPA loadings for 15 min reaction time

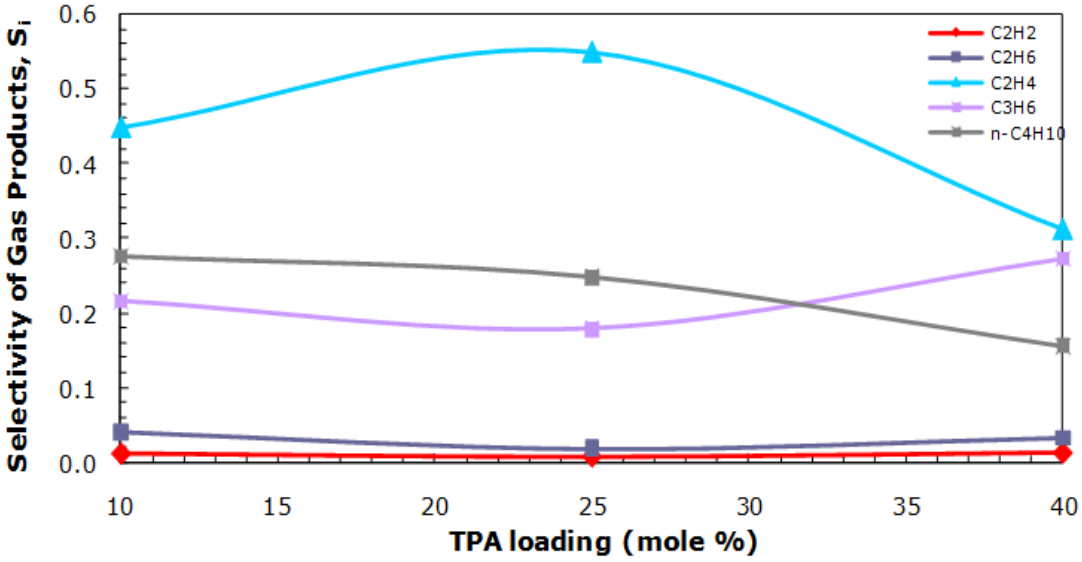

Figure 6.31. Selectivities of gas products obtained from the degradation reactions performed at 390°C using SBA-15 catalysts with different TPA loadings for 15 min reaction time

At 430°C (Figure 6.32-6.33), it was observed that the increase in the ethylene fraction was very significant. This was attributed to the more effective decomposition performance at high acidity levels combined with high reaction temperature. Mole fraction and selectivity values for C2 (acetylene and ethane) and C3 (propane and propylene) hydrocarbons remained almost constant at different TPA loadings. It was observed that mole fraction and selectivity of i-butane was increased and then reached a constant value and mole fraction and selectivitiy values of n-butane were increased and then decreased with more TPA loading.

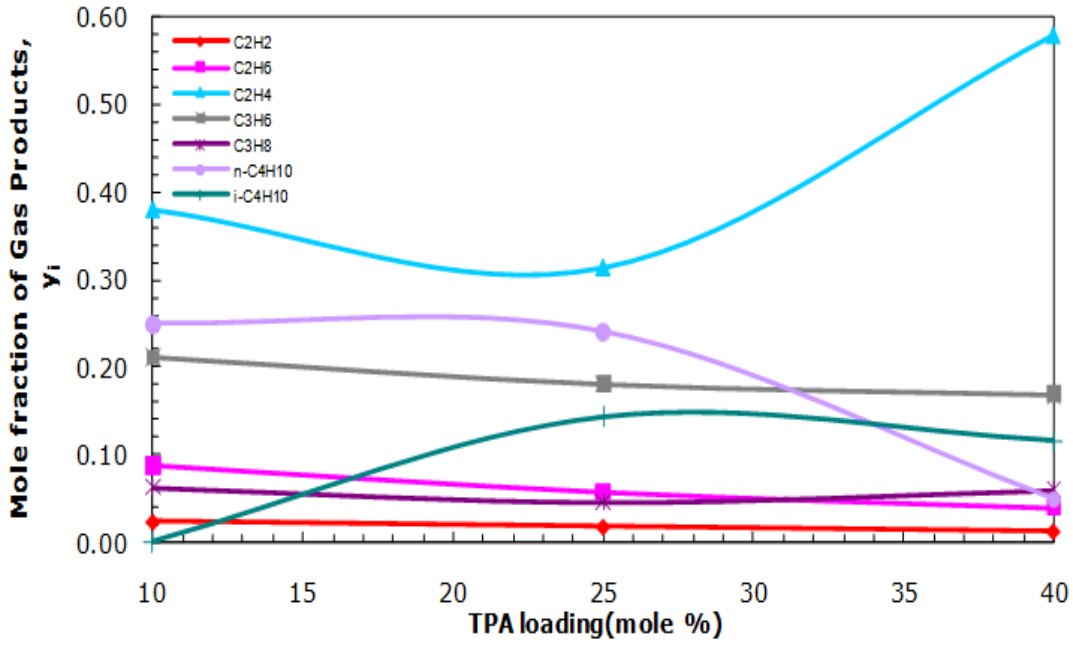

Figure 6.32. Mole fractions of gas products obtained from the degradation reactions performed at 430°C using SBA-15 catalysts with different TPA loadings for 15 min reaction time

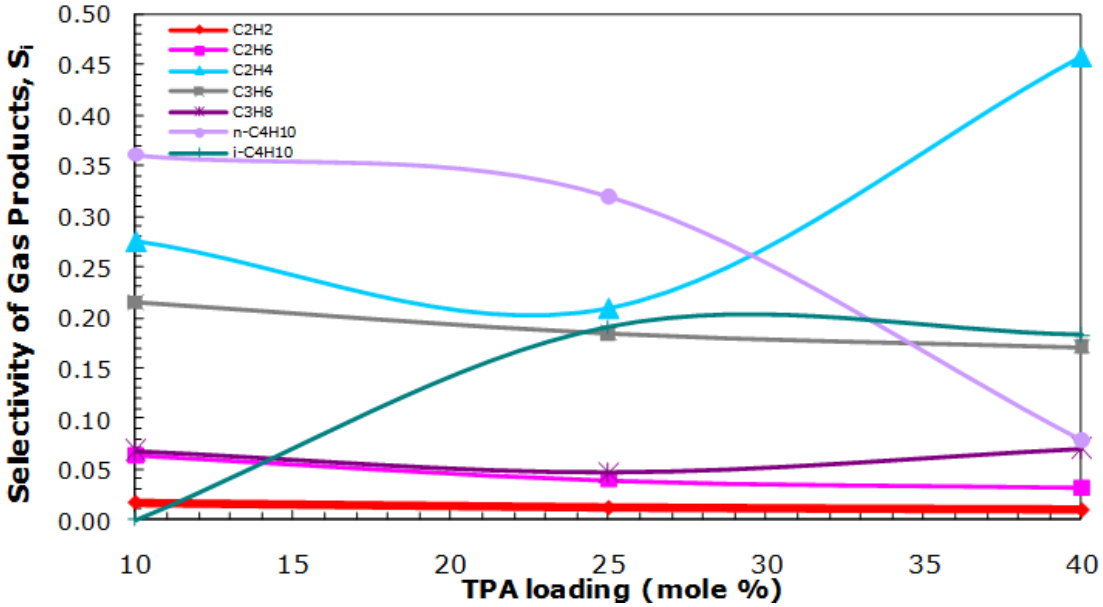

Figure 6.33. Selectivities of gas products obtained from the degradation reactions performed at 430°C using SBA-15 catalysts with different TPA loadings for 15 min reaction time

In Figures 6.34 and 6.35, the comparison of mole fractions and selectivities of gas products obtained from non-catalytic degradation experiment with that of gas products produced from catalytic degradation experiment conducted at 430°C for 15 min reaction time are given. It was observed for non-catalytic pyrolysis of PE that, the majority of the gas products obtained were composed of ethane (C_2H_6) C3 (C_3H_6 & C_3H_8) and C4 (n-C_4H_{10}) gases. On the other hand, for SBA-15 samples the mole fraction of ethylene (C_2H_4) was extremely high when compared to other gaseous products. With increasing TPA content, the amount of ethylene obtained was also increased and reached a maximum level for SBA-0.40 sample. The amount of ethane (C_2H_6), propylene (C_3H_6), and n-butane (n-C_4H_{10}) was also high and their mole fractions were decreased with the increase in the acid content. It was observed that for SBA-0.25 and SBA-0.40 samples the formation of i-butane (i-C_4H_{10}) was observed. For aluminum impregnated MCM-41 samples, the highest mole fractions and selectivites were obtained for n-butane, propylene and i-butane, respectively. When compared in terms of aluminum loading, it was observed that the mole fractions of propylene and n-butane remained constant but the mole fractions of ethylene, ethane and acetylene was increased. It was remarkable that the mole fraction of ethylene was very low when compared to SBA-15 materials.

According to these results, it was observed that TPA loaded SBA-15 materials were selective to ethylene, whereas aluminum loaded MCM-41 materials were selective to n-butane.

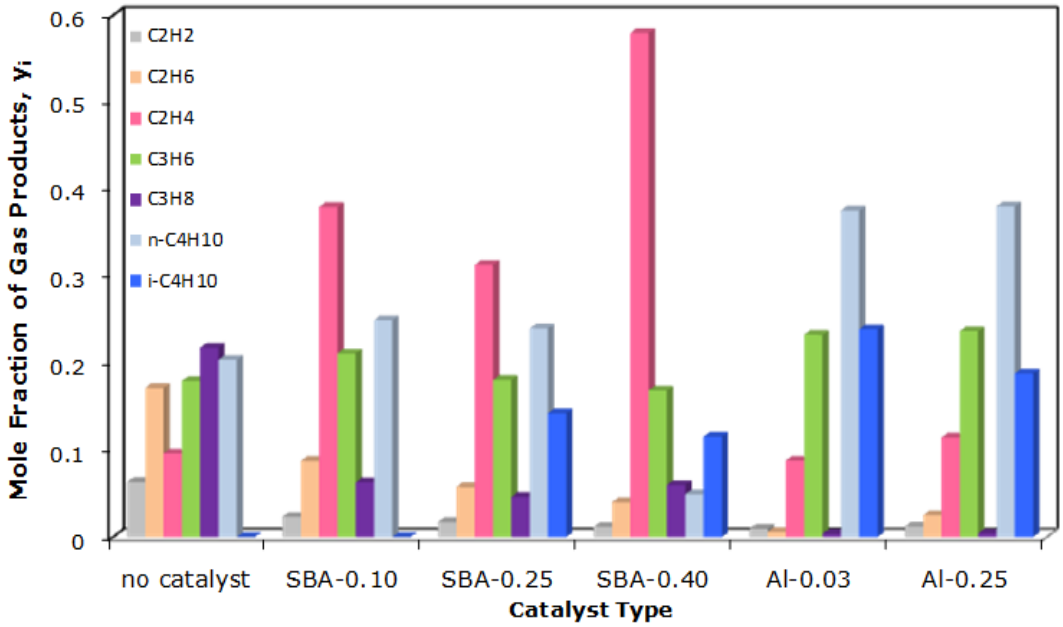

Figure 6.34. Comparison of gas product mole fractions obtained from the degradation reactions performed at 430°C non-catalytically and catalytically for 15 min reaction time

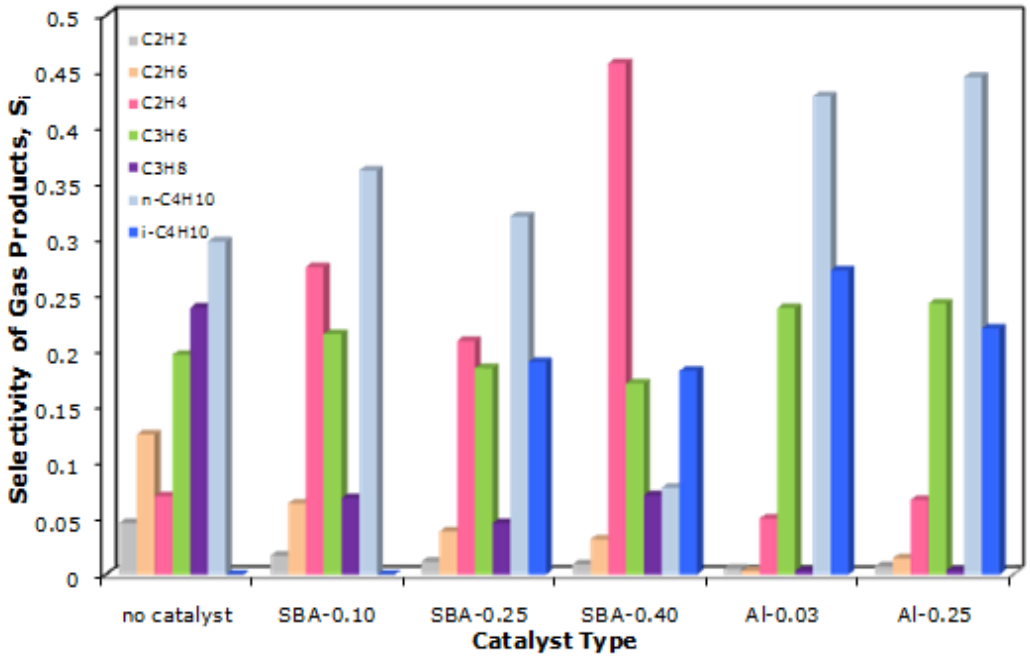

Figure 6.35. Comparison of gas product selectivities of obtained from the degradation reactions performed at 430°C non-catalytically and catalytically for 15 min reaction time

6.4.3 Liquid Analysis of Non-Catalytic and Catalytic Degradation Reactions

6.4.3.1 Liquid Results of Non-Catalytic Degradation Experiments

Liquid products were analyzed qualitatively and quantitatively using GC. For quantitative analysis, calibration factors for liquid products were determined. Calibration factor calculation for liquid products is given in Appendix F. Mole fraction and selectivity results of liquid products were tabulated in Appendix G.

Mole fraction and selectivity of liquid products obtained from non-catalytic degradation of polyethylene are given in Figure 6.36 and Figure 6.37, respectively. It was observed that at 430°C, the majority of the liquid products was greater than C14 and C18. C8-C10 range hydrocarbons had a small share in terms of mole fraction. At 450°C, the highest mole fraction was obtained for C8 hydrocarbons including diisobutylene (C_8H_{16}), n-octane

(C_8H_{18}), ethylbenzene (C_8H_{10}) m,p-xylene ($C_6H_4(CH_3)_2$ and o-xylene ($C_6H_4(CH_3)_2$. It was also remarkable that the fraction of C13, C14 and C18 hydrocarbons were decreased when compared with the results obtained at 430°C. At 480°C reaction temperature, it was observed that C10-C14 hydrocarbons' mole fractions were higher than those of 430°C and 450°C reaction temperatures. Mole fraction of C18 further decreased at 480°C, which was an expected result for higher degradation temperatures.

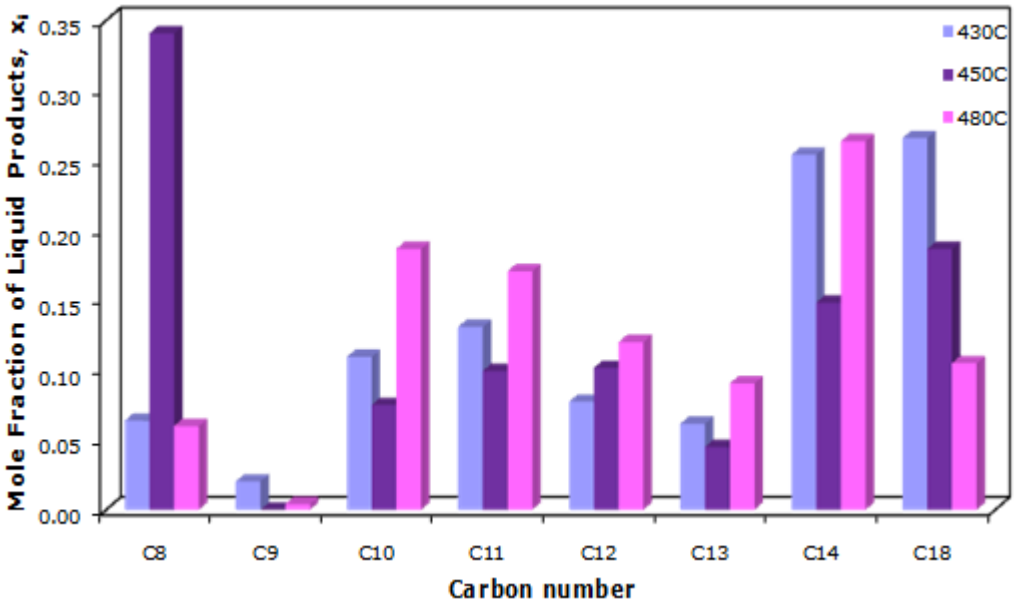

Figure 6.36. Mole fraction of liquid products obtained from the non-catalytic degradation reactions performed at different temperatures (430°C, 450°C, & 480°C) for 10 min reaction time

For non-catalytic thermal degradation experiments, it was observed that selectivity values are higher for higher molecular weight hydrocarbons, C14 and C18. Selectivities of C10-C13 were higher at 480°C degradation reaction temperature than at 430°C and 450°C temperatures. The selectivities of C9 hydrocarbons were very low for all temperatures, and selectivities of C8 hydrocarbons were relatively low when the total product amount was considered. No products lower than C8 was obtained in the liquid products of non-catalytic thermal degradation reactions and a broad range of hydrocarbons having high carbon numbers were obtained. Also, it was observed that hydrocarbons greater than C18 was obtained and with the

increase in reaction temperature, the amount of hydrocarbons greater than C18 was decreased.

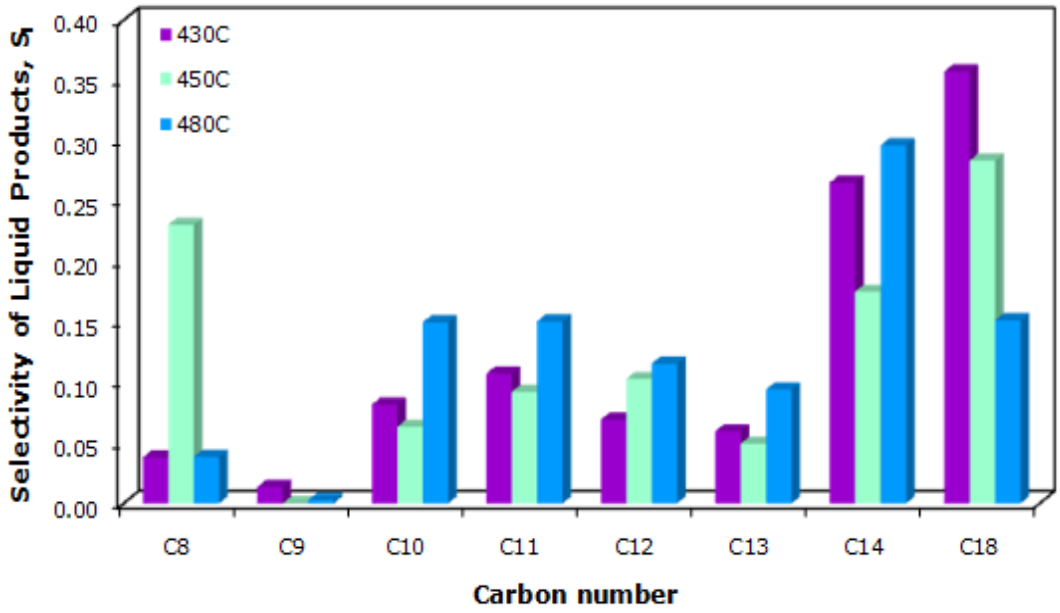

Figure 6.37. Selectivities of liquid products obtained from the non-catalytic degradation reactions performed at different temperatures (430°C, 450°C, & 480°C) for 10 min reaction time

6.4.3.2 Liquid Analysis of Catalytic Degradation Experiments

The effect of temperature change in catalytic degradation of polyethylene was observed by a set of experiments conducted at four different temperatures using SBA-40 catalyst. Mole fraction and selectivity results of liquid products are given in Appendix G. Mole fraction and selectivity of liquid products obtained from these experiments are given in Figure 6.38 and 6.39. First remarkable result when compared to non-catalytic pyrolysis experiments was the decrease in the fraction of C18 hydrocarbons. It was also observed that hydrocarbons greater than C18 were in trace amount and narrow range of product distribution was observed for all synthesized catalysts. This was attributed to the catalytic activity of the SBA-0.40 catalyst, resulting in a product distribution composed of lower carbon number hydrocarbons including C5, which was pentane (C_5H_{12}). Mole fractions of C10 and C11 were higher and mole fractions of C14 were lower at 460°C This showed that the increase in temperature enhanced the production of lower molecular weight

hydrocarbons and decreased the amount of higher molecular weight hydrocarbons. As seen from the figure, the fraction of C14 hydrocarbons decreased with the temperature increase and C18 hydrocarbons almost disappeared at higher temperatures. Mole fraction of n-pentane was found to be the highest for 430°C among four degradation reaction temperatures.

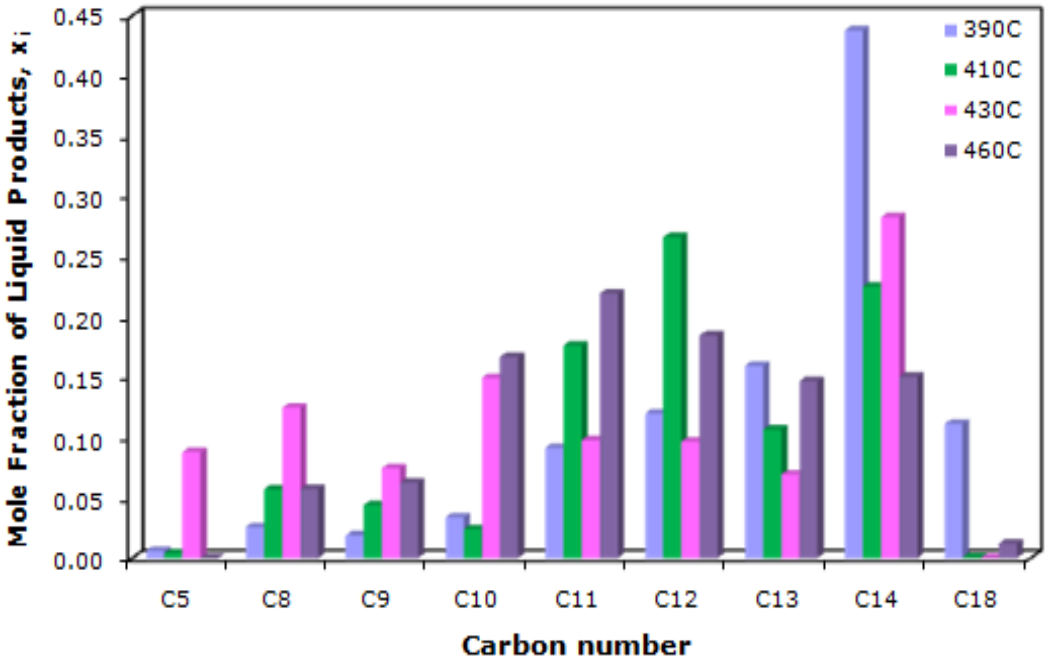

Figure 6.38. Mole fractions of liquid products obtained from the degradation reactions performed using SBA-0.40 catalyst at different temperatures (390°C,410°C, 430°C, & 460°C) for 15 min reaction time

Selectivity of C13 and C14 hydrocarbons at 390°C was the highest ones when compared to the other liquid products. On the other hand, the highest selectivity value was obtained for C12 at 410°C and for C11 at 430°C. This result showed that the increase in temperature resulted in a product distribution more close to gasoline range (C5-C12). Similarly, it was observed that the selectivity values of C9-C11 was increased with increasing reaction temperature. The selectivity of C18 hydrocarbons was decreased below 0.05 for 410, 430 and 460 °C reaction temperatures.

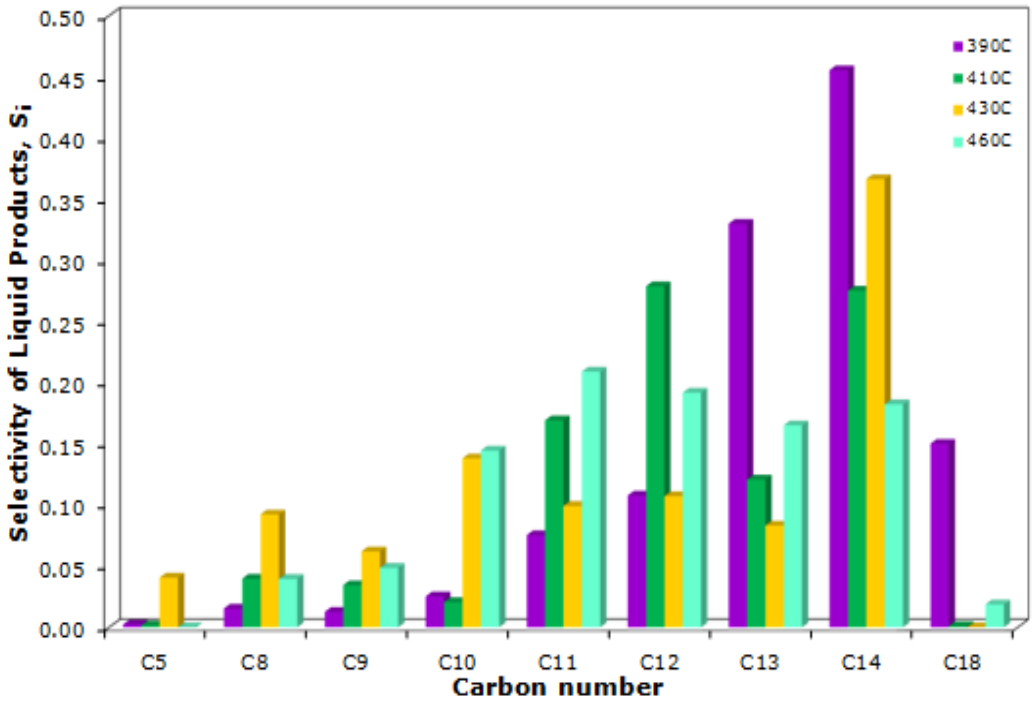

Figure 6.39. Selectivities of liquid products obtained from the degradation reactions performed using SBA-0.40 catalyst at different temperatures (390°C, 410°C, 430°C, & 460°C) for 15 min reaction time

To observe the effect of acidity of the catalyst on PE degradation reactions, degradation experiments were conducted at the same temperature with different TPA loadings for SBA-15 catalysts. In Figures 6.40-6.43, the effect of TPA content on mole fraction and selectivity of liquid products at two different temperatures are shown. At 390°C the mole fraction of C14 hydrocarbons was highest for 40% TPA loaded SBA-15 materials. For 25 % TPA loaded SBA-15 materials the majority of the product distribution was composed of C8, C12 and C14 hydrocarbons. For 10 % TPA loaded SBA-15 materials, C12-C14 hydrocarbons had the major share in the liquid hydrocarbon product distribution. According to these results, it was observed that at 390°C the formation of C8-C14 liquid hydrocarbons was enhanced. The increase in TPA loading resulted in a decrease in C5 and C10 hydrocarbons. In Figure 6.41, it was seen that 40 % TPA loaded SBA-15 caused a decrease in selectivities of C8-C12 hydrocarbons, when compared with 25 % TPA loaded SBA-15 materials.

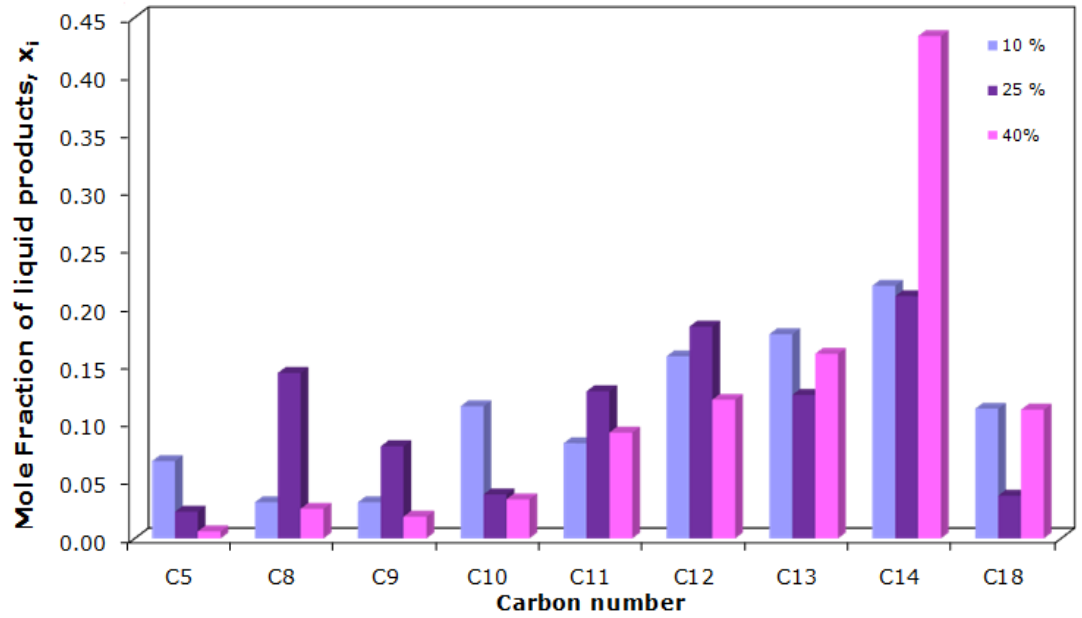

Figure 6.40. Mole fractions of liquid products obtained from the degradation reactions performed at 390°C using SBA-15 catalysts with different TPA loadings

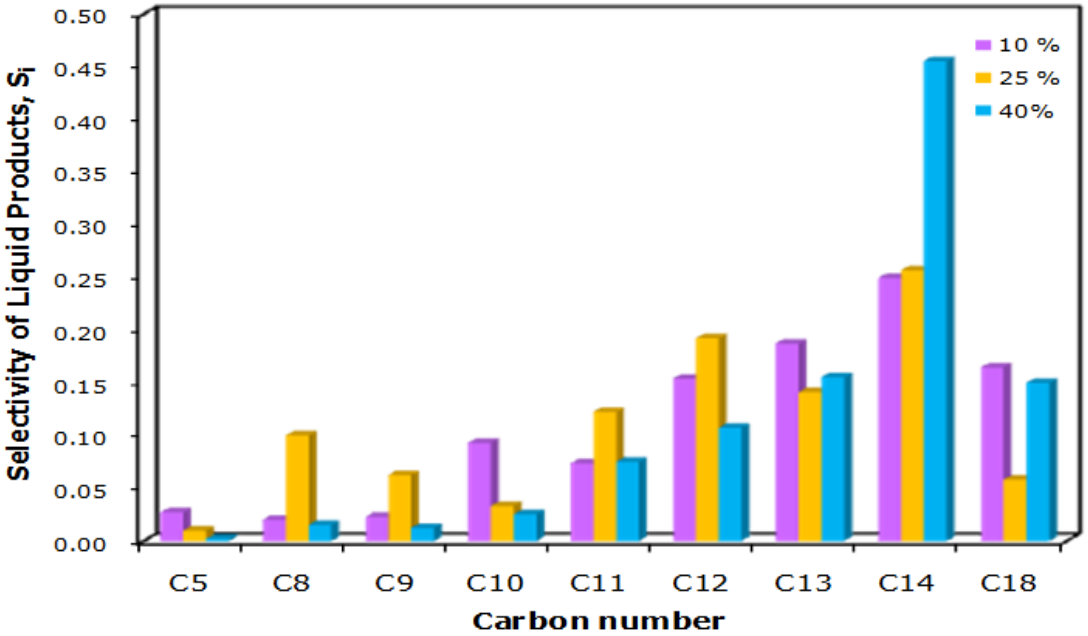

Figure 6.41. Selectivities of liquid products obtained from the degradation reactions performed at 390°C using SBA-15 catalysts with different TPA loadings

At 430°C (Figure 6.42-6.43), it was observed that the lower molecular weight hydrocarbons were obtained when compared with the results of degradation reactions at 390°C carried out with TPA loaded SBA-15 catalysts. C5-C10 range hydrocarbon mole fractions were higher at 40% TPA loading when compared to 10% and 25% TPA loaded SBA-15 materials. This showed the effect of higher acidity enhancing lower molecular weight products. Mole fractions C11-C13 was decreased with 40% TPA loaded SBA-15 catalysts. The majority of the mole fraction values belonged to C11-C14 hydrocarbons for 10% and 25% TPA loaded catalysts, whereas C5, C8, C10 and C14 hydrocarbons had the greatest share of the product distribution for the reactions carried out using SBA-0.40 catalyst. The increase in the mole fraction of C5 (pentane) at 40% TPA loading was also remarkable when the effect of acidity was concerned. When the selectivity of liquid hydrocarbons obtained at 430°C was considered (Figure 6.43), it was observed that there is a remarkable increase in C5, C8, C9 and C14 hydrocarbons and a decrease in C18 hydrocarbons for 40 % TPA loaded SBA-15 material. It was also observed that the liquid hydrocarbon selectivities for all TPA loaded catalysts were obtained in the range of C10-C14 mainly.

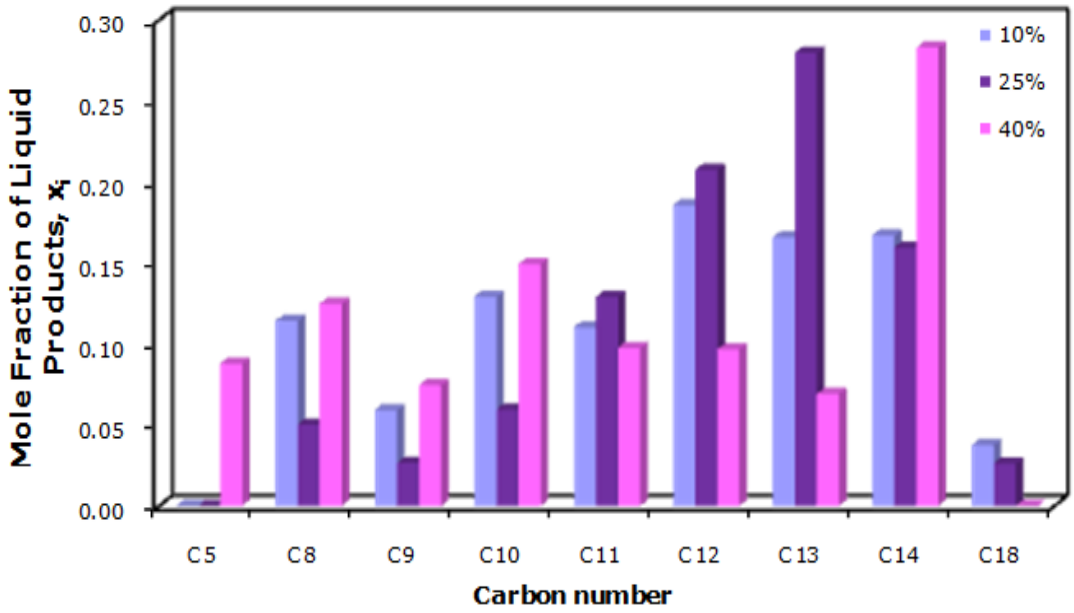

Figure 6.42. Mole fractions of liquid products obtained from the degradation reactions performed at 430°C using SBA-15 catalysts with different TPA loadings

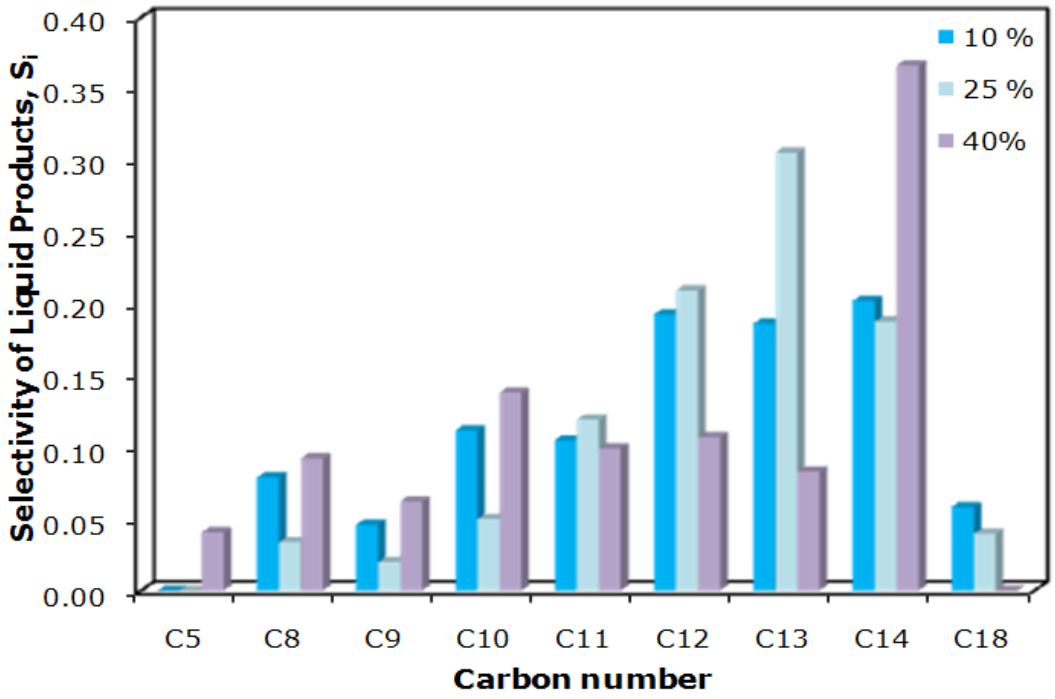

Figure 6.43. Selectivities of liquid products obtained from the degradation reactions performed at 430°C using SBA-15 catalysts with different TPA loadings

In Figures 6.44 and 6.45 the comparison of mole fractions and selectivities of liquid products obtained from non-catalytic and catalytic degradation reactions conducted at 430°C for 15 min reaction time are given. For non-catalytic degradation reaction, it was observed that mole fractions of heavier hydrocarbons were higher than others. For TPA imregnated samples, mole fractions of C5 and C14 were increased with the increase in TPA content. Mole fractions of C12, C13 and C18 hydrocarbons, are decreased to very low fraction for 40 % TPA loaded SBA-15 samples. For aluminum loaded MCM-41 materials on the other hand, mole fractions of C5 and C8 hydrocarbons were very high when compared to other liquid hydrocarbons. With the increase in aluminum content of these samples, mole fractions of C5 and C8 hydrocarbons were also increased, which was attributed to the increase in Bronsted acid sites in the material. The increase in Bronsted acid sites enhanced the production of lower molecular weight hydrocarbons, which are in the gasoline range (C_4-C_{12}). The increase in aluminum content resulted in a

decrease in the mole fraction and selectivities of C10-C18 hydrocarbons, shifting the product distribution to the favor of lighter liquid hydrocarbon products. Hydrocarbon liquid selectivity results (Figure 6.45) exhibited differences for non-catalytic and catalytic degradation of polyethylene. For non catalytic thermal degradation it was observed that the majority of liquid products obtained were in the range above C14 hydrocarbons and hydrocarbon fractions greater than C18 were also present. For TPA loaded SBA-15 materials, the liquid product selectivity range was shifted towards C8-C14 region. The selectivity of C10-C13 compounds was higher for SBA15-0.10 and SBA15-0.25 materials when compared to SBA15-0.40. For aluminum loaded MCM-41 materials, the liquid product selectivity was observed in the range C5-C13 mainly. For higher aluminum loading, it was observed that the selectivity of C5 and C8 hydrocarbons were increased and C13-C18 hydrocarbons were decreased.

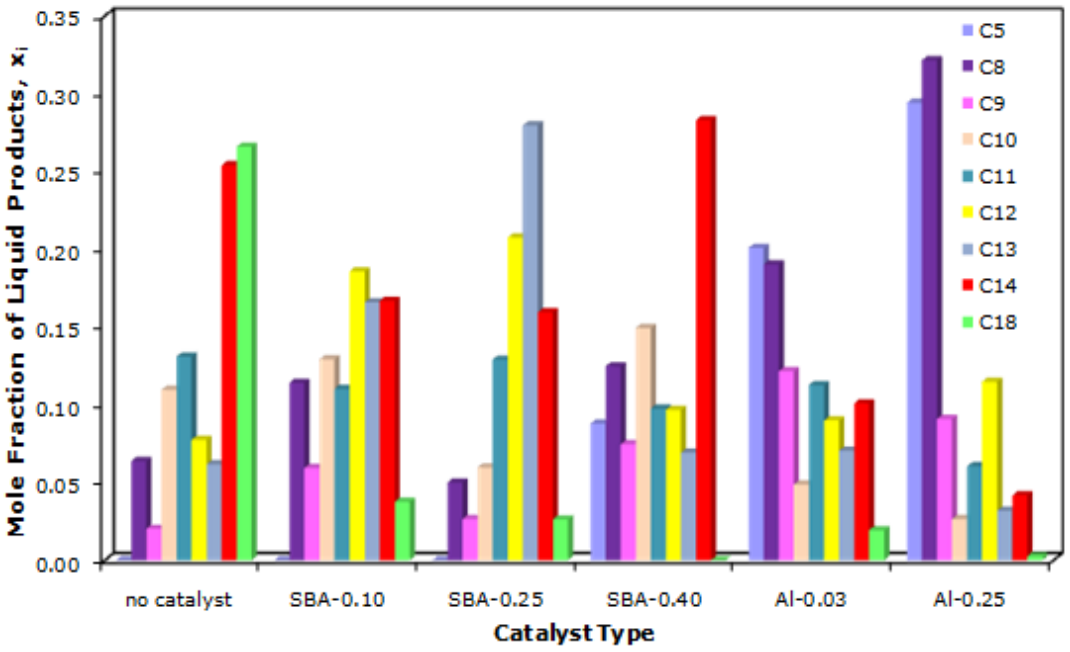

Figure 6.44. Comparison of liquid product mole fractions obtained from the degradation reaction performed at 430°C non-catalytically and catalytically for 15 min reaction time

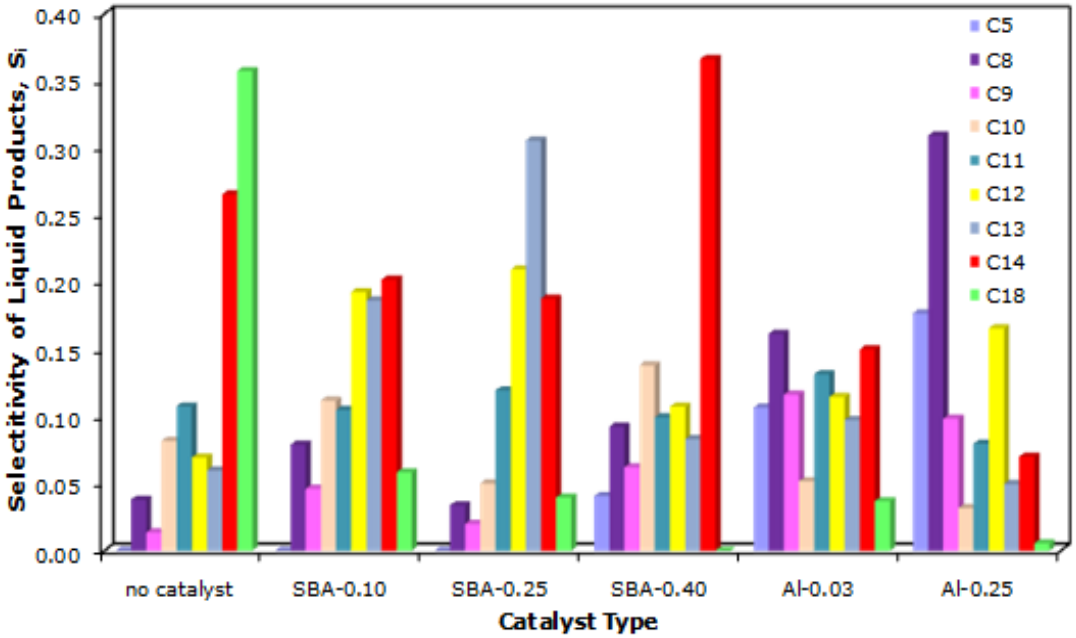

Figure 6.45. Comparison of liquid product selectivities obtained from the degradation reactions performed at 430°C non-catalytically and catalytically for 15 min reaction time

In Figures 6.46 and 6.47, the comparison of liquid product mole fractions and selectivities obtained from catalytic degradation reactions conducted at 390°C for 15 min reaction time are given. At this reaction temperature, liquid product distribution of PE degradation reaction was different from the product distribution at 430°C. For TPA loaded SBA-15 materials, it was observed that mole fractions of C14 hydrocarbons were remarkably increased. On the other hand, mole fractions of lower molecular weight hydrocarbons exhibited a decreasing trend with the increase of acidity. For aluminum loaded MCM-41 materials, mole fractions of C8, C11 and C12 hydrocarbons increased with increasing aluminum content. A remarkable decrease in the mole fraction of C14 hydrocarbons was observed with the increase of acid content of the material. When two reaction temperatures were compared, it was observed that all the catalysts showed a better catalytic activity at 430°C in terms of the liquid product distributions obtained from the analysis of products using GC. At 390°C selectivity results of liquid hydrocarbons for catalytic degradation of polyethylene performed using TPA loaded SBA-15 materials

and aluminum loaded MCM-41 materials exhibited differences (Figure 6.47). The liquid product distribution of catalytic degradation experiments conducted using TPA loaded SBA-15 materials was obtained in the range of C10-C18 majorly. For 10% and 25% TPA loaded SBA-15 materials, this range was narrowed down to C11-C14 mainly. When the selectivity results of aluminum loaded MCM-41 samples were observed, it was seen that the selectivity of C18 hydrocarbons was very low and the product distribution was shifted to C8-C14 range. It was also oserved that the selectivity of C8 hydrocarbons was increased and selectivity of C14 hydrocarbons was decreased with increasing aluminum content.

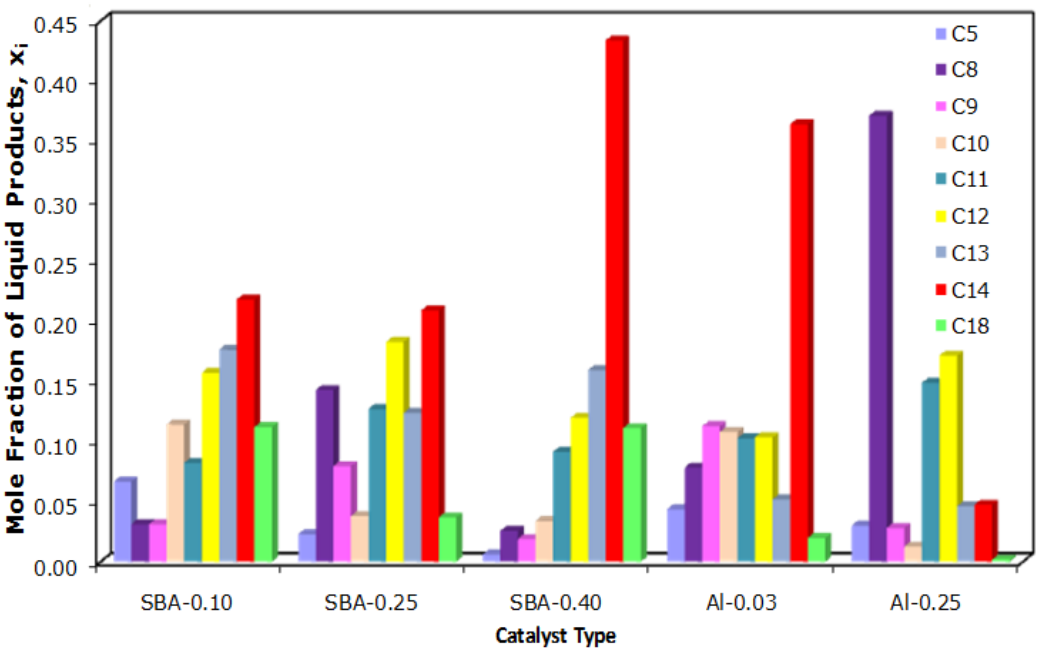

Figure 6.46. Comparison of liquid product mole fractions obtained from the degradation reactions performed at 390°C catalytically for 15 min reaction time

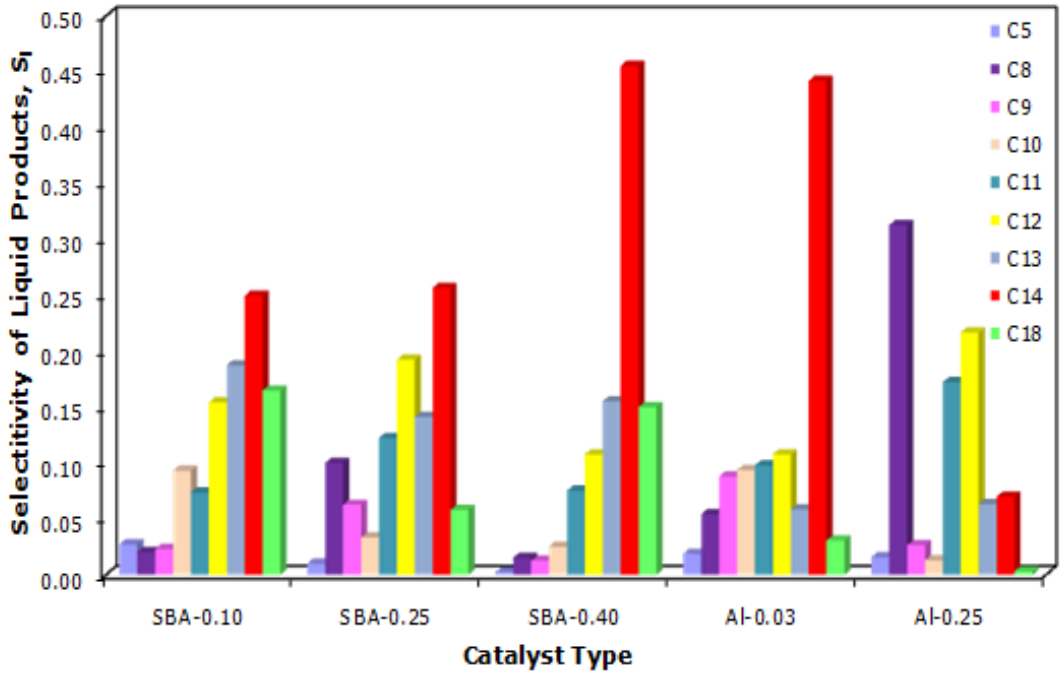

Figure 6.47. Comparison of liquid product selectivities obtained from the degradation reactions performed at 390°C catalytically for 15 min reaction time

CONCLUSIONS

In this study, aluminum containing MCM-41 and TPA loaded SBA-15 materials were synthesized to be used in catalytic degradation reactions of polyethylene. Characterization techniques were effective in understanding the structural properties of the synthesized materials.

XRD analysis of the synthesized materials showed that the regularly ordered structures were not distorted with the addition of aluminum and TPA into the structure. For aluminum containing MCM-41 samples, it was observed that at lower Al/Si ratios, the incorporation was more efficient. For SBA-15 samples, even at high TPA loadings, the incorporation was successful. SEM and TEM images of the synthesized materials revealed the hexagonal, regularly ordered honeycomb pore structures of the synthesized materials. Nitrogen adsorption and desorption analysis showed that the synthesized materials exhibited Type IV isotherms. The surface area of pure and aluminum loaded MCM-41 samples were in the range of 1031-1290 m^2/g and the surface area of pure and TPA containing SBA-15 samples were in the range of 212-825 m^2/g, respectively. Pore size distribution of the synthesized materials revealed their mesoporosity. The average pore sizes of aluminum loaded MCM-41 and TPA impregnated SBA-15 samples were approximately 2.5 nm and 6.5 nm, respectively. ^{27}Al-NMR spectra of aluminum containing MCM-41 materials exhibited octahedrally and tetrahedrally coordinated aluminum species in the structure. DRIFTS analysis of the pyridine adsorbed materials revealed the existence of Bronsted acid sites in the synthesized catalysts in addition to Lewis acid sites.

By thermogravimetric analysis, it was observed that aluminum loaded MCM-41 materials did not caused a significant change in the activation energy of the PE degradation reaction, but TPA modified SBA-15 materials reduced the activation energy effectively. Aluminum impregnated MCM-41 materials on

the other hand, significantly reduced the degradation temperature of PE compared to TPA loaded SBA-15 materials.

Non-catalytic and catalytic degradations of polyethylene were performed in the degradation reaction system. Products were gas and liquid hydrocarbons. Solid residue was also observed at low temperature for non-catalytic degradation reactions. Product yield of non-catalytic degradation reactions was majorly composed of liquids which were obtained in a gel-like form, and the liquid product yield was increased with an increase in reaction temperature. In catalytic degradation reactions carried out using TPA loaded SBA-15 catalysts, the liquid yields were lower and gas yields were higher when compared to non-catalytic pyrolysis product yields. In these reactions performed with SBA-0.40 materials, the liquid product yield increased with the increasing reaction temperature. Increase in TPA loading also increased the liquid product yield, which was due to increase in the acidic content of the material. Catalytic degradation reactions performed using aluminum loaded MCM-41 samples resulted in a product yield of high amount of gases and lower amount of liquids similar to the results obtained for TPA loaded SBA-15 materials. The yield of liquid products were increased with increasing reaction temperature and aluminum loading as well.

The analysis of gaseous products showed that, in non-catalytic degradation of polyethylene, selectivities of C3 and C4 hydrocarbons were very high. The increase in reaction temperature resulted in an increase in selectivity of lower molecular weight hydrocarbons in non-catalytic pyrolysis of PE. In catalytic degradation reactions, it was observed that aluminum loaded MCM-41 materials were selective to higher molecular weight gaseous products; propylene, n-butane and iso-butane On the other hand in catalytic degradation reactions performed using TPA loaded SBA-15 materials, the selectivities of ethylene and n-butane was very high. The maximum ethylene selectivity was obtained for SBA-0.40 material at 430^{o}C reaction temperature.

Analysis of the liquid products showed that, in the non-catalytic degradation reactions, liquid product selectivity of hydrocarbons greater than C18 was high. As the degradation reaction temperature was increased, the selectivity

of these compounds was decreased, shifting the product distribution towards lower molecular weight hydrocarbons was observed. Liquid analysis of the pyrolysis reactions performed using TPA loaded SBA-15 samples were evaluated in terms of reaction temperature and in terms of TPA loading separately. At 390^{o}C reaction temperature, it was observed that selectivity of C14 hydrocarbons was remarkably increased and selectivity of lower molecular weight hydrocarbons exhibited a decreasing trend with the increase of acidity for TPA loaded SBA-15 materials. For aluminum loaded MCM-41 materials, selectivity of C8, C11, and C12 hydrocarbons was increased and selectivity of C14 hydrocarbons was decreased remarkably with the increase in aluminum content of the material. At 430^{o}C reaction temperature, selectivities of C5, C8, C10, and C14 hydrocarbons were increased and selectivities of C12, C13, and C18 were decreased with the increase in TPA loading. For aluminum loaded MCM-41 materials, at 430^{o}C reaction temperature, selectivities of C5 and C8 hydrocarbons were obtained very high when compared to other liquid hydrocarbons. With the increase in aluminum content of these samples, mole fractions of C5 and C8 hydrocarbons were also increased. For both catalysts, the liquid product distribution was shifted to a range of hydrocarbons lower than C18 and it was concluded that the increase in Bronsted acid sites enhanced the production of lower molecular weight hydrocarbons, which are in the gasoline range (C_4-C_{12}). For TPA loaded SBA-15 materials liquid products were distributed in a range of C8 to C14 and for aluminum loaded MCM-41 samples liquid products were distributed in a range of C5-C14. According to these results, both catalysts enhanced the production of gasoline range hydrocarbons.

REFERENCES

Aguado, J., Sotelo, J.L., Serrano, D.P., Calles, J.A., and Escola, J.M.(1997). "*Catalytic Conversion of Polyolefins into Liquid Fuels over MCM-41: Comparison with ZSM-5 and Amorphous SiO_2-Al_2O_3"*, Energy&Fuels **11**, p.1225-1231.

Aguado, J., Serrano, D.P., San Miguel, G., Escola, J. M., Rodriguez, J.M. (2007) *"Catalytic activity of zeolitic and mesostructured catalysts in the cracking of pure and waste polyolefins*, J. Anal. Appl. Pyrolysis **78**, p.153-161.

Akpanudoh, N. S., Gobin, K., Manos, G. (2005) *"Catalytic degradation of plastic waste to liquid fuel over commercial cracking catalysts: Effect of polymer to catalyst ratio/acidity content"*, Journal of Molecular Catalysis A: Chemical **235**, p.67-7.

Beck, J. S., Vartuli, J.C., Roth, W.J., Leonowicz, M.E., Kresge, C.T., Schmitt, K.D., Chu, C.t-W., Olson, D.H., Sheppard, E.W., McCullen, S.B., Higgins, J.B., Schlenker, J.L. (1992). "*A New Family of Mesoporous Molecular Sieves Prepared with Liquid Crystal Templates*", J. Am. Chem. Soc. **114**, p.10834-10843.

Bhaskar, T., Uddin, M. A., Murai, K., Kaneko, J., Hamano, K., Kusaba, T., Muto, A., Sakata, Y. (2003). *"Comparison of thermal degradation products from real municipal waste plastic and model mixed plastics"*, J. Anal. Appl. Pyrolysis **70**, p.579-587.

Biz, S. and White, M. G. (1999). *"Syntheses of aluminosilicate mesostructures with high aluminum content"*, J. Phys. Chem. B, **103**, p.8432–8442.

Brodie-Linder, N., Dosseh, G., Alba-Simonesco, C., Audonnet, F., Impéror-Clerc, M, (2008).“*SBA-15 synthesis: Are there lasting effects of temperature change within the first 10 min of TEOS polymerization?”,* Materials Chemistry and Physics **108**, p.73-81.

Cesteros, Y., Haller, G.L. (2001) “*Several factors affecting Al-MCM-41 synthesis*”, Microporous and Mesoporous Materials **43**, p.171-179

Chaianansutcharit, S., Katsutath, R., Chaisuwan, A., Bhaskar, T., Nigo, A., Muto, A., Sakata, Y. (2007). “*Catalytic degradation of polyolefins over hexagonal mesoporous silica: Effect of aluminum addition*”, J. Anal. Appl. Pyrolysis **80**, p.360-368.

Ciesla, U., Schüth, F. (1999). “*Ordered mesoporous materials*”, Microporous and Mesoporous Materials **27**, p.131-149.

Coats, A.W., Redfern, J.P. (1964).*“Kinetic parameters from thermogravimetric data”*, *Nature* **201**, p.68-69.

Corma, A. (1995) “*Inorganic Solid Acids and Their Use in Acid-Catalyzed Hydrocarbon Reactions*”, Chem. Rev. **95**, p.559-614.

Dufaud, V., Lefebvre, F., Niccolai, G. P., Aouie M. (2009). *“New insights into encapsulation and stabilization of heteropolyacids inside the pore walls of mesostructured silica materials”*, Journal of Materials Chemistry **19**, p. 1142-1150.

Eimer, G. A., Pierella, L. B., Monti, G. A., and Anunziata, O. A. (2003). *“Preparation and characterization of aluminum-containing MCM-41”*, Catal. Commun., **4**, p.118–123.

Fulvio, P. F., Pikus, S., Jaroniec, M. (2005) “*Short-time synthesis of SBA-15 using various silica sources*”, Journal of Colloid and Interface Science **287**, p.717-720.

Garforth, A., Fiddy, S., Lin, Y.-H., Ghanbari-Siakhali, A., Sharatt, P.N., Dwyer, J. (1997) "*Catalytic degradation of high density polyethylene: An evaluation of mesoporous and microporous catalysts using thermal analysis*", Thermochimica Acta **294**, p.65-69.

Güçbilmez, Y., (2005) "*Vanadium and Molybdenum Incorporated MCM-41 Catalysts for Selective Oxidation of Ethanol*", MSc Thesis, Middle East Technical University, Ankara, Turkey.

He, N. Woo, C., Kim, H., Lee, H. (2005) *"Catalytic formation of acetic anhydride over tungstophosphoric acid modified SBA-15 mesoporous materials"*, applied Catalysis A: General **281**, p.167-178.

Holmes,S. M., Zholobenko V. L., Thursfield, A., Plaisted, R. J., Cundy, C. S., Dwyer, J. (1998) *"In situ FTIR study of the formation of MCM-41"*, J. Chem. Soc. **94**, p.2025-2032.

Isoda, T., Nakahara, T., Kusakabe, K., Shigeharu, M. (1998). "Catalytic Cracking of Polyethylene-Liquefied Oil over Amorphous Aluminosilicate Catalysts", Energy&Fuels **12**, p.1161-1167.

Jalil, P.A. (2002). *"Investigations on polyethylene degradation into fuel oil over tungstophosphoric acid supported on MCM-41 mesoporous silica"*, J. Anal. Appl. Pyrolysis **65**, p.185-195.

Jana, S. K., Takahashi, H., Nakamura, M., Kaneko, M., Nishida, R., Shimizu, H., Kugita, T., Namba, S. (2003). "*Aluminum incorporation in mesoporous MCM-41 molecular sieves and their catalytic performance in acid-catalyzed reactions*", Applied Catalysis A: General **245**, p. 33-41.

Kaminsky, W., Zorriqueta I.N., (2007) *"Catalytical and thermal pyrolysis of polyolefins",* J. Anal. Appl. Pyrolysis **79**, p.368-374.

Kozhevnikov, I.V. (1998). *"Catalysis by Heteropoly Acids and Multicomponent Polyoxometalates in Liquid-Phase Reactions"*, Chem. Rev. **98**, p.171-198.

Kresge, C. T., Leonowicz, M. E., Roth, W. J., Vartuli, J. C., Beck, J. S. (1992). "*Ordered mesoporous molecular sieves synthesized by a liquid-crystal template mechanism*", Nature **359**, p.710-712.

Kumar, G. S., Vishnuvarthan, M., Palanichamy, M., Murugesan, V. (2006). *"SBA-15 supported HPW: Effective catalytic performance in the alkylation of phenol"*, Journal of Molecular Catalysis A: Chemical, **260**, p.49-55.

Liu, Q., Wu, W., Wang, J., Ren, X., Wang, Y. (2004) "*Characterization of 12-tungstophosphoric acid impregnated on mesoporous silica SBA-15 and its catalytic performance in isopropylation of naphthalene with isopropanol",* Microporous and Mesoporous Materials **76**, p 51-60.

Luan, Z., Cheng, C., Zhou, W., Klinowski, J. (1995) "*Mesopore Molecular Sieve Containing Framework Aluminum*", J. Phys. Chem. **99**, p. 1018-1024.

Marcilla, A., Gómez, A., García, A.N., Olaya, M. M. (2002). *"Kinetic study of the catalytic decomposition of different commercial polyethylenes over an MCM-41 catalyst"*, J. Anal. Appl. Pyrolysis **64**, p.85-101.

Miskolczi, N., Bartha, L., Deák, G., Jóver, B., Kalló, D. (2004) "*Thermal and thermo-catalytic degradation of high-density polyethylene waste*", J. Anal. Appl. Pyrolysis **72**, p.235-242.

Obalı, Z., Sezgi, N. A., Doğu, T. (2009) "Performance of Acidic MCM-like Aluminosilicate Catalysts in Pyrolysis of Polypropylene", Chem. Eng. Comm. **196**, p.116-130.

Obalı, Z. (2010) *"Synthesis of Aluminum Incorporated Mesoporous Catalysts for Pyrolysis of Polypropylene"*, MSc Thesis, Middle East Technical University, Ankara, Turkey.

Ohkita, H., Nishiyama, R., Tochihara, Y., Mizushima, T., Kakuta, N., Morioka, Y., Ueno, A., Namiki, Y., Tanifuji, S., Katoh, H., Sunazuka, H., Nakayama, R., Kuroyanagi, T. (1993) "*Acid Properties of Silica-Alumina Catalysts and Catalytic Degradation of Polyethylene*", Ind. Eng. Chem. Res. **32**, p.3112-3116.

Palcheva, R., Spojakina, A., Dimitrov, L., Jiratova, K. (2009) *"12-Tungstophosphoric heteropolyacid supported on modified SBA-15 as catalyst in HDS of thiophene"*, Microporous and Mesoporous Materials **122**, p.128-134.

Peterson, J. D.; Vyazovkin, S.; Wight, C. A. (2009) *"Kinetics of the Thermal and Therno-Oxidative Degradation of Polystyrene Polyethylene and Poly(propylene)"*, Macromol. Chem. Phys. **202**, p.775-784.

Roth, W. J. and Vartuli, J. R. (2005) "*Synthesis of mesoporous molecular sieves*", Studies in Surface Science and Catalysis **157**, p.91-110.

Sakata, Y., Uddin, M. A., Muto, A., Kanada, Y., Koizumi, K., Murata, K. (1997). "*Catalytic degradation of polyethylene into fuel oil over mesoporous silica (KFS-16) catalyst*", Journal of Analytical and Applied Pyrolysis **43**, p.15-25.

Sawant, D. P., Vinu, A.; Jacob, N. E., Lefebvre, F., Halligudi, S.B. (2005) "*Formation of nanosized zirconia-supported 12-tungstophosphoric acid in mesoporous silica SBA-15: A stable and versatile solid acid catalyst for benzylation of pheno",* Journal of Catalysis **235**, p.341-352.

Sayari, A. (1996). "*Periodic mesoporous materials: synthesis, characterization and potential applications*", Recent Advances and New Horizons in Zeolite Science and Technology Studies in Surface Science and Catalysis **102**, p.1-46.

Scheirs, J. and Kaminsky, W. "*Feedstock Recycling and Pyrolysis of Waste Plastics: Converting Waste Plastics into Diesel and Other Fuels*", 1st Ed., John Wiley & Sons, West Sussex, 2006.

Schmidt, R., Akporiaye, D., Stöcker, M., Ellestad, O. H. (1994) "*Synthesis of a Mesoporous MCM-41 Material with High Levels of Tetrahedral Aluminum"*, J. Chem. Soc., Chem. Commun. p.1493-1494.

Sing, K.S.W., Everett, D.H., Haul, R.A.W., Moscou, L., Pierrotti, R.A., Jouquerol, J., Siemieniewska, T. (1985). "*Reporting Physisorption Data for Gas/Solid Systems with Special Reference to the Determination of Surface Area and Porosity*", Pure and Appl. Chem. **57**, p.603-619.

Sonwane, C. G. and Ludovice, P. J. (2005). "*A note on micro- and mesopores in the walls of SBA-15 and hysteresis of adsorption isotherms*", Journal of Molecular Catalysis A: Chemical **238**, p. 135-137.

Sun, Y., Yue, Y., Gao, Z. (1997). "*Synthesis and characterization of AlMCM-41 molecular sieves*", Applied Catalysis A: General **161**, p.121-127.

Taguchi, A. and Schüth, F. (2005) "*Ordered mesoporous materials in catalysis*", Microporous and Mesoporous Materials **77**, p.1-45.

Uddin, M. A., Koizumi, K., Murata, K., Sakata, Y. (1997) *"Thermal and catalytic degradation of structurally different types of polyethylene into fuel oil"*, Polymer Degradation and Stability **56**, p.37-44.

van Grieken, R., Serrano, D.P., Aguado, J., Garcia, R., Rojo, C. (2001). *"Thermal and catalytic cracking of polyethylene under mild conditions"*, J. Anal. Appl. Pyrolysis **58-59**, p.127-142.

Vinu, A., Murugesan, V., Böhlmann, W., Hartmann, M. (2004) *"An Optimized Procedure for the Synthesis of ALSBA-15 with Large Pore Diameter and High Aluminum Content"*, J. Phys. Chem. B **108**, p.11496-11505.

Walendziewski, J. (2002) *"Engine fuel derived from waste plastics by thermal treatment"*, Fuel **81**, p.473-481.

Walendziewski, J., Steininger, M. (2001) "*Thermal and catalytic degradation of waste polyolefines"*, Catalysis Today **65**, p.323-330.

Wan, Y., Ma, J., Wang, Z., Zhou, W. (2004) "*Synthesis of MCM-41 with high content of framework aluminum using mixed templates*", Microporous and Mesoporous Materials **76**, p. 35-40.

Vazquez, P., Pizzio, L., Caceres, C., Blanco, M., Thomas, H., Alesso, E., Finkielsztein, L., Lantano, B., Moltrasio, G. and Aguirre, J. (2000). "*Silica-supported heteropolyacids as catalysts in alcohol dehydration reactions"*. Molecular Catalysis A: Chemical **161**, p. 223-232.

Zhao, X.S., Lu, G.Q., Whittaker, A.K., Millar, G.J., Zhu, H.Y. (1997). *"Comprehensive Study of Surface Chemistry of MCM-41 Using ^{29}Si CP/MAS NMR, FTIR Pyridine-TPD, and TGA."* J. Phys. Chem. B. **101**, p.6525-6531.

The University of Texas, http://www.utdallas.edu/~balkus/drop.jpg, last accessed date: 10.10.2010

Wikipedia, http://en.wikipedia.org/wiki/Keggin_structure, last accessed date: 10.10.2010

Wikipedia, http://en.wikipedia.org/wiki/Heteropoly_acid, last accessed date: 10.10.2010

Wikipedia, http://en.wikipedia.org/wiki/Polymer, last accessed date: 10.10.2010

Wikipedia, http://en.wikipedia.org/wiki/Polyethylene , last accessed date: 10.10.2010

Wikipedia, http://en.wikipedia.org/wiki/Polypropylene, last accessed date: 10.10.2010

Wikipedia, http://en.wikipedia.org/wiki/Polystyrene, last accessed date: 10.10.2010

Wikipedia, http://en.wikipedia.org/wiki/Polyvinyl_chloride, last accessed date: 10.10.2010

Wikipedia, http://en.wikipedia.org/wiki/Polyethylene_terephthalate, last accessed date: 10.10.2010

Wikipedia, http://en.wikipedia.org/wiki/Nylon, last accessed date: 10.10.2010

Wikipedia, http://en.wikipedia.org/wiki/X-ray_scattering_techniques, last accessed date: 10.10.2010

Zhao, D., Feng, J., Huo, Q., Melosh, N., Frederickson, G. H., Chmelka, B. F., Stucky, G. D. (1998) "*Triblock Copolymer Syntheses of Mesoporous Silica with Periodic 50 to 300 Angstom Pores*", Science **279**, p.548-552.

Zhao, X.S., Lu, G.Q., Whittaker, A.K., Millar, G.J., Zhu, H.Y. (1997). *"Comprehensive Study of Surface Chemistry of MCM-41 Using ^{29}Si CP/MAS NMR, FTIR, Pyridine-TPD, and TGA",* J. Phys. Chem. B **101**, p.6525-6531.

Zholobenko, V.L., Holmes, S.M., Cundy, C.S., Dwyer, J. (1997). *"Synthesis of MCM-41 materials: an in situ FTIR study", Microporous Materials* **11**, p.83-86.

APPENDIX A

CALCULATION OF ALUMINUM AND TUNGSTOPHOSPHORIC ACID AMOUNTS TO BE IMPREGNATED INTO SYNTHESIZED MCM-41 AND SBA-15 MATERIALS

A.1 Calculation of Aluminum Amount to be Impregnated into MCM-41 Material

First of all, the calculation was based on the assumption that MCM-41 was purely composed of SiO_2. Therefore, the weighed amount of MCM-41 was equal to the amount of SiO_2.

The amount of aluminum source (aluminum triisopropylate) to be used for impregnation was calculated according to the following;

Approximately 0.8 g of MCM-41 was weighed to be used for impregnation and using the molecular weight of SiO_2 (60 g/mol), mole number of SiO_2 was found using equation A.1;

$$n_{SiO2} = m_{SiO2} / MW_{SiO2} \quad (A.1)$$

where m_{SiO2} and n_{SiO2} are the mass of MCM-41 (SiO_2) material weighed and mole number of SiO_2, respectively.

For a desired ratio of Al/Si, mole number of aluminum was calculated using equation A.2;

$$n_{Al}/n_{SiO2} = n_{Al}/n_{Si} = R \quad (A.2)$$

where R is the ratio of Al/Si desired to be produced and n_{Al} is the mole number of aluminum triisopropylate.

When the mole number of aluminyum isopropylate was calculated, knowing that in 1 mole of aluminum triisopropylate ($C_9H_{21}AlO_3$), there is 1 mole of aluminum; number of moles of aluminum triisopropylate is equal to number of moles of aluminum. Therefore, the amount of aluminum triisopropylate to be used was found using equation A.3;

$$m_{Al} = n_{Al} \times MW_{Al} \qquad (A.3)$$

where m_{Al} is mass of aluminum trisipropylate ($C_9H_{21}AlO_3$) and MW_{Al} is the molecular weight of aluminum triisopropylate, 204.25 g/mol.

A.2 Calculation of Tungstophosphoric Acid Amount to be Impregnated into SBA-15 Material

First of all, the calculation was based on the assumption that SBA-15 was purely composed of SiO_2. Therefore, the weighed amount of SBA-15 was equal to the amount of SiO_2.

The amount of tungstophosphoric acid (TPA) that will be used for impregnation was calculated according to the following;

Approximately 0.8 g of SBA-15 was weighed to be used for impregnation and using the molecular weight of SiO_2 (60 g/mol), mole number of SiO_2 was found using equation A.4;

$$n_{SiO2} = m_{SiO2} / MW_{SiO2} \quad (A.4)$$

where m_{SiO2} and n_{SiO2} are the mass of SBA-15 (SiO_2) material weighed and mole number of SiO_2, respectively.

For a desired ratio of W/Si, mole number of tungsten was calculated using equation A.5;

$$n_W / n_{SiO2} = R \quad (A.5)$$

where n_w is the mole number of W and R is the desired ratio of W/Si.

When the mole number of tungsten was calculated, knowing that in 1 mole of TPA ($H_3PW_{12}O_{40}$), there is 12 moles of tungsten; number of moles of TPA is 1/12 of n_W Therefore, the amount of TPA to be used was found using equation A.6;

$$m_{TPA} = (n_W / 12) x\ MW_{TPA} \quad (A.6)$$

where m_{TPA} is mass of TPA and MW_{TPA} is the molecular weight of TPA, 2880 g/mol.

APPENDIX B

EDS RESULTS OF THE SYNTHESIZED MATERIALS

EDS results of the synthesized materials are given in Figures B1-B7.

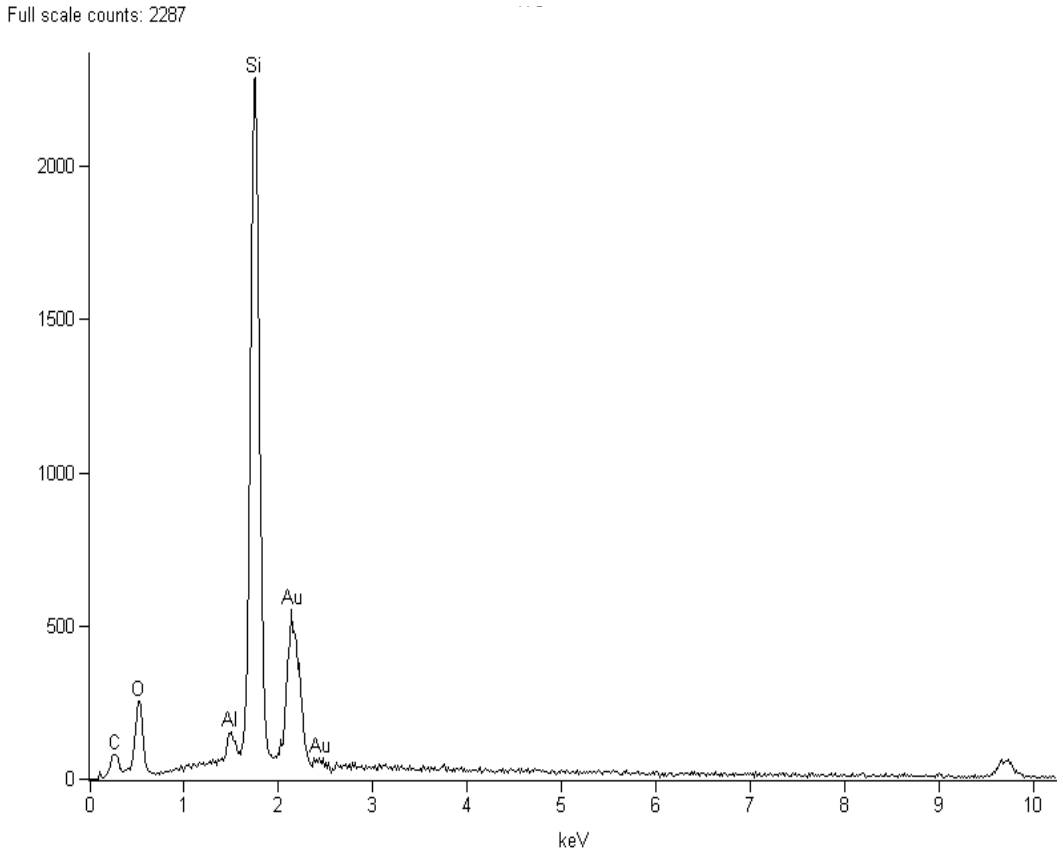

Al-0.03

Element	*Weight Conc %*	*Atom Conc %*
Al	3.01	3.13
Si	96.99	96.87

Figure B.1. EDS result of Al-0.03 material

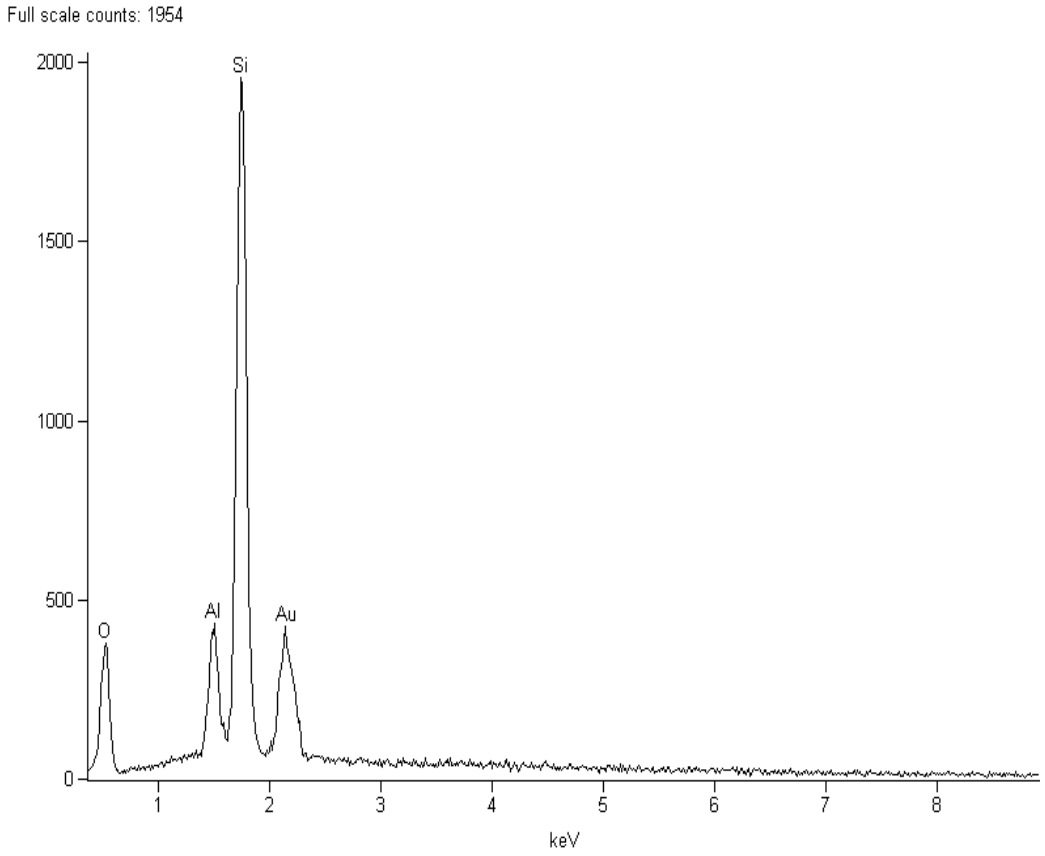

Al-0.10

Element	*Weight Conc %*	*Atom Conc %*
Al	13.14	13.60
Si	86.86	86.40

Figure B.2. EDS result of Al-0.10 material

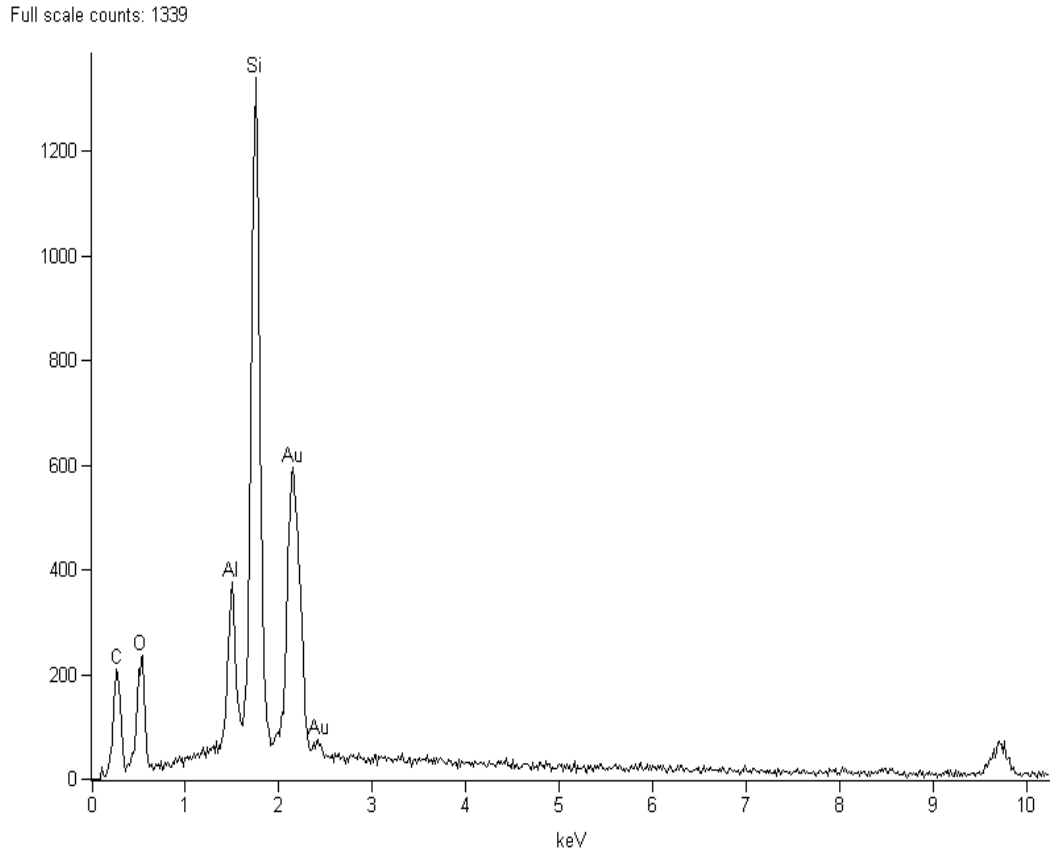

Al-0.25

Element	*Weight Conc %*	*Atom Conc %*
Al	15.00	15.52
Si	85.00	84.48

Figure B.3. EDS result of Al-0.25 material

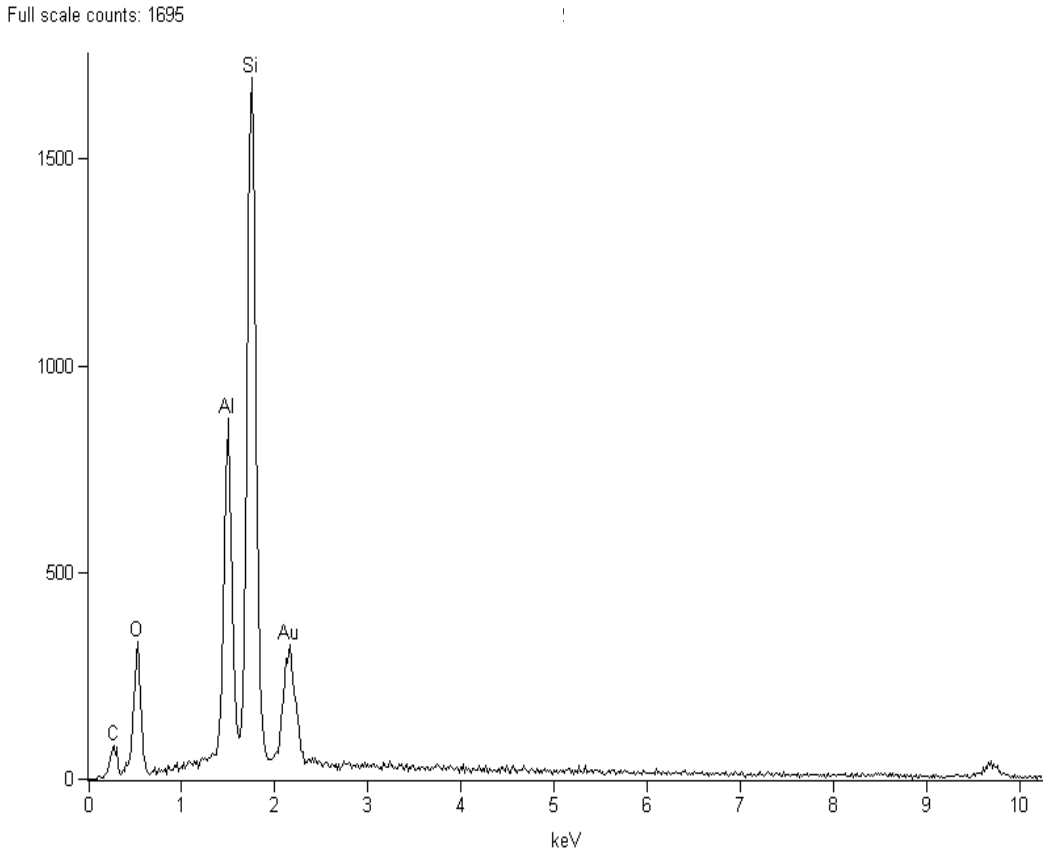

Al-0.50

Element	*Weight Conc %*	*Atom Conc %*
Al	25.46	26.23
Si	74.54	73.77

Figure B.4. EDS result of Al-0.50 material

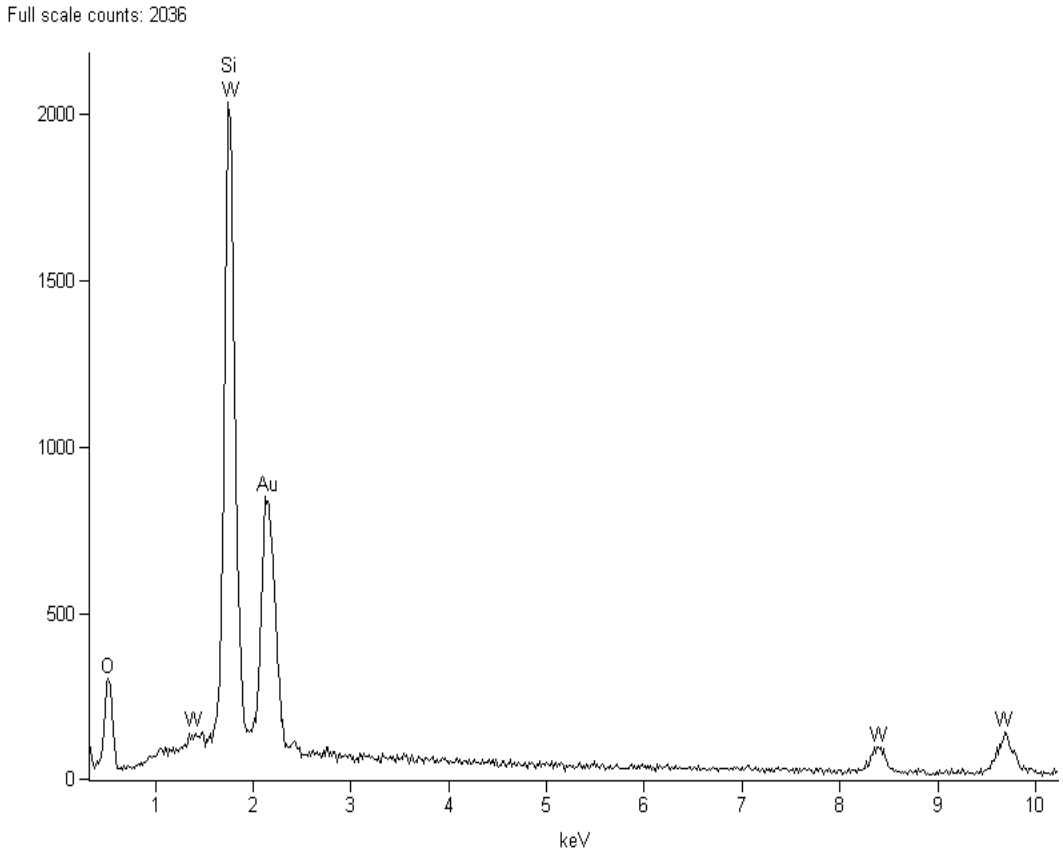

SBA-0.10

Element	*Weight Conc %*	*Atom Conc %*
Si	48.01	85.80
W	51.99	14.20

Figure B.5. EDS result of SBA-0.10 material

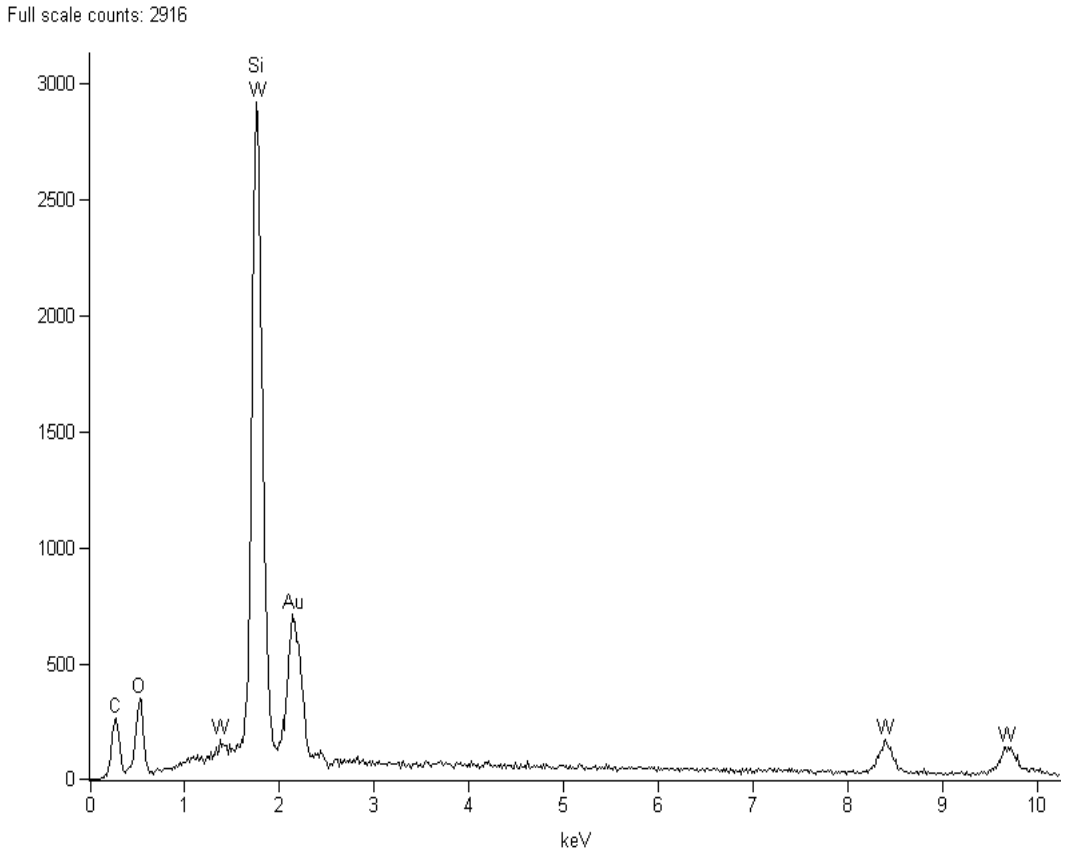

SBA-0.25

Element	*Weight Conc %*	*Atom Conc %*
Si	38.20	80.18
W	61.80	19.82

Figure B.6. EDS result of SBA-0.25 material

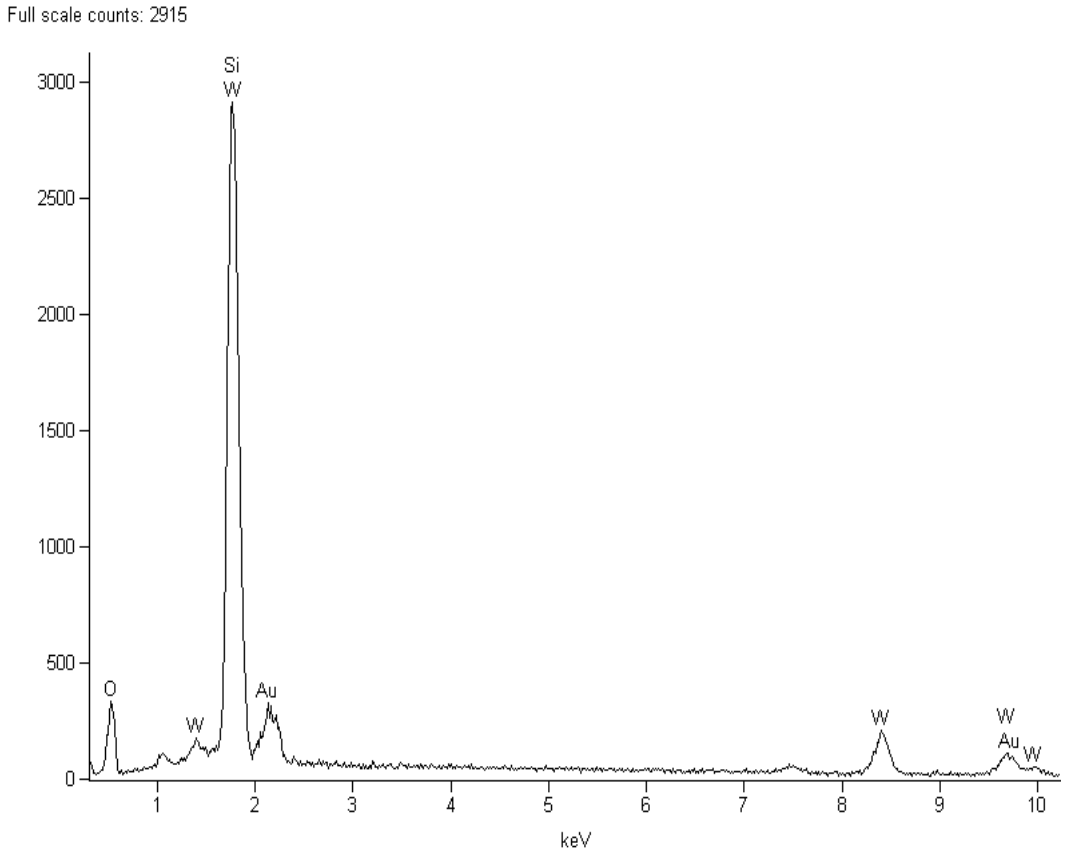

SBA-0.40

Element	*Weight Conc %*	*Atom Conc %*
Si	26.95	70.71
W	73.05	29.29

Figure B.7. EDS result of SBA-0.40 material

APPENDIX C

CALCULATION OF GAS CHROMATOGRAPHY CALIBRATION FACTORS FOR GAS PRODUCTS

In order to identify the gaseous products obtained from the catalytic and non-catalytic degradation of polyethylene, firstly, calibration by standart gas mixtures was carried out. By the use of these calibration runs, retention times and calibration factors of the products were determined. Two standard gas mixtures were used in the calibration trials. The qualifications of these mixtures are given in Table C.1.

Table C.1. Contents of the standart gas mixtures used for calibration

Mixture 1		Mixture 2	
Gas ID	**Mole (%)**	**Gas ID**	**Mole (%)**
CO	1	CH_4	1
CO_2	1	C_2H_6	1
CH_4	1	C_3H_6	1
C_2H_6	1	C_3H_8	1
C_2H_4	1	C_4H_{10}	1
C_2H_2	1	N_2	95
N_2	94		

Gas Products:

A:CH_4 (methane)

B:C_2H_6 (ethane)

C:C_2H_2 (acetylene)

D:C_2H_4 (ethylene)

E:C_3H_6 (propylene)

F:C_3H_8 (propane)

G:C_4H_{10} (butane)

Total amount of gas products was calculated from equation C.1 by taking N_2 as free basis.

$$n_{total} = A_A \beta_A + A_B \beta_B + A_E \beta_E + A_F \beta_F + A_G \beta_G \quad \text{(C.1)}$$

The mole fraction of compound i in the gas is equal to equation C.2;

$$y_i = \frac{n_i \beta}{n_{total} \beta} = \frac{A_i \beta_i}{A_A \beta_A + A_B \beta_B + A_E \beta_E + A_F \beta_F + A_G \beta_G} \quad \text{(C.2)}$$

and the ratio of CH_4 mole fraction to mole fraction of compound i is given as follows,

$$\frac{y_A}{y_i} = \frac{n_A}{n_i} = \frac{A \beta_A}{A \beta_i} \quad \text{(C.3)}$$

A_A and A_i are gas chromatography area data obtained from the analysis and β_A was assigned as 1.0. Calibration factor of component i (β_i) was calculated using equation C.3. Calibration factors of other products were calculated similarly and the calibration factors were tabulated in Table C.2.

Table C.2. Retention times and average areas obtained from the gas chromatograph analysis and calculated calibration factors

Gas ID	Retention Time (min)	$A_{average}$ (mVolt.sec)	Calibration Factor, β
CH_4	0.58	13.2	1
C_2H_6	2.1	19.2	0.69
C_2H_2	1.57	29.8	0.44
C_2H_4	3.14	31.7	0.42
C_3H_6	6.97	24.7	0.54
C_3H_8	7.91	23.7	0.56
$n\text{-}C_4H_{10}$	28.9	22.6	0.59
$i\text{-}C_4H_{10}$	26.1	22.6	0.59

APPENDIX D

CALCULATION OF MOLE AND WEIGHT FRACTIONS AND SELECTIVITIES OF GAS PRODUCTS

D.1 Calculation of Gas Product Mole and Weight Fractions and Selectivities

Mole and weight fractions of compound i were found from equations D.1 and D.2 respectively.

$$y_i = \frac{n_i \beta}{n_{total} \beta} = \frac{A_{i\ i}}{A_A \beta_A + A_B \beta_B + A_C \beta + A_D \beta_D + A_E \beta_E + \ _F \ _F} \qquad (D.1)$$

$$w_i = \frac{m_i}{m_{total}} = \frac{y_i MW_i}{y_A MW_A + y_B MW_B + y_C MW_C + y_D MW_D + y_E MW_E + y_F MW_F} \qquad (D.2)$$

By making carbon balance, selectivity of compound i was determined from equation D.3.

$$S_A = \frac{n_A}{n_A + 2n_B + 2n_C + 2n_D + 3n_E + 3n_F} \qquad (D.3)$$

D.2 Sample Calculation for CH_4 component

Mole and weight fractions and selectivity of CH_4 component were calculated for the experiment performed at 450°C for 15 min without catalyst. GC area data of the gas products and the calculated mole numbers were tabulated in Table D.1.

Table D.1 Compounds and area values obtained for the degradation reaction carried out at 450°C for 15 min.

Compound	Area (mV.sec)	Calibration Factor, β	Mole, n
A:CH_4	1.88	1	1.88
B:C_2H_2	1.35	0.69	0.594
C:C_2H_6	2.95	0.44	2.036
D:C_2H_4	4.74	0.42	1.99
E:C_3H_6	2.44	0.54	1.32
F:C_3H_8	4.35	0.56	2.44

For methane, mole fraction was calculated as;

$$y_A = \frac{n_A}{n_{total}} = \frac{1.88}{1.88 + 0.594 + 2.036 + 1.99 + 1.32 + 2.44} = 0.18$$

Weight fraction of this compound was calculated using equation D.2,

$$w_A = \frac{m_A}{m_{total}} = \frac{0.18 \times 16}{0.18 \times 16 + 0.058 \times 26 + 0.2 \times 30 + 0.194 \times 28 + 0.128 \times 42 + 0.238 \times 44} = 0.9$$

Selectivity was calculated from equation, D.3,

$$S_A = \frac{1.88}{1.88 + 2 \times 0.594 + 2 \times 2.036 + 2 \times 1.99 + 3 \times 1.32 + 3 \times 2.44} = 0.084$$

APPENDIX E

MOLE FRACTION, WEIGHT FRACTION AND SELECTIVITY RESULTS OF GAS PRODUCTS

Mole and weight fractions and selectivities calculated for the non-catalytic and catalytic degradation experiments are tabulated in Tables E.1-E.19.

Table E.1. Mole Fraction and selectivity results obtained from the analysis of gas products (420^{o}C, 45 min, polyethylene)

Gas ID	Mole Fraction	Weight Fraction	Selectivity
C_2H_2	0.044	0.044	0.030
C_2H_6	0.172	0.172	0.134
C_2H_4	0.253	0.253	0.183
C_3H_6	0.158	0.158	0.172
C_3H_8	0.216	0.216	0.246
n-C_4H_{10}	0.157	0.157	0.235

Table E.2. Mole Fraction and selectivity results obtained from the analysis of gas products (430^{o}C, 10 min, polyethylene)

Gas ID	Mole Fraction	Weight Fraction	Selectivity
C_2H_2	0.051	0.032	0.035
C_2H_6	0.178	0.129	0.124
C_2H_4	0.153	0.103	0.106
C_3H_6	0.148	0.151	0.155
C_3H_8	0.218	0.231	0.227
n-C_4H_{10}	0.253	0.354	0.352

Table E.3. Mole Fraction and selectivity results obtained from the analysis of gas products (430°C, 15 min, polyethylene)

Gas ID	Mole Fraction	Weight Fraction	Selectivity
CH_4	0.069	0.028	0.025
C_2H_2	0.063	0.042	0.046
C_2H_6	0.171	0.130	0.125
C_2H_4	0.096	0.068	0.070
C_3H_6	0.179	0.191	0.197
C_3H_8	0.218	0.243	0.239
$n\text{-}C_4H_{10}$	0.204	0.299	0.298

Table E.4. Mole Fraction and selectivity results obtained from the analysis of gas products (450°C, 10 min, polyethylene)

Gas ID	Mole Fraction	Weight Fraction	Selectivity
C_2H_2	0.024	0.020	0.022
C_2H_6	0.069	0.065	0.061
C_2H_4	0.708	0.620	0.627
C_3H_6	0.060	0.079	0.079
C_3H_8	0.080	0.111	0.107
$n\text{-}C_4H_{10}$	0.058	0.106	0.104

Table E.5. Mole Fraction and selectivity results obtained from the analysis of gas products (450°C, 15 min, polyethylene)

Gas ID	Mole Fraction	Weight Fraction	Selectivity
CH_4	0.183	0.093	0.084
C_2H_2	0.058	0.048	0.053
C_2H_6	0.199	0.188	0.182
C_2H_4	0.194	0.172	0.178
C_3H_6	0.128	0.170	0.177
C_3H_8	0.238	0.330	0.327

Table E.6. Mole Fraction and selectivity results obtained from the analysis of gas products (480°C, 5 min, polyethylene)

Gas ID	Mole Fraction	Weight Fraction	Selectivity
C_2H_2	0.055	0.039	0.043
C_2H_6	0.127	0.105	0.100
C_2H_4	0.374	0.287	0.293
C_3H_6	0.165	0.191	0.195
C_3H_8	0.173	0.209	0.203
n-C_4H_{10}	0.106	0.169	0.166

Table E.7. Mole Fraction and selectivity results obtained from the analysis of gas products (480°C, 10 min, polyethylene)

Gas ID	Mole Fraction	Weight Fraction	Selectivity
C_2H_2	0.055	0.039	0.042
C_2H_6	0.112	0.091	0.086
C_2H_4	0.379	0.288	0.294
C_3H_6	0.147	0.168	0.171
C_3H_8	0.178	0.212	0.207
n-C_4H_{10}	0.129	0.203	0.200

Table E.8. Mole Fraction and selectivity results obtained from the analysis of gas products (390^{o}C, 15 min, Polyethylene + SBA-0.10)

Gas ID	Mole Fraction	Weight Fraction	Selectivity
C_2H_2	0.014	0.014	0.011
C_2H_6	0.051	0.059	0.041
C_2H_4	0.569	0.612	0.447
C_3H_6	0.182	0.295	0.215
C_3H_8	0.009	0.015	0.010
n-C_4H_{10}	0.175	0.390	0.275

Table E.9. Mole Fraction and selectivity results obtained from the analysis of gas products (430^{o}C, 15 min, Polyethylene + SBA-0.10)

Gas ID	Mole Fraction	Weight Fraction	Selectivity
C_2H_2	0.023	0.015	0.017
C_2H_6	0.087	0.067	0.063
C_2H_4	0.379	0.270	0.275
C_3H_6	0.198	0.211	0.215
C_3H_8	0.063	0.070	0.068
n-C_4H_{10}	0.249	0.367	0.361

Table E.10. Mole Fraction and selectivity results obtained from the analysis of gas products (390°C, 15 min, Polyethylene + SBA-0.25)

Gas ID	Mole Fraction	Weight Fraction	Selectivity
C_2H_2	0.009	0.006	0.007
C_2H_6	0.023	0.020	0.018
C_2H_4	0.671	0.543	0.548
C_3H_6	0.146	0.177	0.178
n-C_4H_{10}	0.152	0.254	0.248

Table E.11. Mole Fraction and selectivity results obtained from the analysis of gas products (430°C, 15 min, Polyethylene + SBA-0.25)

Gas ID	Mole Fraction	Weight Fraction	Selectivity
C_2H_2	0.017	0.010	0.011
C_2H_6	0.058	0.040	0.038
C_2H_4	0.313	0.204	0.209
C_3H_6	0.184	0.181	0.185
C_3H_8	0.046	0.047	0.046
i-C_4H_{10}	0.142	0.193	0.190
n-C_4H_{10}	0.240	0.325	0.320

Table E.12. Mole Fraction and selectivity results obtained from the analysis of gas products (390°C, 15 min, Polyethylene + SBA-0.40)

Gas ID	Mole Fraction	Weight Fraction	Selectivity
C_2H_2	0.016	0.011	0.012
C_2H_6	0.045	0.035	0.033
C_2H_4	0.423	0.306	0.311
C_3H_6	0.247	0.268	0.273
C_3H_8	0.065	0.074	0.071
i-C_4H_{10}	0.098	0.147	0.144
n-C_4H_{10}	0.106	0.159	0.156

Table E.13. Mole Fraction and selectivity results obtained from the analysis of gas products (410°C, 15 min, Polyethylene + SBA-0.40)

Gas ID	Mole Fraction	Weight Fraction	Selectivity
C_2H_2	0.017	0.012	0.013
C_2H_6	0.051	0.044	0.041
C_2H_4	0.573	0.454	0.460
C_3H_6	0.157	0.187	0.189
C_3H_8	0.068	0.085	0.082
i-C_4H_{10}	0.041	0.067	0.066
n-C_4H_{10}	0.092	0.150	0.147

Table E.14. Mole Fraction and selectivity results obtained from the analysis of gas products (430°C, 15 min, Polyethylene + SBA-0.40)

Gas ID	Mole Fraction	Weight Fraction	Selectivity
C_2H_2	0.012	0.008	0.009
C_2H_6	0.040	0.033	0.031
C_2H_4	0.580	0.451	0.457
C_3H_6	0.144	0.169	0.171
C_3H_8	0.060	0.073	0.071
i-C_4H_{10}	0.116	0.186	0.182
n-C_4H_{10}	0.049	0.079	0.078

Table E.15. Mole Fraction and selectivity results obtained from the analysis of gas products (460°C, 15 min, Polyethylene + SBA-0.40)

Gas ID	Mole Fraction	Weight Fraction	Selectivity
CH_4	0.168	0.078	0.070
C_2H_2	0.028	0.021	0.024
C_2H_6	0.116	0.100	0.097
C_2H_4	0.401	0.324	0.334
i-C_4H_{10}	0.165	0.275	0.274
n-C_4H_{10}	0.121	0.202	0.201

Table E.16. Mole Fraction and selectivity results obtained from the analysis of gas products (390°C, 15 min, Polyethylene + Al-0.03)

Gas ID	Mole Fraction	Weight Fraction	Selectivity
CH_4	0.263	0.111	0.100
C_2H_2	0.007	0.005	0.005
C_2H_6	0.004	0.003	0.003
C_2H_4	0.150	0.111	0.115
C_3H_6	0.263	0.292	0.301
C_3H_8	0.002	0.003	0.003
i-C_4H_{10}	0.103	0.157	0.157
n-C_4H_{10}	0.207	0.318	0.316

Table E.17. Mole Fraction and selectivity results obtained from the analysis of gas products (430°C, 15 min, Polyethylene + Al-0.03)

Gas ID	Mole Fraction	Weight Fraction	Selectivity
C_2H_2	0.009	0.005	0.005
C_2H_6	0.006	0.004	0.003
C_2H_4	0.088	0.049	0.050
C_3H_6	0.279	0.233	0.238
C_3H_8	0.004	0.003	0.003
i-C_4H_{10}	0.239	0.275	0.272
n-C_4H_{10}	0.375	0.432	0.428

Table E.18. Mole Fraction and selectivity results obtained from the analysis of gas products (390°C, 15 min, Polyethylene + Al-0.25)

Gas ID	Mole Fraction	Weight Fraction	Selectivity
C_2H_2	0.008	0.004	0.005
C_2H_6	0.005	0.003	0.003
C_2H_4	0.119	0.067	0.069
C_3H_6	0.265	0.224	0.229
C_3H_8	0.004	0.004	0.004
i-C_4H_{10}	0.245	0.285	0.282
n-C_4H_{10}	0.354	0.413	0.408

Table E.19. Mole Fraction and selectivity results obtained from the analysis of gas products (430^{o}C, 15 min, Polyethylene + Al-0.25)

Gas ID	Mole Fraction	Weight Fraction	Selectivity
C_2H_2	0.012	0.006	0.007
C_2H_6	0.025	0.015	0.015
C_2H_4	0.114	0.065	0.067
C_3H_6	0.276	0.237	0.243
C_3H_8	0.004	0.004	0.003
i-C_4H_{10}	0.188	0.223	0.220
n-C_4H_{10}	0.380	0.450	0.445

APPENDIX F

CALCULATION OF GAS CHROMATOGRAPHY CALIBRATION FACTORS FOR LIQUID PRODUCTS

In order to identify the liquid products obtained from the catalytic and non-catalytic degradation of polyethylene, firstly, calibration by standart liquids was performed. By the use of these calibration runs, retention times and calibration factors of the products were determined. For the identification of liquid products, five paraffin mixtures were used. These mixtures are given in Table F.1.

Table F.1. Standard paraffin mixtures used for calibration (C_5-C_{18})

Mixture 1		Mixture 2		Mixture 3		Mixture 4		Mixture 5	
Liq. ID	Wt. (%)	Liq. ID	Wt. (%)	Liq. ID	Wt. (%)	Liq. ID	Wt. (%)	Liq. ID	Wt. (%)
n-C_5H_{12}	25	n-C_7H_{16}	25	n-C_9H_{20}	25	n-$C_{11}H_{24}$	25	n-$C_{12}H_{26}$	25
n-C_6H_{14}	25	n-C_8H_{18}	25	n-$C_{10}H_{22}$	25	n-$C_{12}H_{26}$	25	n-$C_{14}H_{30}$	25
n-C_7H_{16}	25	n-C_9H_{20}	25	n-$C_{11}H_{24}$	25	n-$C_{13}H_{28}$	25	n-$C_{16}H_{34}$	25
n-C_8H_{18}	25	n-$C_{10}H_{22}$	25	n-$C_{12}H_{26}$	25	n-$C_{14}H_{29}$	25	n-$C_{18}H_{38}$	25

In addition to the mixtures given above, also equal volume mixtures were prepared. Hexane was chosen as the common compound for these mixtures which are given in Table F.2.

Table F.2. Calibration mixtures prepared in equal volumes

Mixture	Compounds	Volume (%)
1	n-hexane+isooctane	50-50
2	n-hexane+diisobutylene	50-50
3	n-hexane+cyclohexane	50-50
4	n-hexane+benzene	50-50
5	n-hexane+xylene	50-50
6	n-hexane+toluene	50-50
7	n-hexane+ethylbenzene	50-50

The procedure for calculation of calibration factor is given for 1st paraffin mixture;

A:n-C_5H_{12}

B:n-C_6H_{14}

C:n-C_7H_{16}

D:n-C_8H_{18}

Total amount of gas products was calculated from equation F.1;

$$n_{total} = A_A \beta_A + A_B \beta_B + A_C \beta_C + A_D \beta_D \quad \text{(F.1)}$$

and mole fractions of the liquid compounds were calculated using equation F.2;

$$x_i = \frac{n_i \beta}{n_{total} \beta} = \frac{A_{i\ i}}{A_A \beta_A + A_B \beta_B + A_C \beta_C + \ _D \ D} \quad \text{(F.2)}$$

$$\frac{x_A}{x_i} = \frac{n_A}{n_i} = \frac{A\beta_A}{A\beta_i} \qquad \text{(F.3)}$$

Volume fraction of the components were calculated as;

$$z_A = x_A \frac{MW_A}{\rho_A} \qquad \text{(F.4)}$$

In the calculations, for n-hexane a calibration factor of 1.0 was randomly chosen. Using equation F.3, calibration factor of component i, β_i was calculated since the other parameters were already known. Calibration factors of other compounds in all mixtures were calculated in a similar way and in Table F.3, calculated calibration factors and retention times of the liquid hydrocarbons are given.

Table F.3. Calibration factors and retention times of the liquid hydrocarbons

Liquid Compounds	Retention Time (min)	Calibration Factor, β
n-Pentane (C_5H_{12})	3.39	2.98
n-Hexane (C_6H_{14})	4.16	1.0
Cyclohexane (C_6H_{12})	6.03	0.51
Benzene (C_6H_6)	6.11	0.87
n-Heptane (C_7H_{16})	6.56	0.93
i-octane (i-C_8H_{18})	7.07	0.49
Diisobutylene (C_8H_{16})	7.97	0.75
Toluene (C_7H_8)	11.7	0.78
n-Octane (n-C_8H_{18})	12.9	0.87
Ethylbenzene (C_8H_{10})	17.4	0.51
m,p-xylene ($C_6H_4(CH_3)_2$)	17.9	0.51
o-xylene ($C_6H_4(CH_3)_2$)	18.2	0.51
n-Nonane (C_9H_{20})	18.4	0.64
n-Decane ($C_{10}H_{22}$)	23.3	0.56
n-Undecane ($C_{11}H_{24}$)	27.0	0.45
n-Dodecane ($C_{12}H_{26}$)	30.7	0.42
n-Tridecane ($C_{13}H_{28}$)	33.9	0.33
n-Tetradecane ($C_{14}H_{30}$)	38.1	0.41
n-Hexadecane ($C_{16}H_{34}$)	51.2	0.69
n-Octadecane ($C_{18}H_{38}$)	69.4	0.90

APPENDIX G

MOLE FRACTION AND SELECTIVITY RESULTS OF LIQUID PRODUCTS

Mole and selectivities calculated for the non-catalytic and catalytic degradation experiments are given in Tables G.1-G-17.

Table G.1. Mole Fraction and selectivity results obtained from the analysis of liquid products (420^{o}C, 45 min, Polyethylene)

Liquid ID	Mole Fraction	Selectivity
n-Nonane (C_9H_{20})	0.000	0.000
n-Decane ($C_{10}H_{22}$)	0.000	0.000
n-Undecane ($C_{11}H_{24}$)	0.003	0.002
n-Dodecane ($C_{12}H_{26}$)	0.006	0.004
n-Tridecane ($C_{13}H_{28}$)	0.006	0.004
n-Tetradecane ($C_{14}H_{30}$)	0.022	0.017
n-Hexadecane ($C_{14}H_{30}$)	0.063	0.050
n-Octadecane ($C_{18}H_{38}$)	0.900	0.922

Table G.2. Mole Fraction and selectivity results obtained from the analysis of liquid products (430^{o}C, 10 min, Polyethylene)

Liquid ID	Mole Fraction	Selectivity
n-Pentane (C_5H_{12})	0.012	0.004
n-Octane (n-C_8H_{18})	0.013	0.007
m,p-xylene ($C_6H_4(CH_3)_2$)	0.024	0.014
o-xylene ($C_6H_4(CH_3)_2$)	0.027	0.016
n-Nonane (C_9H_{20})	0.020	0.014
n-Decane ($C_{10}H_{22}$)	0.109	0.082
n-Undecane ($C_{11}H_{24}$)	0.131	0.107
n-Dodecane ($C_{12}H_{26}$)	0.077	0.069
n-Tridecane ($C_{13}H_{28}$)	0.062	0.060
n-Tetradecane ($C_{14}H_{30}$)	0.112	0.117
n-Hexadecane ($C_{14}H_{30}$)	0.142	0.149
n-Octadecane ($C_{18}H_{38}$)	0.266	0.357

Table G.3. Mole Fraction and selectivity results obtained from the analysis of liquid products (430°C, 15 min, Polyethylene)

Liquid ID	Mole Fraction	Selectivity
n-Pentane (C_5H_{12})	0.018	0.002
m,p-xylene ($C_6H_4(CH_3)_2$)	0.028	0.005
o-xylene ($C_6H_4(CH_3)_2$)	0.005	0.000
n-Nonane (C_9H_{20})	0.009	0.000
n-Decane ($C_{10}H_{22}$)	0.133	0.113
n-Undecane ($C_{11}H_{24}$)	0.087	0.049
n-Dodecane ($C_{12}H_{26}$)	0.106	0.072
n-Tridecane ($C_{13}H_{28}$)	0.060	0.023
n-Tetradecane ($C_{14}H_{30}$)	0.110	0.077
n-Hexadecane ($C_{14}H_{30}$)	0.181	0.211
n-Octadecane ($C_{18}H_{38}$)	0.264	0.447

Table G.4. Mole Fraction and selectivity results obtained from the analysis of liquid products (450°C, 10 min, Polyethylene)

Liquid ID	Mole Fraction	Selectivity
Diisobutylene (C_8H_{16})	0.118	0.080
n-Octane (n-C_8H_{18})	0.004	0.003
Ethylbenzene (C_8H_{10})	0.112	0.076
m,p-xylene ($C_6H_4(CH_3)_2$)	0.054	0.037
o-xylene ($C_6H_4(CH_3)_2$)	0.053	0.036
n-Nonane (C_9H_{20})	0.000	0.000
n-Decane ($C_{10}H_{22}$)	0.075	0.063
n-Undecane ($C_{11}H_{24}$)	0.099	0.092
n-Dodecane ($C_{12}H_{26}$)	0.102	0.103
n-Tridecane ($C_{13}H_{28}$)	0.045	0.049
n-Tetradecane ($C_{14}H_{30}$)	0.049	0.059
n-Hexadecane ($C_{14}H_{30}$)	0.099	0.117
n-Octadecane ($C_{18}H_{38}$)	0.187	0.284

Table G.5. Mole Fraction and selectivity results obtained from the analysis of liquid products (480°C, 10 min, Polyethylene)

Liquid ID	Mole Fraction	Selectivity
Ethylbenzene (C_8H_{10})	0.053	0.034
m,p-xylene ($C_6H_4(CH_3)_2$)	0.007	0.004
o-xylene ($C_6H_4(CH_3)_2$)	0.000	0.000
n-Nonane (C_9H_{20})	0.004	0.003
n-Decane ($C_{10}H_{22}$)	0.187	0.150
n-Undecane ($C_{11}H_{24}$)	0.171	0.151
n-Dodecane ($C_{12}H_{26}$)	0.120	0.116
n-Tridecane ($C_{13}H_{28}$)	0.090	0.094
n-Tetradecane ($C_{14}H_{30}$)	0.146	0.164
n-Hexadecane ($C_{14}H_{30}$)	0.118	0.133
n-Octadecane ($C_{18}H_{38}$)	0.105	0.152

Table G.6. Mole Fraction and selectivity results obtained from the analysis of liquid products (390°C, 15 min, Polyethylene+SBA15-0.10)

Liquid ID	Mole Fraction	Selectivity
n-Pentane (C_5H_{12})	0.067	0.027
n-Hexane (C_6H_{14})	0.005	0.002
n-Octane (n-C_8H_{18})	0.003	0.002
Ethylbenzene (C_8H_{10})	0.020	0.013
m,p-xylene ($C_6H_4(CH_3)_2$)	0.008	0.005
o-xylene ($C_6H_4(CH_3)_2$)	0.000	0.000
n-Nonane (C_9H_{20})	0.031	0.023
n-Decane ($C_{10}H_{22}$)	0.114	0.093
n-Undecane ($C_{11}H_{24}$)	0.082	0.074
n-Dodecane ($C_{12}H_{26}$)	0.157	0.154
n-Tridecane ($C_{13}H_{28}$)	0.176	0.188
n-Tetradecane ($C_{14}H_{30}$)	0.138	0.158
n-Hexadecane ($C_{14}H_{30}$)	0.080	0.092
n-Octadecane ($C_{18}H_{38}$)	0.112	0.165

Table G.7. Mole Fraction and selectivity results obtained from the analysis of liquid products (390°C, 15 min, Polyethylene+SBA15-0.25)

Liquid ID	Mole Fraction	Selectivity
n-Pentane (C_5H_{12})	0.023	0.010
n-Octane (n-C_8H_{18})	0.028	0.020
Ethylbenzene (C_8H_{10})	0.070	0.049
m,p-xylene ($C_6H_4(CH_3)_2$)	0.028	0.020
o-xylene ($C_6H_4(CH_3)_2$)	0.017	0.012
n-Nonane (C_9H_{20})	0.080	0.063
n-Decane ($C_{10}H_{22}$)	0.038	0.033
n-Undecane ($C_{11}H_{24}$)	0.127	0.123
n-Dodecane ($C_{12}H_{26}$)	0.183	0.193
n-Tridecane ($C_{13}H_{28}$)	0.124	0.141
n-Tetradecane ($C_{14}H_{30}$)	0.160	0.196
n-Hexadecane ($C_{14}H_{30}$)	0.049	0.060
n-Octadecane ($C_{18}H_{38}$)	0.037	0.058

Table G.8. Mole Fraction and selectivity results obtained from the analysis of liquid products (390°C, 15 min, Polyethylene+SBA15-0.40)

Liquid ID	Mole Fraction	Selectivity
n-Pentane (C_5H_{12})	0.006	0.002
n-Octane (n-C_8H_{18})	0.006	0.004
Ethylbenzene (C_8H_{10})	0.007	0.004
m,p-xylene ($C_6H_4(CH_3)_2$)	0.007	0.004
o-xylene ($C_6H_4(CH_3)_2$)	0.006	0.004
n-Nonane (C_9H_{20})	0.019	0.013
n-Decane ($C_{10}H_{22}$)	0.034	0.025
n-Undecane ($C_{11}H_{24}$)	0.091	0.075
n-Dodecane ($C_{12}H_{26}$)	0.120	0.108
n-Tridecane ($C_{13}H_{28}$)	0.159	0.155
n-Tetradecane ($C_{14}H_{30}$)	0.356	0.374
n-Hexadecane ($C_{14}H_{30}$)	0.077	0.081
n-Octadecane ($C_{18}H_{38}$)	0.111	0.150

Table G.9. Mole Fraction and selectivity results obtained from the analysis of liquid products (410°C, 15 min, Polyethylene+SBA15-0.40)

Liquid ID	Mole Fraction	Selectivity
n-Pentane (C_5H_{12})	0.004	0.002
i-octane (i-C_8H_{18})	0.005	0.004
n-Octane (n-C_8H_{18})	0.021	0.015
Ethylbenzene (C_8H_{10})	0.009	0.006
m,p-xylene ($C_6H_4(CH_3)_2$)	0.015	0.010
o-xylene ($C_6H_4(CH_3)_2$)	0.012	0.008
n-Nonane (C_9H_{20})	0.044	0.034
n-Decane ($C_{10}H_{22}$)	0.024	0.021
n-Undecane ($C_{11}H_{24}$)	0.176	0.169
n-Dodecane ($C_{12}H_{26}$)	0.266	0.279
n-Tridecane ($C_{13}H_{28}$)	0.107	0.121
n-Tetradecane ($C_{14}H_{30}$)	0.194	0.237
n-Hexadecane ($C_{14}H_{30}$)	0.031	0.038
n-Octadecane ($C_{18}H_{38}$)	0.001	0.001

Table G.10. Mole Fraction and selectivity results obtained from the analysis of liquid products (430°C, 15 min, Polyethylene+SBA15-0.10)

Liquid ID	Mole Fraction	Selectivity
n-Octane (n-C_8H_{18})	0.002	0.002
Ethylbenzene (C_8H_{10})	0.075	0.052
m,p-xylene ($C_6H_4(CH_3)_2$)	0.017	0.012
o-xylene ($C_6H_4(CH_3)_2$)	0.020	0.014
n-Nonane (C_9H_{20})	0.059	0.046
n-Decane ($C_{10}H_{22}$)	0.129	0.112
n-Undecane ($C_{11}H_{24}$)	0.110	0.105
n-Dodecane ($C_{12}H_{26}$)	0.186	0.193
n-Tridecane ($C_{13}H_{28}$)	0.166	0.186
n-Tetradecane ($C_{14}H_{30}$)	0.126	0.153
n-Hexadecane ($C_{14}H_{30}$)	0.041	0.049
n-Octadecane ($C_{18}H_{38}$)	0.037	0.058

Table G.11. Mole Fraction and selectivity results obtained from the analysis of liquid products (430°C, 15 min, Polyethylene+SBA15-0.25)

Liquid ID	Mole Fraction	Selectivity
i-octane (i-C_8H_{18})	0.004	0.002
Ethylbenzene (C_8H_{10})	0.024	0.016
m,p-xylene ($C_6H_4(CH_3)_2$)	0.019	0.013
o-xylene ($C_6H_4(CH_3)_2$)	0.004	0.002
n-Nonane (C_9H_{20})	0.026	0.020
n-Decane ($C_{10}H_{22}$)	0.060	0.050
n-Undecane ($C_{11}H_{24}$)	0.129	0.119
n-Dodecane ($C_{12}H_{26}$)	0.208	0.209
n-Tridecane ($C_{13}H_{28}$)	0.280	0.306
n-Tetradecane ($C_{14}H_{30}$)	0.140	0.165
n-Hexadecane ($C_{14}H_{30}$)	0.020	0.023
n-Octadecane ($C_{18}H_{38}$)	0.026	0.040

Table G.12. Mole Fraction and selectivity results obtained from the analysis of liquid products (430°C, 15 min, Polyethylene+SBA15-0.40)

Liquid ID	Mole Fraction	Selectivity
n-Pentane (C_5H_{12})	0.088	0.041
i-octane (i-C_8H_{18})	0.002	0.001
Toluene (C_7H_8)	0.011	0.007
n-Octane (n-C_8H_{18})	0.029	0.021
Ethylbenzene (C_8H_{10})	0.030	0.022
m,p-xylene ($C_6H_4(CH_3)_2$)	0.031	0.023
o-xylene ($C_6H_4(CH_3)_2$)	0.034	0.025
n-Nonane (C_9H_{20})	0.075	0.062
n-Decane ($C_{10}H_{22}$)	0.149	0.138
n-Undecane ($C_{11}H_{24}$)	0.098	0.099
n-Dodecane ($C_{12}H_{26}$)	0.097	0.107
n-Tridecane ($C_{13}H_{28}$)	0.069	0.083
n-Tetradecane ($C_{14}H_{30}$)	0.125	0.162
n-Hexadecane ($C_{14}H_{30}$)	0.158	0.205

Table G.13. Mole Fraction and selectivity results obtained from the analysis of liquid products (460°C, 15 min, Polyethylene+SBA15-0.40)

Liquid ID	Mole Fraction	Selectivity
n-Octane (n-C_8H_{18})	0.002	0.002
Ethylbenzene (C_8H_{10})	0.012	0.008
m,p-xylene ($C_6H_4(CH_3)_2$)	0.019	0.013
o-xylene ($C_6H_4(CH_3)_2$)	0.024	0.016
n-Nonane (C_9H_{20})	0.063	0.049
n-Decane ($C_{10}H_{22}$)	0.167	0.144
n-Undecane ($C_{11}H_{24}$)	0.219	0.209
n-Dodecane ($C_{12}H_{26}$)	0.185	0.192
n-Tridecane ($C_{13}H_{28}$)	0.147	0.165
n-Tetradecane ($C_{14}H_{30}$)	0.139	0.168
n-Hexadecane ($C_{14}H_{30}$)	0.012	0.014
n-Octadecane ($C_{18}H_{38}$)	0.012	0.019
n-Octane (n-C_8H_{18})	0.002	0.002

Table G.14. Mole Fraction and selectivity results obtained from the analysis of liquid products (390°C, 15 min, Polyethylene+Al-0.03)

Liquid ID	Mole Fraction	Selectivity
n-Pentane (C_5H_{12})	0.04	0.02
n-Hexane (C_6H_{14})	0.01	0.01
Ethylbenzene (C_8H_{10})	0.01	0.01
m,p-xylene ($C_6H_4(CH_3)_2$)	0.04	0.03
o-xylene ($C_6H_4(CH_3)_2$)	0.02	0.02
n-Nonane (C_9H_{20})	0.11	0.09
n-Decane ($C_{10}H_{22}$)	0.11	0.09
n-Undecane ($C_{11}H_{24}$)	0.10	0.10
n-Dodecane ($C_{12}H_{26}$)	0.10	0.11
n-Tridecane ($C_{13}H_{28}$)	0.05	0.06
n-Tetradecane ($C_{14}H_{30}$)	0.09	0.10
n-Hexadecane ($C_{14}H_{30}$)	0.28	0.34
n-Octadecane ($C_{18}H_{38}$)	0.02	0.03

Table G.15. Mole Fraction and selectivity results obtained from the analysis of liquid products (390°C, 15 min, Polyethylene+Al-0.25)

Liquid ID	Mole Fraction	Selectivity
n-Pentane (C_5H_{12})	0.03	0.02
Diisobutylene (C_8H_{16})	0.02	0.01
n-Octane (n-C_8H_{18})	0.23	0.19
Ethylbenzene (C_8H_{10})	0.05	0.04
m,p-xylene ($C_6H_4(CH_3)_2$)	0.02	0.01
o-xylene ($C_6H_4(CH_3)_2$)	0.06	0.05
n-Nonane (C_9H_{20})	0.03	0.03
n-Decane ($C_{10}H_{22}$)	0.01	0.01
n-Undecane ($C_{11}H_{24}$)	0.15	0.17
n-Dodecane ($C_{12}H_{26}$)	0.17	0.22
n-Tridecane ($C_{13}H_{28}$)	0.05	0.06
n-Tetradecane ($C_{14}H_{30}$)	0.04	0.06
n-Hexadecane ($C_{14}H_{30}$)	0.01	0.01

Table G.16. Mole Fraction and selectivity results obtained from the analysis of liquid products (430°C, 15 min, Polyethylene+Al-0.03)

Liquid ID	Mole Fraction	Selectivity
n-Pentane (C_5H_{12})	0.20	0.11
i-octane (i-C_8H_{18})	0.00	0.00
n-Octane (n-C_8H_{18})	0.06	0.05
Ethylbenzene (C_8H_{10})	0.06	0.05
m,p-xylene ($C_6H_4(CH_3)_2$)	0.05	0.04
o-xylene ($C_6H_4(CH_3)_2$)	0.02	0.02
n-Nonane (C_9H_{20})	0.12	0.12
n-Decane ($C_{10}H_{22}$)	0.05	0.05
n-Undecane ($C_{11}H_{24}$)	0.11	0.13
n-Dodecane ($C_{12}H_{26}$)	0.09	0.11
n-Tridecane ($C_{13}H_{28}$)	0.07	0.10
n-Tetradecane ($C_{14}H_{30}$)	0.09	0.13
n-Hexadecane ($C_{14}H_{30}$)	0.01	0.02
n-Octadecane ($C_{18}H_{38}$)	0.02	0.04

Table G.17. Mole Fraction and selectivity results obtained from the analysis of liquid products (430^{o}C, 15 min, Polyethylene+Al-0.25)

Liquid ID	Mole Fraction	Selectivity
n-Pentane (C_5H_{12})	0.29	0.18
Diisobutylene (C_8H_{16})	0.01	0.01
n-Octane (n-C_8H_{18})	0.19	0.19
Ethylbenzene (C_8H_{10})	0.02	0.01
m,p-xylene ($C_6H_4(CH_3)_2$)	0.01	0.01
o-xylene ($C_6H_4(CH_3)_2$)	0.09	0.09
n-Nonane (C_9H_{20})	0.09	0.10
n-Decane ($C_{10}H_{22}$)	0.03	0.03
n-Undecane ($C_{11}H_{24}$)	0.06	0.08
n-Dodecane ($C_{12}H_{26}$)	0.11	0.17
n-Tridecane ($C_{13}H_{28}$)	0.03	0.05
n-Tetradecane ($C_{14}H_{30}$)	0.03	0.05
n-Hexadecane ($C_{14}H_{30}$)	0.01	0.02
n-Octadecane ($C_{18}H_{38}$)	0.00	0.01